INFORMATION TO USERS

This manuscript has been reproduced from the microfilm master. UMI films the text directly from the original or copy submitted. Thus, some thesis and dissertation copies are in typewriter face, while others may be from any type of computer printer.

The quality of this reproduction is dependent upon the quality of the copy submitted. Broken or indistinct print, colored or poor quality illustrations and photographs, print bleedthrough, substandard margins, and improper alignment can adversely affect reproduction.

In the unlikely event that the author did not send UMI a complete manuscript and there are missing pages, these will be noted. Also, if unauthorized copyright material had to be removed, a note will indicate the deletion.

Oversize materials (e.g., maps, drawings, charts) are reproduced by sectioning the original, beginning at the upper left-hand corner and continuing from left to right in equal sections with small overlaps. Each original is also photographed in one exposure and is included in reduced form at the back of the book.

Photographs included in the original manuscript have been reproduced xerographically in this copy. Higher quality 6" x 9" black and white photographic prints are available for any photographs or illustrations appearing in this copy for an additional charge. Contact UMI directly to order.

UMI

A Bell & Howell Information Company
300 North Zeeb Road, Ann Arbor MI 48106-1346 USA
313/761-4700 800/521-0600

CHARACTERIZATION AND OPTIMIZATION OF ORDERING IN THIN FILMS OF (2,3,9,10,16,17,23,24-OKTAKIS((2-BENZYLOXY)ETHOXY) PHTHALOCYANINATO COPPER AND ITS METAL FREE ANALOGUE

by

Rebecca Anne Peterson

A Thesis Submitted to the Faculty of the

DEPARTMENT OF CHEMISTRY

In Partial Fulfillment of the Requirements
For the Degree of

MASTER OF SCIENCE

In the Graduate College

THE UNIVERSITY OF ARIZONA

1998

STATEMENT BY AUTHOR

This thesis has been submitted in partial fulfillment of requirements for an advanced degree at The University of Arizona and is deposited in the University Library to be made available to borrowers under rules of the Library.

Brief quotations from this thesis are allowable without special permission, provided that accurate acknowledgment of source is made. Requests for permission for extended quotation from or reproduction of this manuscript in whole or in part may be granted by the head of the major department or the Dean of the Graduate College when in his or her judgment the proposed use of the material is in the interests of scholarship. In all other instances, however, permission must be obtained from the author.

SIGNED: 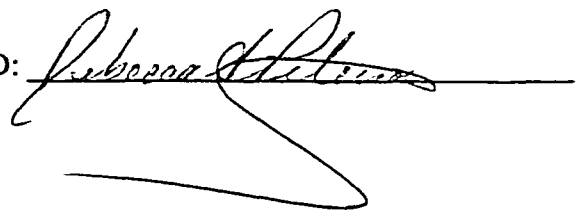

APPROVAL BY THESIS DIRECTOR

This thesis has been approved on the date shown below:

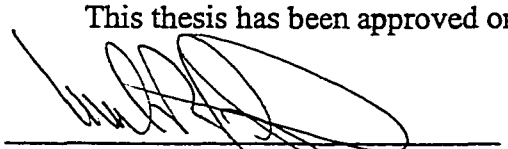

Neal R. Armstrong
Professor of Chemistry

12/7/98
Date

ACKNOWLEDGMENTS

There are many people who deserve credit for their contributions to this document. First, my collaborators: SAXS expert, Dr. Simon Bates at Kratos Analytical, TFT expert, Dr. Zhenan Bao at Lucent Technologies, Bell Laboratories, and our resident AFM expert Dr. Ken Nebesny. Secondly, my research advisors Dr. Neal Armstrong and Dr. David O'Brien, and Dr. Jeanne Pemberton for their intellectual guidance and support in an endeavor that has strengthened my scientific abilities as well as my character. Lastly, I'd like to thank the people who have given me unconditional support and encouragement, my family and my best friend, Chris.

TABLE OF CONTENTS

LIST OF FIGURES.....viii

LIST OF TABLES.....xii

ABSTRACT.....xiv

CHAPTER 1: INTRODUCTION.....1

1.1 The Phthalocyanines.....1

1.1.1 Origins.....1

1.1.2 Focus of Recent Research.....1

1.2 Previously Characterized Properties of $CuPc(OC_2OBz)_8$ and $H_2Pc(OC_2OBz)_8$

.....3

1.3 Overview of Experiments.....7

1.4 Summary of Results.....8

CHAPTER 2: EXPERIMENTAL.....10

2.1 Studied Molecules.....10

2.2 Langmuir-Blodgett Materials and Techniques.....10

2.3 Substrate Surface Preparation and Modification.....11

2.4 Contact Angle Measurements.....12

2.5 Small Angle X-ray Scattering Measurements.....12

2.6 Atomic Force Microscopy.....13

2.7 Infrared Spectroscopy.....14

2.7.1 Transmission Experiments.....14

TABLE OF CONTENTS - Continued

2.7.2 LB Multilayer Thin Films.....14

2.7.3 Reflection Absorption Infrared Spectroscopy.....14

2.8 X-ray Photoelectron Spectroscopy.....15

2.9 Thin Film Field-Effect Transistor Mobility Measurements.....15

CHAPTER 3: MACROSCOPIC ORDERING OF LB THIN FILMS.....18

3.1 Overview of Experiments.....18

3.2 Importance of Substrate Surface Treatment.....18

3.2.1 Choice of Substrate Materials and Surface Modifiers.....19

3.2.3 Contact Angle Theory.....20

3.2.4 Measured Contact Angles of Modified Surfaces.....20

3.2.5 Significance of Measured Contact Angles.....24

3.3 SAXS Theory.....24

3.3.1 Bragg Diffraction Peak (Angle) Measurements.....25

3.3.2 Effects of Annealing.....30

3.3.3 Dimensional Information in Context of Molecular Ordering.....32

3.4 Atomic Force Microscopy.....33

3.4.1 Considerations of using AFM as an Imaging Tool of Soft Materials.....33

3.4.2 Images of Single bilayer films of $CuPc(OC_2OBz)_8$ and $H_2Pc(OC_2OBz)_8$...34

3.4.3 Comparison with SAXS Experiments.....41

TABLE OF CONTENTS - Continued

CHAPTER 4: MICROSCOPIC ORDERING DETERMINED BY IR SPECTROSCOPY 42

4.1 Overview of Experimental Parameters 42

4.2 Bulk Transmission IR Spectroscopy 42

4.3 Transmission IR Spectroscopy with Polarized Excitation Source 46

4.3.1 Introduction 46

4.3.2 Overview of the Experiment 49

4.3.3 Spectroscopic Results 51

4.3.4 Definition and Evaluation of Semi-quantitative Parameters 51

4.4 Transmission Polarized IR Spectroscopy of Annealed films 68

4.5 Reflection Absorption Infrared Spectroscopy (RAIRS) 71

4.5.1 RAIRS Theory 74

4.5.2 Debe Theory on Determination of Molecular Orientation 72

4.5.3 Qualitative Evaluation of Spectroscopic Results 79

4.5.4 Quantitative Analysis: Evaluation of Debe Theory 85

4.6 Summary of IR Results 89

CHAPTER 5: CHARGE MOBILITIES AND DOPING EFFECTS IN LB THIN FILMS OF $CuPc(OC_2OBz)_8$ 94

5.1 $CuPc(OC_2OBz)_8$ as a Thin Film Transistor Semiconducting Material 94

5.2 Determination of Charge Mobilities 96

TABLE OF CONTENTS - Continued

5.3 Evaluation of $CuPc(OC_2OBz)_8$ as a Semi-Conducting Material in TFT's.....99

5.2 Electrochemical Doping of $CuPc(OC_2OBz)_8$ LB Thin Films with the ClO_4^- Anion.....103

5.2.1 Theoretical Effects of Doping an Organic Thin Film.....103

5.2.2 Quantitation of the Extent of Doping by XPS.....106

5.2.3 Hypotheses on the Interactions of ClO_4^- Anions in these Pc Thin Films.110

CHAPTER 6: CONCLUSIONS.....112

6.1 Summary of Results.....112

6.2 Future Directions.....116

REFERENCES.....118

LIST OF FIGURES

Figure 1.1, The phthalocyanine molecule.....2

Figure 1.2, Structures of (a) $CuPc(OC_2OBz)_8$ and (b) $H_2Pc(OC_2OBz)_8$.....4

Figure 1.3, $CuPc(OC_2OBz)_8$ and $H_2Pc(OC_2OBz)_8$ at the air-water interface: (a) Surface pressure versus area isotherm showing two transitions of the monolayer and bilayer formation respectively, (b) Physical deposition variables.....5

Figure 2.1, Configuration of TFT substrate from a side view showing the layers of the gate (2) and from a top view of the Si wafer (b) showing the different channel widths available for measurement.....16

Figure 3.1, Schematic of proposed surface composition upon reaction of (a) HMDS and (b) DPTMDS with a glass slide 21

Figure 3.2, Surface tension components of a sessile drop.....22

Figure 3.3, Diagram of path length difference of two x-rays off of adjacent lattice planes (a) and SAXS experimental configuration (b).....26

Figure 3.4, SAXS spectrum of a 15 bilayer thin film of $CuPc(OC_2OBz)_8$ on Si(100)..27

Figure 3.5, SAXS spectrum of a 15 bilayer thin film of $H_2Pc(OC_2OBz)_8$ on Si(100) before (a) and after (b) annealing for 2 hours at 100°C in air.....29

Figure 3.6, SAXS spectrum of a 15 bilayer thin film of $CuPc(OC_2OBz)_8$ on Si(100) after annealing for 2 hours at 100°C in air.....31

Figure 3.7, Force distance curves for a partially hydrophilic tip (a) and a fully hydrophilic tip(b).....35

Figure 3.8, Tapping AFM images of a one bilayer LB thin film of $CuPc(OC_2OBz)_8$ showing long range ordering.....36

Figure 3.9, Tapping AFM images of a one bilayer LB thin film of $CuPc(OC_2OBz)_8$ showing short range ordering over 50 nm^2 with divergence of columns (a), and highly organized parallel columns (b).....38

Figure 3.10, Tapping AFM images of one bilayer LB thin films of $H_2Pc(OC_2OBz)_8$ showing columnar order over 50 nm^2, scanning perpendicular (a) and off-

LIST OF FIGURES - Continued

angle (b).....39

Figure 3.11, View of an edge of a $H_2Pc(OC_2OBz)_8$ monolayer within the center of an LB thin film sample.....40

Figure 4.1, Geometric relation between the electric field vectors associated with RAIRS (E_{RAIRS}) and transmission (E_{TE} and E_{TM}) experiments.....43

Figure 4.2, IR transmission spectrum of KBr pressed pellet of $CuPc(OC_2OBz)_8$.....44

Figure 4.3, IR transmission spectrum of KBr pressed pellet of $H_2Pc(OC_2OBz)_8$.....47

Figure 4.4, IR linear dichroism spectra of 7 bilayer films of $CuPc(OC_2OBz)_8$ on Si(100) modified with HMDS deposited at (a) 1.0°C and (b) 30.0°C.....52

Figure 4.5, IR linear dichroism spectra of 7 bilayer films of $CuPc(OC_2OBz)_8$ on Si(100) modified with DPTMDS deposited at (a) 0.3°C and (b) 30.0°C...53

Figure 4.6, IR linear dichroism spectra of 7 bilayer films of $H_2Pc(OC_2OBz)_8$ on Si(100) modified with HMDS deposited at (a) 1.0°C and (b) 34.7°C.....54

Figure 4.7, IR linear dichroism spectra of 7 bilayer films of $H_2Pc(OC_2OBz)_8$ on Si(100) modified with DPTMDS deposited at (a) 1.0°C and (b) 30.0°C.....55

Figure 4.8, Definition of deviation angle, ψ, from the dipping direction based on dipole moments in the plane and out of the plane of the Pc molecule.....61

Figure 4.9, Definition of ψ for $CuPc(OC_2OBz)_8$ and $H_2Pc(OC_2OBz)_8$ Pc systems.....63

Figure 4.10, Plot of tilt angle, ψ, versus the dichroic ratio, R, showing large changes in tilt angle per unit change at low dichroic ratios and small changes in tilt angle per unit change at high dichroic ratios. Shaded region encompasses dichroic ratio range used to determine ψ in these experiments.....65

Figure 4.11, The difference in tilt angle, ψ, as indicated by the side chain and Pc macrocycle vibrations of $CuPc(OC_2OBz)_8$ (a). The difference in tilt angles may be quantitatively determined by WAXS reflections from the correspondin differences in lattice spacings (b).....67

Figure 4.12, IR linear dichroism spectra of 7 bilayer films of $CuPc(OC_2OBz)_8$ (a) before

LIST OF FIGURES - Continued

annealing and (b) after annealing for 2 hours at 100°C in air.....69

Figure 4.13, Configuration of RAIRS experiment at grazing incidence. The p-polarized IR standing wave has perpendicular and parallel components with respect to the surface, whereas the s-polarized light has both components parallel to the surface.....72

Figure 4.14, The molecular plane , defined by the orthogonal vibration pair, is perpendicular to the Pc macrocyle plane.....75

Figure 4.15, Definition of Euler anges, ψ_{Debe} and θ, with respect to the molecular plane defined by IR active vibrations in and out of the plane of the phthalocyanine molecule.....76

Figure 4.16, RAIRS spectra of 1 bilayer films of $CuPc(OC_2OBz)_8$ deposited on Au (a) un-modified, (b) modified with 1-octanethiol, and (c) modified with benzyloxyethanethiol.....80

Figure 4.17, RAIRS spectra of 1 bilayer films of $H_2Pc(OC_2OBz)_8$ deposited on Au (a) un-modified, (b) modified with 1-octanethiol, and (c) modified with benzyloxyethanethiol.....81

Figure 4.18, RAIRS spectra of 3 bilayer films of $CuPc(OC_2OBz)_8$ deposited on Au (a) un-modified, (b) modified with 1-octanethiol, and (c) modified with benzyloxyethanethiol.....83

Figure 4.19, RAIRS spectra of 3 bilayer films of $H_2Pc(OC_2OBz)_8$ deposited on Au (a) un-modified, (b) modified with 1-octanethiol, and (c) modified with benzyloxyethane thiol.....84

Figure 4.20, Molecular plane with respect to the surface coordinates x, y, z and with respect to orientation coordinates x′, y′, z′, in (a) a three dimensional perspective, (b) along the z axis, and (c) along the x axis.....86

Figure 4.21, Pc macrocycle plane with respect to the surface coordinates x, y, z and with respect to orientation coordinates x′, y′, z′, in (a) a three dimensional perspective, (b) along the z axis, and (c) along the x axis.....86

Figure 4.22, Top view of columnar assemblies viewed along y axis (a) before any rotations, (b) after rotation through ψ, and (c) after rotation through θ.....91

LIST OF FIGURES - Continued

Figure 5.1, Directional transfer of LB films of $CuPc(OC_2OBz)_8$ (a) perpendicular ($\perp$), and (b) parallel ($\parallel$) with respect to the channel walls.....97

Figure 5.2, Typical current-voltage curves for a field-effect transistor with a p-type semiconducting layer at varying gate voltages (V_g).....98

Figure 5.3, Current-voltage curves for 3 bilayer films of $CuPc(OC_2OBz)_8$ deposited (a) parallel with and (b) perpendicular to the channel walls of the TFT substrate.....100

Figure 5.4, Current-voltage curves for 6 bilayer films of $CuPc(OC_2OBz)_8$ deposited (a) parallel with and (b) perpendicular to the channel walls of the TFT substrate.....101

Figure 5.5, Cyclic voltammetry of un-annealed and annealed 15 bilayer films of $CuPc(OC_2OBz)_8$ on ITO in the presence of 0.1 M $LiClO_4$ as the supporting electrolyte.....104

Figure 5.6, Photoelectron Spectra of C 1s (a) and (b), N 1s (c) and (d), Cl 2p (e) and (f) and Cu 2p (g) and (h) peaks of doped and undoped films respectively....108

Figure 6.1, Possible packing arrangements of elliptical $CuPc(OC_2OBz)_8$ and $H_2Pc(OC_2OBz)_8$ molecules: (a) rombehedral packing of columnar layer on top of columnar layer, (b) overlap of elliptical projections in hexagonal close packing, (c) deformation of Pc substituents, creating a possible hexagonal close packing, while maintaining the elliptical projection of the Pc macrocyle core.....115

LIST OF TABLES

Table 3.1, Contact angles measured on un-modified and modified glass, Si(100), and ITO surfaces.....23

Table 4.1, Assignment of IR bands of $CuPc(OC_2OBz)_8$ in KBr pressed pellet.....45

Table 4.2, Assignment of IR bands of $H_2Pc(OC_2OBz)_8$ in KBr pressed pellet.....48

Table 4.3, Absorbance intensities for 7 bilayer film of $CuPc(OC_2OBz)_8$ on Si(100) modified with HMDS at 1.0°C upon transfer.....56

Table 4.4, Absorbance intensities for 7 bilayer film of $CuPc(OC_2OBz)_8$ on Si(100) modified with HMDS at 30.0°C upon transfer.....56

Table 4.5, Absorbance intensities for 7 bilayer film of $CuPc(OC_2OBz)_8$ on Si(100) modified with DPTMDS at 0.3°C upon transfer.....57

Table 4.6, Absorbance intensities for 7 bilayer film of $CuPc(OC_2OBz)_8$ on Si(100) modified with DPTMDS at 30.0°C upon transfer.....57

Table 4.7, Absorbance intensities for 7 bilayer film of $H_2Pc(OC_2OBz)_8$ on Si(100) modified with HMDS at 1.0°C upon transfer.....58

Table 4.8, Absorbance intensities for 7 bilayer film of $H_2Pc(OC_2OBz)_8$ on Si(100) modified with HMDS at 34.7°C upon transfer.....58

Table 4.9, Absorbance intensities for 7 bilayer film of $H_2Pc(OC_2OBz)_8$ on Si(100) modified with DPTMDS at 1.0°C upon transfer.....59

Table 4.10, Absorbance intensities for 7 bilayer film of $H_2Pc(OC_2OBz)_8$ on Si(100) modified with DPTMDS at 34.7°C upon transfer.....59

Table 4.11, Tilt angles, ψ, for varying subphase temperatures and substrate modifications.....64

Table 4.12, Order parameter, S_2, values for varying subphase temperatures and substrate modifications.....66

Table 4.13, Absorbance intensities for un-annealed 7 bilayer films of $CuPc(OC_2OBz)_8$ on Si(100) modified with HMDS at 23.4°C upon transfer.....70

LIST OF TABLES - Continued

Table 4.14, Absorbance intensities for annealed 7 bilayer films of $CuPc(OC_2OBz)_8$ on Si(100) modified with HMDS at 23.4°C upon transfer.....70

Table 4.15, Absorbances of $CuPc(OC_2OBz)_8$ orthogonal mode pairs used to define the molecular plane.....87

Table 4.16, Absorbances of $H_2Pc(OC_2OBz)_8$ orthogonal mode pairs used to define the molecular plane.....87

Table 5.1, Threshold voltage and field-effect mobilites for LB films of $CuPc(OC_2OBz)_8$ 102

Table 5.2, XPS data from undoped films of $CuPc(OC_2OBz)_8$.....109

Table 5.3, XPS data from ClO_4^- doped films of $CuPc(OC_2OBz)_8$.....109

ABSTRACT

The variables which control the degree of molecular ordering of $CuPc(OC_2OBz)_8$ and $H_2Pc(OC_2OBz)_8$ within Langmuir-Blodgett (LB) thin films were identified and optimized. Stabilizing the Langmuir film, lowering the subphase temperature, transferring to phenyl terminated substrates, and annealing lead to enhanced ordering.

Infrared data confirms increased anisotropy (dichroic ratio, R~4.6) and order (order parameter, S_2~0.65) within these films, and predicts a tilted elliptical orientation of the molecules. Small angle X-ray scattering data and atomic force microscopy images correlate, giving a column-to-column spacing of ca. 27Å and ca. 29Å, respectively.

Ordered LB thin films have charge transport mobilities of ca. $1x10^{-4}$ $cm^2V^{-1}s^{-1}$ that may increase with ClO_4^- anion insertion.

The degree of achieved ordering leads to further investigations into the applicability of LB thin films of $CuPc(OC_2OBz)_8$ and $H_2Pc(OC_2OBz)_8$ in molecular electronic devices.

CHAPTER 1: INTRODUCTION

1.1 The Phthalocyanines

The phthalocyanine molecule, shown in Figure 1.1, is a conjugated discotic molecule that is stable in its metal free version, but can also bind a number of different metals in its core. The periphery of the molecule is available for functionalization at all, or only a few of the available sites. Functionalization has made the phthalocyanine molecule more processable and offers ways to alter the optical, electrical, and physical properties compared with the properties of the base molecule.

1.1.1 Origins

The discovery of an iron phthalocyanine molecule happened by serendipity. A blue impurity was found and isolated in the manufacturing of phthalimide from phthalic anhydride.[1] The blue impurity was identified as an iron phthalocyanine molecule. It had formed spontaneously in the reaction mixture when a portion of the ceramic coating chipped off of the cast iron vat releasing iron into solution. Because of their stability, light fastness, economic value and intense blue and green hues, phthlocyanines have been used profusely as dyes and pigments in consumer products such as paint, plastics, inks, and textiles.[2]

1.1.2 Focus of Recent Research

Recent research using phthalocyanines (Pcs) is driven by the potential applications of these molecules. High absorption coefficients enable Pcs to act as

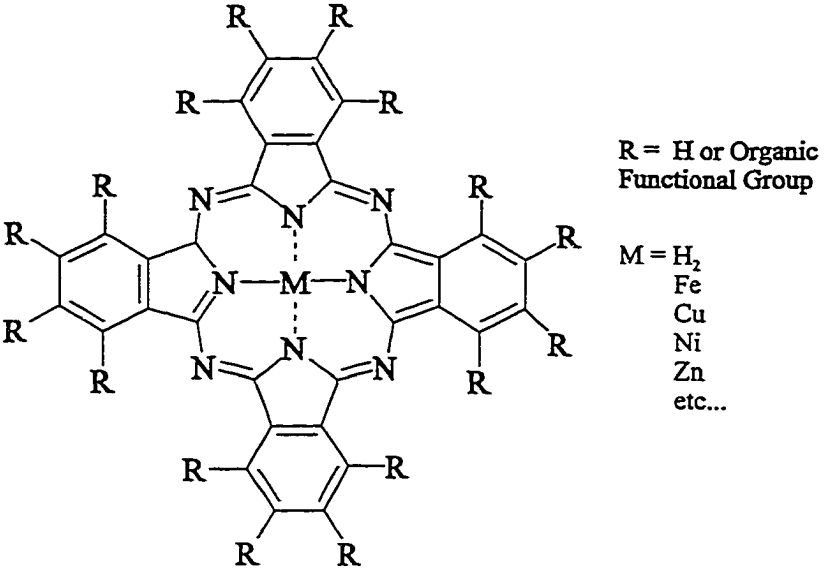

Figure 1.1, The phthalocyanine molecule.

photosensitisers in the area of photodynamic cancer therapy;[3] electrochromic properties of certain Pcs have been probed for new type displays;[4] photochromic properties have been probed for use in optical data storage. Successful gas sensors have been constructed of Pc thin films for the detection of toxic gases such as 2,4-toluene diisocyanate.[5] Well ordered semiconducting pthalocyanines offer the promise of flexible circuitry.[6] The viability of these applications is based on the ability to manipulate Pc macroscopic properties, such as morphology, molecular ordering, and crystallinity.

Peripheral substitution is one way of inducing self assembly characteristics. Deposition of phthalocyanines by the Langmuir-Blodgett technique was first shown to be possible when a Pc with tetra-t-butyl peripheral substitution was used.[7] Cook et al. have reported anisotropic films of amphiphilic phthalocyanines deposited by the LB technique,[8] and cofacial, siloxane-polymerized phthalocyaninatopolysiloxane (PcPS) molecules with peripheral substitution are known as "hairy rod" polymers and are able to be transferred via LB techniques onto rigid substrates.[9]

1.2 Previously Characterized Properties of $CuPc(OC_2OBz)_8$ and $H_2Pc(OC_2OBz)_8$

$CuPc(OC_2OBz)_8$ and $H_2Pc(OC_2OBz)_8$ (Figure 1.2) have been thoroughly characterized spectroscopically and electrochemically in solution, cast films, and LB films.[10,11,12] References to this work will be made periodically throughout this thesis. The most interesting aspect of these molecules is the overall ordering and rigidity of the films at the air-water interface and in LB thin films.[10]

The pressure vs. area isotherm shows two distinct phase transitions (Figure 1.3.a)

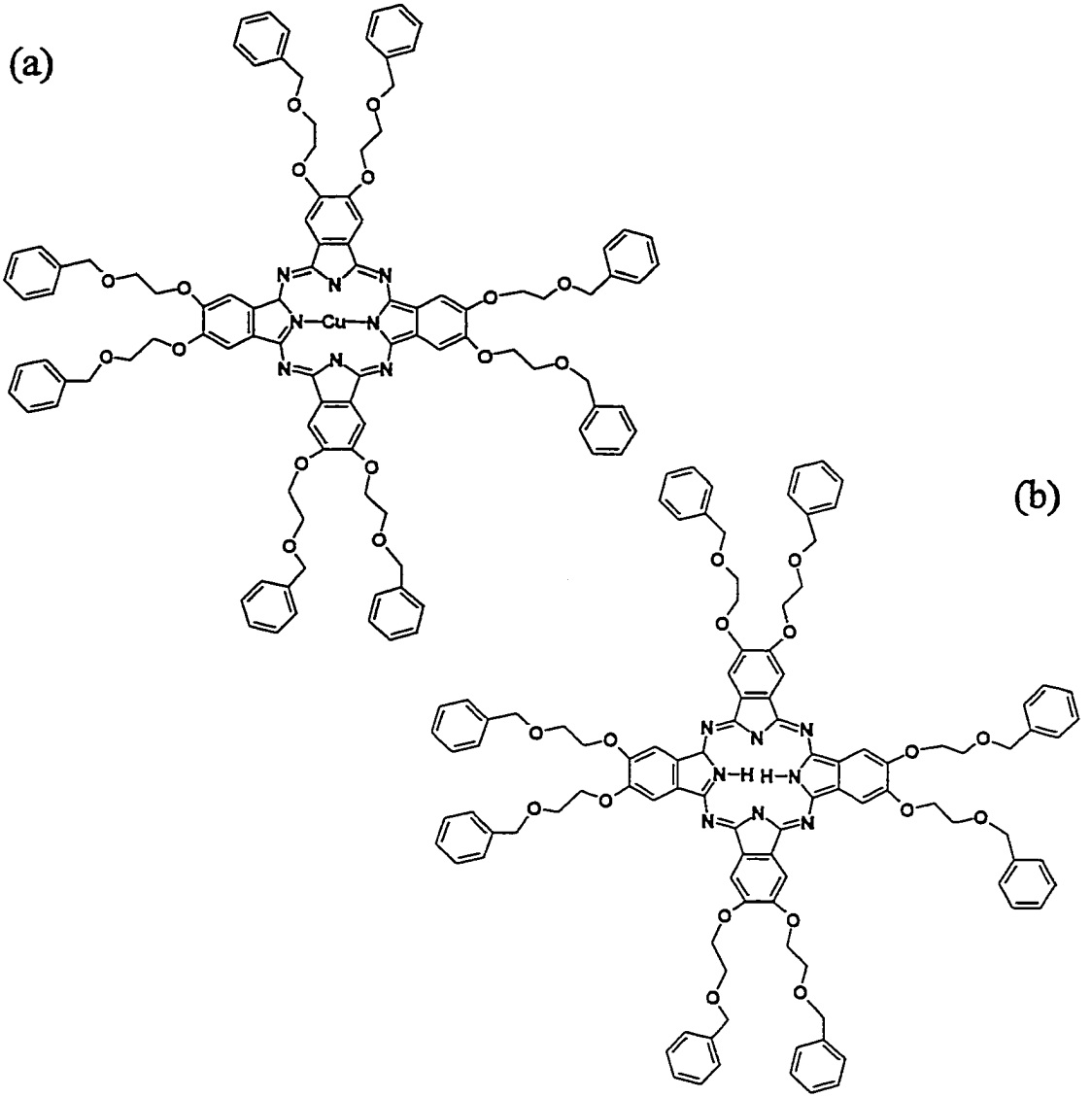

Figure 1.2, Structures of (a) $CuPc(OC_2OBz)_8$ and (b) $H_2Pc(OC_2OBz)_8$.

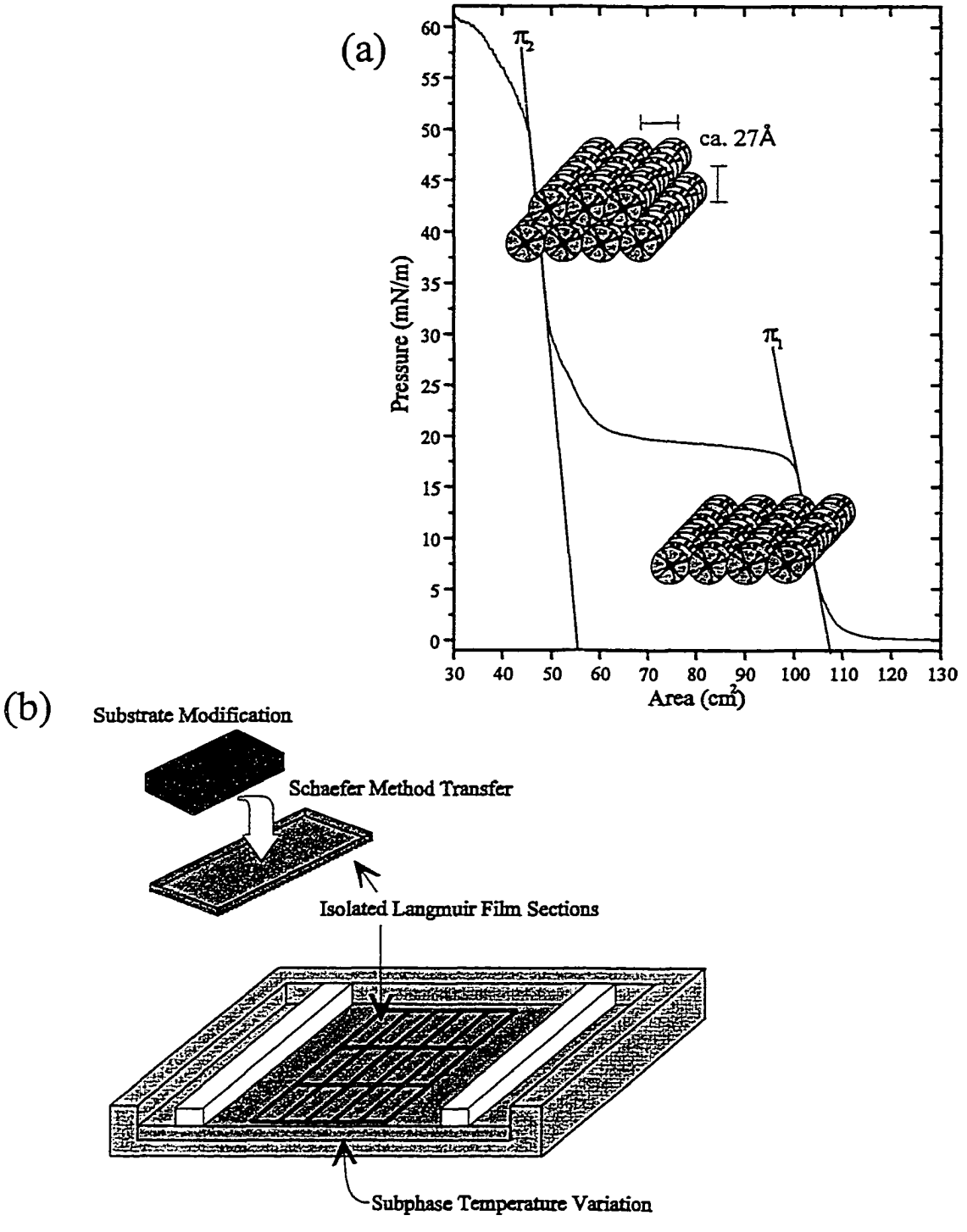

Figure 1.3, $CuPc(OC_2OBz)_8$ and $H_2Pc(OC_2OBz)_8$ at the air-water interface: (a) Surface pressure versus area isotherm showing two transitions of the monolayer and bilayer formation respectively, (b) Physical deposition variables.

seen also for the PcPS system, and an stereoisomerically pure form of a substituted Pc developed by Nolte et al.[13] From area/molecule calculations, the first transition corresponds with the formation of a monolayer of the material, and the second transition corresponds with the formation of a bilayer structure.[12] Upon further compression a folding up of the bilayer structure occurs, creating fiber like structures on the surface of the water. The bilayer structure has proven to be more rigid and more ordered than the monolayer structure.[12,14,15] These mono- and bi- layer structures were found to be composed of a series of columnar assemblies of cofacially stacked $CuPc(OC_2OBz)_8$ and $H_2Pc(OC_2OBz)_8$ molecules.[12,14,15]

UV-visible and IR spectroscopy have indicated a great deal of anisotropy in LB thin films. Calculated molecular tilt angles were reported as ranging from 50° to 60°.[10] Early WAXS data, taken of $CuPc(OC_2OBz)_8$ fibers indicated a Pc cofacial separation of 3.36 Å, with a correlation length of 81 Å, or 24 molecules, and a center to center column distance of 27.8 ± 0.3 Å.[10] STM images taken of 1 monolayer and 1 bilayer films of $CuPc(OC_2OBz)_8$ LB thin films, reconfirmed the center to center column distance, but also revealed the existence of ordered domains within a thin film.[15]

Transfer of the bilayers to substrates was first done with the traditional vertical dipping technique.[10,11] It was found that better transfer, and the preservation of ordering found in the Langmuir layer remained by using the Schaefer method[16] (horizontal dipping).[12,14,15] The transfer of films was once more improved by the introduction of a metal baffle that was placed in the subphase before the Langmuir film was formed.[14,15]

The water level in the LB trough was then reduced, lowering the Langmuir film onto the baffle, which sectionalized the films into 15 separate films. These films were isolated so that the transfer of a film in one area would not effect the structure of the films in another area.

Previous characterization of macroscopic and microscopic ordering of these films were done on films that do not approach the preservation of ordering that can be achieved presently. The improvements in transfer techniques lead to the most recent agenda of finding the conditions that produce the most ordered films, and characterizing the resulting order.

1.3 Overview of the Experiments

The focus of this thesis is to explain the steps that were taken and the success that was made in improving the ordering within these thin films. Ideal deposition conditions were identified using the Schaefer method of transfer, using a baffle to sectionalize the Langmuir film, varying subphase water temperatures, and varying substrate surface modifications (Figure 1.3.b). The success of annealing was evaluated as a way to reorganize the molecules into a more tightly packed arrangement within the thin films.

Macroscopic ordering was probed by small angle x-ray scattering (SAXS) and atomic force microscopy (AFM). Microscopic ordering was probed with infrared spectroscopy. Two IR experiments were completed to determine the Pc molecular orientation within the thin films. Transmission IR spectroscopy, using polarized radiation, probed vibrational transitions in the plane of the thin film; reflection absorption

IR spectroscopy (RAIRS) probed vibrational transitions perpendicular to the plane of the thin films.

Preliminary investigations as to the applicability of LB thin films of $CuPc(OC_2OBz)_8$ in electronic applications were done. Charge transfer mobilities were measured for these films in a thin film transistor (TFT) configuration, and the possibility of doping thin films with perchlorate anions was determined by a semiquatitative analysis using x-ray photoelectron spectroscopy (XPS).

1.4 Summary of Results

Improvement in ordering in LB films of $CuPc(OC_2OBz)_8$ and $H_2Pc(OC_2OBz)_8$ was accomplished when the Langmuir film was formed and transfer occurred at lower temperatures. Better transfer occurred with substrate surface modifications that provided a phenyl functionality on the surface, such as 1,3-Diphenyl-1,1,3,3-tetramethyldisilazane (DPTMDS). Single bilayer transfers onto Au surfaces retained molecular ordering almost exclusively when transferred to a surface modified with benzyloxyethanethiol.

SAXS results showed center to center column distances of ca. 27 Å. This was confirmed by AFM images that showed an average distance of ca. 29 Å. SAXS data also confirmed 27 Å as the thickness of the molecular layers within the thin films as well.

Transmission IR linear dichroism experiments identified two quantitative parameters that defined the order within a particular film. Order parameters for these films approached 0.47 in un-annealed films and 0.65 in annealed films (with 1 being maximum ordering). Average deviation angles of the columnar assemblies ranged from

ca. 25° to 40°.

Molecular orientations calculations based on the RAIRS data determined that the molecules are tilted ca. 30 ° away from the substrate surface normal, and are rotated ca. 15 ° around the Pc column long axis resulting in an elliptical orientation of the Pc molecules within a columnar assembly.

Annealed films of $CuPc(OC_2OBz)_8$ were found to have overall increase order seen in IR dichroic ratios, and the appearance of Kiessig fringes in the SAXS data.

Preliminary mobility and doping measurements suggest that the $CuPc(OC_2OBz)_8$ molecule would be suitable for some electronic applications. The highest mobilities observed were ca. 1×10^{-4} $cm^2V^{-1}s^{-1}$, leaving room for improvement. Further investigations into the effects of annealing and doping will likely improve field-effect mobilities.

CHAPTER 2: EXPERIMENTAL

2.1 Studied Molecules

All molecules used were synthesized previously by Smolenyak.[12] (2,3,9,10,16,17,23,24-Octakis((2-benzyloxy)ethoxy)phthalocayninato) copper and (2,3,9,10,16,17,23,24-Octakis((2-benzyloxy)ethoxy)phthalocayninato) dihydrogen were synthesized as reported by Smolenyak[12] and Osburn.[11] Solutions of $CuPc(OC_2OBz)_8$ and $H_2Pc(OC_2OBz)_8$ were prepared using HPLC grade chloroform (Aldrich).

2.2 Langmuir-Blodgett Materials and Techniques

Langmuir-Blodgett films were prepared on a Riegler & Kerstein RK3 LB trough. The trough was equipped with a Whilhemy balance (WS1) mounted midway between the compression barriers. The water subphase was purified using a Millipore Milli-Q system. The temperature of the water subphase was controlled with a Coolflow CFT-33 Refrigerated Recirculator (Neslab Instruments Inc.), down to ca. 0° C. Temperature control at higher temperatures (ca. 30° C) was obtained by pre-heating the water sub-phase prior to filling the trough, and by using heating tapes under the trough to maintain temperature.

All films were prepared by expanding the barriers completely, zeroing the balance, applying the material, letting solvent evaporate for 15 min, and compressing at 29.6 cm^2/s to a set pressure. Langmuir films were lowered onto a baffle already beneath the air-water interface, partioning the film into fifteen separate rectangular isolated

regions, as developed by Smolenyak.[14] Transfers were made using the horizontal or Schaefer transfer method.[16] A motor mounted above the trough drove the substrate into the film at ca. 0.15 cm^2/s, paused at the interface for 10 seconds, and lifted the film up at ca. 0.01 cm^2/s (The implications of the speed at which the films are transferred has yet to be investigated). Each bilayer transfer was done in a separate section of the baffle. Any remaining water left on the LB film after transfer was removed with dry nitrogen gas.

2.3 Substrate Surface Preparation and Modification

Si(100) wafers (MEMC Electronic Materials, Inc.) and indium tin oxide (ITO) coated glass (Balzer's) substrates were sonicated for 15 min in subsequent washes of a dilute solution of Alconox in Millipore Milli-Q water, Millipore Milli-Q water, and Ethanol. They were then dried in air at ca. 100° C for 15 min. The substrates were activated by two different procedures to ensure a fully hydroxylated surface before hydrophobization. They were hung over a volume of concentrated HCl until a layer of vapor appeared on the surface or were heated to 40° C in a 10% solution of HNO_3 for 15 min. The substrates were then washed with water leaving a fully hydroxylated surface.

The substrates were then hydrophobized by heating (ca. 40° C) and sonicating for 15 min in a 20% solution of 1,1,1,3,3,3-hexamethyldisilazane, 99.9% (Aldrich) in HPLC grade chloroform (Aldrich) or a 20% solution of 1,3-diphenyl-1,1,3,3-tetramethyldisilazane, 96% (Aldrich) in HPLC grade chloroform. The substrates were stored in these solutions after heating. At time of use, the substrate was rinsed with chloroform, removing any unreacted silazane, and dried in a stream of nitrogen.

Au substrates consisting of a ca. 1000 Å Au layer on a titanium treated float glass were obtained from Evaporated Metal Films (Ithaca, NY), donated by Dr. J. E. Pemberton. The Au slides were cleaned by immersing in a 1:4 solution of H_2O_2:H_2SO_4 for 10 seconds and then rinsing with water. Unmodified slides were stored in water. Other slides were modified by immersing in a 0.10 mM solution of a reactive thiol.[17] 1-Octanethiol, 98.5+% was purchased from Aldrich; benzyloxyethoxythiol was synthesized previously in our lab.[14] The modified substrates were washed with ethanol to remove unreacted thiols, dried in a stream of nitrogen and stored in a sealed container.

2.4 Contact Angle Measurements

Evaluation of the substrate hydrophobicity was made by measuring the contact angles using the sessile drop method.[18] The substrate was placed onto a small platform in front of a Pulnix TM-7CN video camera. A 10 μL syringe was used to place a drop of Millipore Milli-Q water onto the substrate. The drop was back lit using a Fiber-Lite® model 190 fiber optic illuminator (Dolan-Jenner Industries, Inc.) and diffused by a piece of filter paper. An image of the drop at the surface was taken using a Video Snapshot Snappy and was converted into a tagged image file using Snappy Software 1.0 (Play Incorporated). The angle of interest was measured using Image-Pro Plus 1.3 software (Media Cybernetics).

2.5 Small Angle X-ray Scattering Measurements

Small angle x-ray scattering (SAXS) measurements of 15 bilayer annealed and unannealed samples of $CuPc(OC_2OBz)_8$ and $H_2Pc(OC_2OBz)_8$ on Si(100) were obtained in

collaboration with Dr. Simon Bates at Kratos Analytical. A XRD-6000 instrument, with Bragg-Brentano optics (Kratos) was used in the analysis.

2.6 Atomic Force Microscopy

A Nanoscope IIIa scanning probe microscope (Digital Instruments) was used to image bilayer films of $CuPc(OC_2OBz)_8$ and $H_2Pc(OC_2OBz)_8$ on Si(100). Special care was taken to prepare the Si(100) surface for these studies. A procedure similar to Watanabe's method was used to remove any oxide surface.[19] The substrates were boiled in 1:1:4 solution of $HCl:H_2O_2:H_2O$ for 10 min and then immersed in 1% HF solution for 2 min, then boiled in water for 10 min. Substrates were stored in water to avoid contamination and contact with dust until used.

Silicon nitride contact tips (Digital Instruments) were used in tapping mode in the fluid cell. It became apparent that the condition of the tips had dramatic effects on the quality of images obtainable, especially for the $H_2Pc(OC_2OBz)_8$ films. Any carbon present on the tip surface was removed by oxidization to carbon dioxide by ozone cleaning under a UV ozone lamp for up to 8 hours before imaging, making the tip completely hydrophilic. This cleaning process was used periodically throughout an analysis day.

The hydrophilicity was determined by measuring the force curve of each tip. Any attraction of the tip to the surface, resulting in a deflection in the force curve, indicated that there was still some degree of hydrophobicity on the tip. Even a small degree of hydrophobicity negatively influenced the ability to obtain good images of the

$H_2Pc(OC_2OBz)_8$ films as will be discussed further in Section 3.4.1.

2.7 Infrared Spectroscopy

All FT-IR spectra were obtained on a dry air purged Nicolet 550 series spectrometer equipped with a tungsten source and a MCT detector. A Au wire grid polarizer (Cambridge Physical Sciences) was used in the thin film transmission and RAIRS experiments.

2.7.1 Transmission Experiments

A bulk transmission spectrum of $CuPc(OC_2OBz)_8$ was obtained by mixing ca. 1mL of 0.45 mM $CuPc(OC_2OBz)_8$ in chloroform with ca. 1 g of KBr (standard infrared grade, Aldrich). The chloroform was allowed to evaporate during the mixing time and a pellet was pressed.

2.7.2 LB Mulitlayer Thin Films

A film thickness of 7 bilayers were used for transmission FT-IR of the Langmuir-Blodgett films. Two spectra were obtained for each sample: 0° and 90° polarization with substrate normal to incident. Blank spectra of the bare Si(100) substrates at the sample polarization and angles were taken for each sample prior to deposition. These blank spectra served as a background correction, accounting for differences in absorption due to reflection and difference in path length. This was done to minimize the effects of the substrate due to polarization and incident beam angle.

2.7.3 Reflection Absorption Infrared Spectroscopy

RAIRS spectra were obtained with a FT-80 Fixed 80° Grazing Angle Accessory

(Spectra-Tech). One and three bilayer films were applied to each of three Au surfaces with no modification, or with modification by a self assembled monolayer of 1-octanethiol or benzyloxyethoxythiol. A blank spectrum was taken from a bare Au surface.

2.8 X-ray Photoelectron Spectroscopy

XPS was used to quantitate the amount of doping of the ClO_4^- anion into the $CuPc(OC_2OBz)_8$ versus the oxidative potential applied. XPS data were collected at the Laboratory for Electron Spectroscopy and Surface Analysis (LESSA, University of Arizona), using a VG ESCALAB MK II spectrometer. More recent data was acquired using a Kratos Axis-Ultra spectrometer, with monochromatic Al(Kα) radiation and multichannel detection .

2.9 Thin Film Field-Effect Transistor Mobility Measurements

The compatibility of $CuPc(OC_2OBz)_8$ for use as the semiconducting layer in an OFET was evaluated by determining the charge mobilities within the films in the OFET configuration. Compatibility measurements were made by Dr. Zhenan Bao at Lucent Technologies, Bell Laboratories.

Langmuir-Blodgett bilayers of $CuPc(OC_2OBz)_8$ were deposited on a pre-fabricated thin film transistor made and provided by Bell Labs. The thin film transistor (TFT) substrate, diagramed in Figure 2.1.a, consists of several layers of materials. The gate of the TFT is constructed of a n-doped silicon wafer base, a 3000 Å layer of SiO_2 dielectric layer, and evaporated gold source and drain contacts. There are several gold

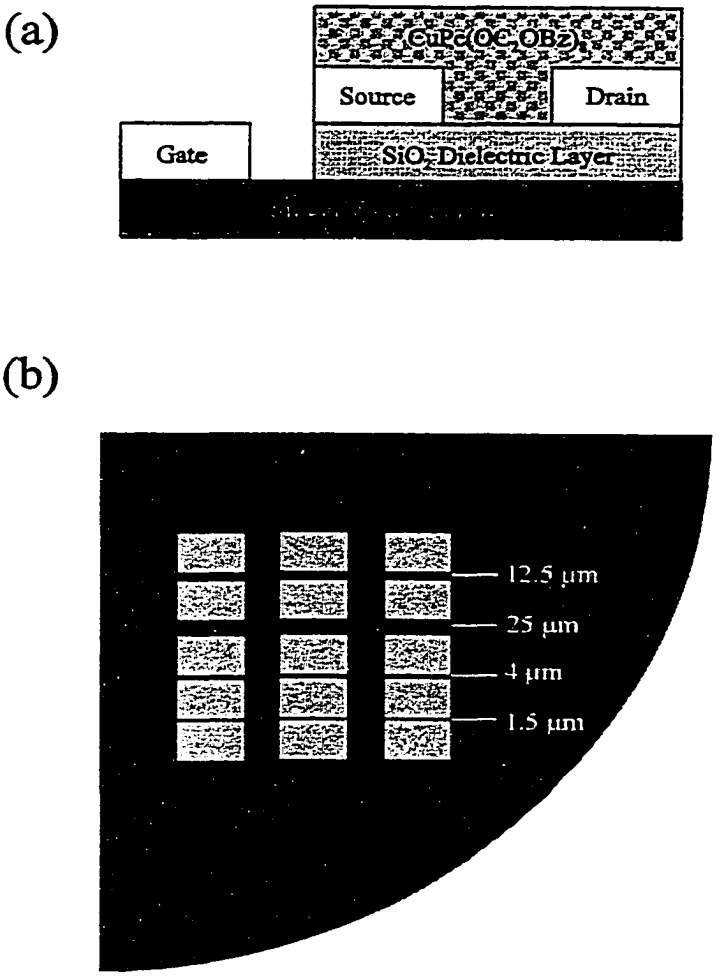

Figure 2.1, Configuration of TFT substrate from a side view showing the layers of the gate (a) and from a top view of the Si wafer (b) showing the different channel widths available for measurement.

contacts spaced at specified distances to create a variety of channel width regions (Figure 2.1.b).

The LB layer was deposited onto of the TFT substrate with the main Pc column axis parallel and perpendicular to the channel walls as a measure of expected anisotropy within the film.

CHAPTER 3: MACROSCOPIC ORDERING OF LB THIN FILMS

3.1 Overview of Experiments

Two experiments were done to determine the macroscopic ordering of the phthalocyanine columnar assemblies formed by $CuPc(OC_2OBz)_8$ and $H_2Pc(OC_2OBz)_8$ in LB thin films.[12] Small angle x-ray scattering measurements (SAXS) were made on multilayer films of $CuPc(OC_2OBz)_8$ that were un-annealed and annealed. This experiment gives quantitative lattice spacings between layers of phathacyanine assemblies, and qualitatively information about any degree of crystallinity within the film. AFM images of single bilayer films of $CuPc(OC_2OBz)_8$ and $H_2Pc(OC_2OBz)_8$ were achieved, and give an approximate intercolumnar spacing, as well as images of long range order within a single bilayer film.

The success of these two experiments were dependent on the quality of the film transferred from the LB trough. Several different substrates and surface modification procedures were investigated to insure the greatest transfer of film, while retaining the greatest order as achieved on the LB trough.

Therefore, the remaining sections of this chapter describe the substrate surface treatments, the SAXS experiment and results, and AFM images of these LB films.

3.2 Importance of Substrate Surface Treatment

While trying to characterize and accentuate the order of the thin films of $CuPc(OC_2OBz)_8$ and $H_2Pc(OC_2OBz)_8$ it is advantageous to maintain the order achieved

on the Langmuir trough during the transfer to the Langmuir-Blodgett layer. As was discussed previously, the use of a baffle to sectionalize the Langmuir film and stabilize it during horizontal transferring is one way to maintain that order. An additional means developed here is to functionalize the substrate onto which transfer will occur to avoid any repulsive interactions.

3.2.1 Choice of Substrate Materials and Surface Modifiers

Certain substrates where chosen because of their suitability to the analytical techniques that were used to characterize the thin films. ITO was chosen because it provides a thin, optically transparent electrode through which electrochemical contact to the thin films are made. Si(100) was chosen for the transmission IR studies because it does not absorb IR radiation in the window we wish to use. Si(100) wafers were also used as the substrates for the X-ray reflectance and the conductance measurements because it provides a nearly atomically flat surface. Au substrates were used in the RAIRS experiment because of their reflective surface and the ability to functionalize the surface with thiol self-assembled monolayers, which is discussed in Section 4.4.3. None of the above mentioned substrates, before modification, provide a sufficiently hydrophobic surface for a Pc bilayer to transfer and still maintain optimum ordering. Because of the benzyl terminated substituents on the Pc molecules, it is supposed that an alkylated surface would interact preferentially over a bare Si surface or an oxide layer, and that a phenylated surface would interact even more preferentially. Two silazane molecules were chosen to modify glass, ITO, and Si(100) surfaces. 1,1,1,3,3,3-

hexamethyldisilazane (HMDS) provided a methyl terminated surface and 1,3-diphenyl-1,1,3,3-tetramethyldisilazane (DPTMDS) provided a phenyl terminated surface (Figure 3.1).

3.2.3 Contact Angle Theory

The extent of hydrophobization by these silazane molecules was evaluated using contact angle measurements. The behavior of a drop of liquid on a solid surface is predictable. It may remain as a drop of finite area, or it may spread over the surface. Young first explained this behavior based upon surface tensions between the liquid-vapor, $\gamma_{L\text{-}V}$, liquid-solid, $\gamma_{L\text{-}S}$, and solid-vapor ,$\gamma_{S\text{-}V}$, interfaces.[18] The magnitude of these surface tensions create an equilibrium contact angle, θ, which is defined in Figure 3.2 and is expressed in terms of the surface tensions as:

$$\gamma_{SV} - \gamma_{SL} = \gamma_{LV} \cos\theta \qquad \text{(Eq. 3.1)}$$

When a liquid spreads freely over a surface then $\theta = 0°$, and when the liquid is non-spreading $\theta \neq 0°$. Based on early experiments, there is no liquid-solid combination that results in $\theta = 180°$.[18] The water contact angle with a close packed methyl layer on a smooth surface under ideal conditions is ca. 111°-115°.[18]

3.2.4 Measure Contact Angles of Modified Surfaces

Contact angle measurements were made on unmodified glass, Si(100), and ITO and on those modified with HMDS and DPTMDS. These angles are listed in Table 3.1. Six contact angle measurements were made on different areas of the substrate surfaces.

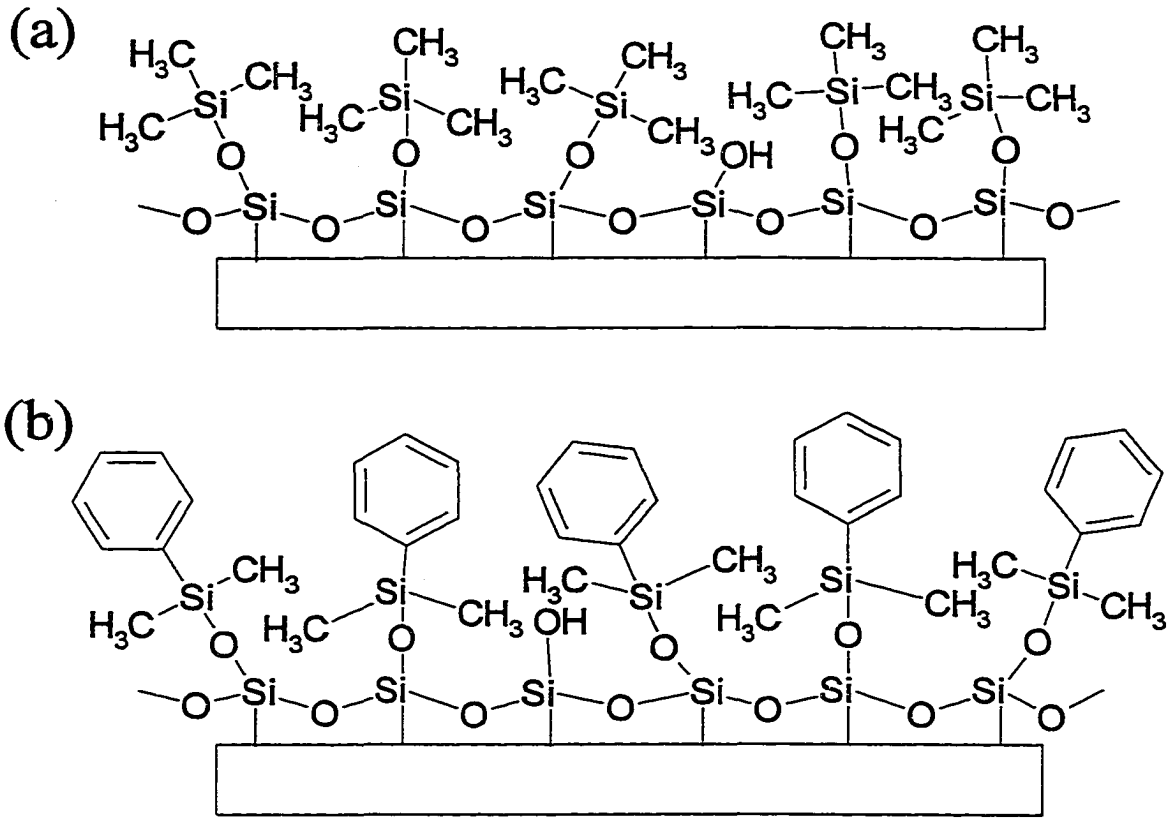

Figure 3.1, Schematic of proposed surface composition upon reaction of (a) HMDS and (b) DPTMDS with a glass slide.

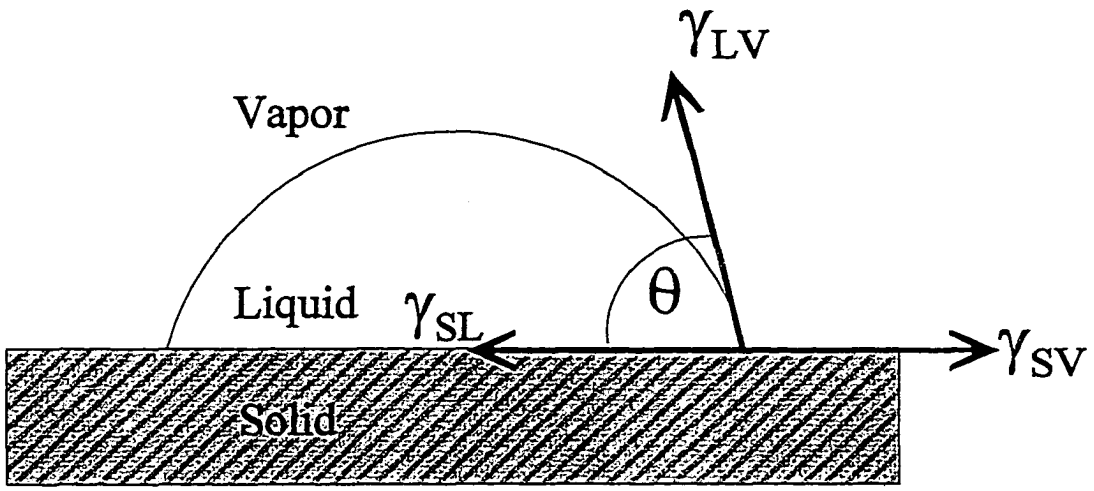

Figure 3.2, Surface tension components of a sessile drop.

Table 3.1, Contact angles measured on un-modified and modified glass, Si(100), and ITO surfaces.

Surface	Modification	Contact Angle
Glass microscope slide	None	8.29 ± 1.32
	HMDS	78.45 ± 3.73
	DPTMDS	69.22 ± 4.67
Si (100) wafer	None	47.83 ± 2.04
	HMDS	85.97 ± 3.53
	DPTMDS	83.84 ± 2.92
ITO	None	41.26 ± 7.93
	HMDS	49.20 ± 8.33
	DPTMDS	47.21 ± 5.24

This was done as a measure of the homogeneity of the surface after hydrophobization and is expressed in the units of error in Table 3.1.

3.2.5 Significance of Measured Contact Angles

The smallest contact angle observed was for the un-modified glass surface. This is expected because of free oxide and hydroxyl groups present at the surface which can hydrogen bond with the water droplet. After hydrophobization, the contact angle of the HMDS glass surface was greater by ca. 9° than that of the DPTMDS glass surface. This difference is also seen in the Si(100) and ITO samples, but not to as great of an extent. As shown in Figure 3.1.b, there may be a larger population of exposed residual hydroxyl groups, or there may be induced dipole interactions between the polar water molecules and the pi electrons of the phenyl groups which would allow the drop to spread out more over the surface, creating a smaller contact angle.

The distribution of contact angles on the glass and Si(100) surfaces is relatively small, indicated by the standard deviation values. This shows that the surfaces are being hydrophobized uniformly. The difference in the contact angles between the unmodified and modified ITO surfaces was minimal. This seems to be a result of poor reactivity of these silanes with the ITO surface, the reason for which is still not clear, and is under further investigation.

3.3 SAXS Theory

X-ray diffraction and scattering measurements are based on the interactions between X-rays and the lattice planes of a given crystal, since the wavelengths of x-ray

radiation are on the order of lattice plane spacings in crystalline solids (ie. CuKα radiation with a wavelength of 1.54 Å). If the lattice planes are regarded as partially reflective mirrors separated by a distinct distance, d, then there will be constructive interference of the incoming x-ray beam at a specific angles.

The difference in the path length is shown in Figure 3.3.a. When the difference in path length is equivalent to an integral number of wavelengths then constructive interference occurs and a large x-ray reflection intensity occurs at that angle. The Bragg law (Equation 3.1) describes the relationship between the wavelength, λ, the incoming angle, θ, and the lattice spacing distance, d:

$$n\lambda = 2d\sin\theta \qquad \text{(Eq. 3.1)}$$

Once the angle, θ, has been determined, the lattice spacing, d, can be readily deduced.

3.3.1 Bragg Diffraction Peak (Angle) Measurements

A small angle X-ray scattering experiment was used to probe un-annealed and annealed 15 bilayer thin films of $CuPc(OC_2OBz)_8$ and $H_2Pc(OC_2OBz)_8$ on Si(100). Small incident glancing angles were used as the intensities of the 2θ reflections were monitored (Figure 3.3.b).

A Bragg reflection at 3.745° in 2θ was observed for the un-annealed LB film of $CuPc(OC_2OBz)_8$ (Figure 3.4). This angle of reflection corresponds with a d spacing of 23.6 Å. A small, poorly defined reflection peak is shown in the inset of Figure 3.4. This reflection peak has also been seen in previous SAXS experiments on this same material.[14]

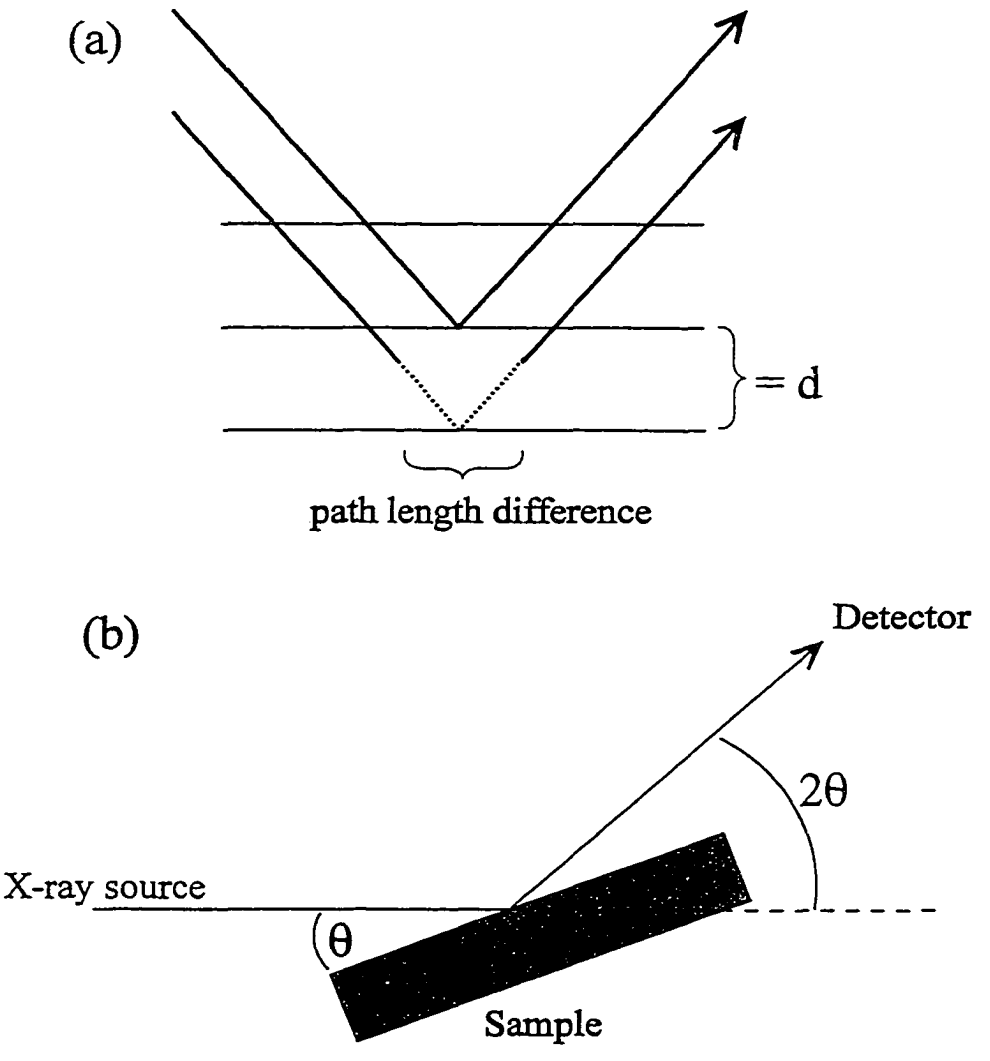

Figure 3.3, Diagram of path length difference of two x-rays off of adjacent lattice planes (a) and the SAXS experimental configuration (b).

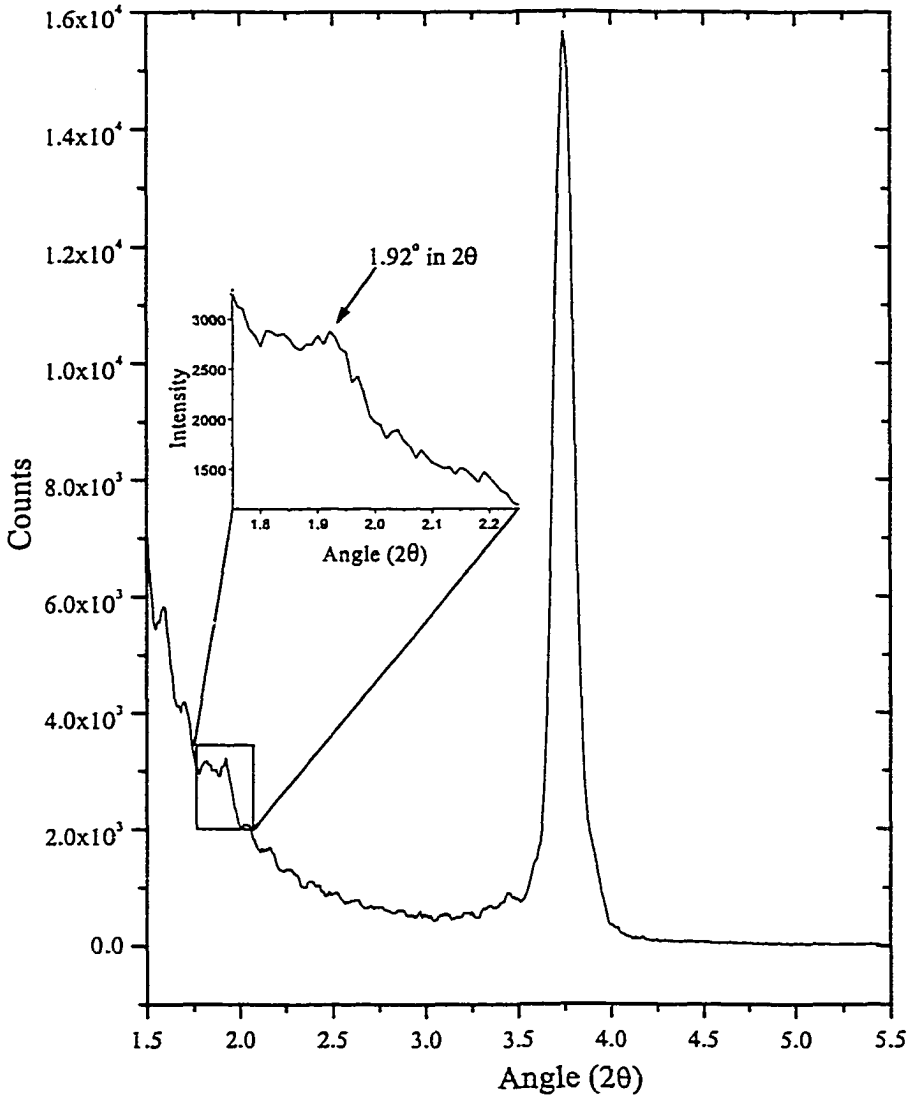

Figure 3.4, SAXS spectrum of a 15 bilayer thin film of $CuPc(OC_2OBz)_8$ on Si(100).

The angle of this reflection, 1.92° in 2θ, corresponds with a lattice spacing of 45.9 Å. This is almost twice the spacing found for the main Bragg reflection peak, and corresponds to bilayer structures within the thin film.[20] Since this reflection peak is not well resolved, we can say that although discrete bilayers were transferred to construct the thin films, the bilayers, on the whole, do not stay resolved in the multilayer structure.

The Scherrer equation, initially used as an approximate measure of crystallite size in a powder sample, can be used as an approximation of the correlation length of the vertical thickness of the thin film.[21] The Scherrer equation (Equation 3.2) relates, L, the correlation length with, Δ(2θ), the peak width at half height of a Bragg reflection peak, and K, a constant commonly assigned the value of 0.9.[21]

$$L = \frac{\lambda \cdot K}{\cos\theta \cdot \Delta(2\theta)} \qquad \text{(Eq. 3.2)}$$

The peak width at half height is 0.126° in 2θ, which determines a correlation length of 632 Å for a 15 bilayer film.

A very small Bragg reflection at 3.76° in 2θ was seen for an un-annealed 15 bilayer sample of $H_2Pc(OC_2OBz)_8$ on Si(100) (Figure 3.5.a). The quality of the reflection intensity suggests that this film is not well ordered at all, although we see no significant difference in d spacing, 23.5 Å versus 23.6 Å for the $CuPc(OC_2OBz)_8$ thin film. The correlation length for the un-annealed film, 177 Å, is much shorter than that for the un-annealed $CuPc(OC_2OBz)_8$ film and for annealed films of $CuPc(OC_2OBz)_8$ and

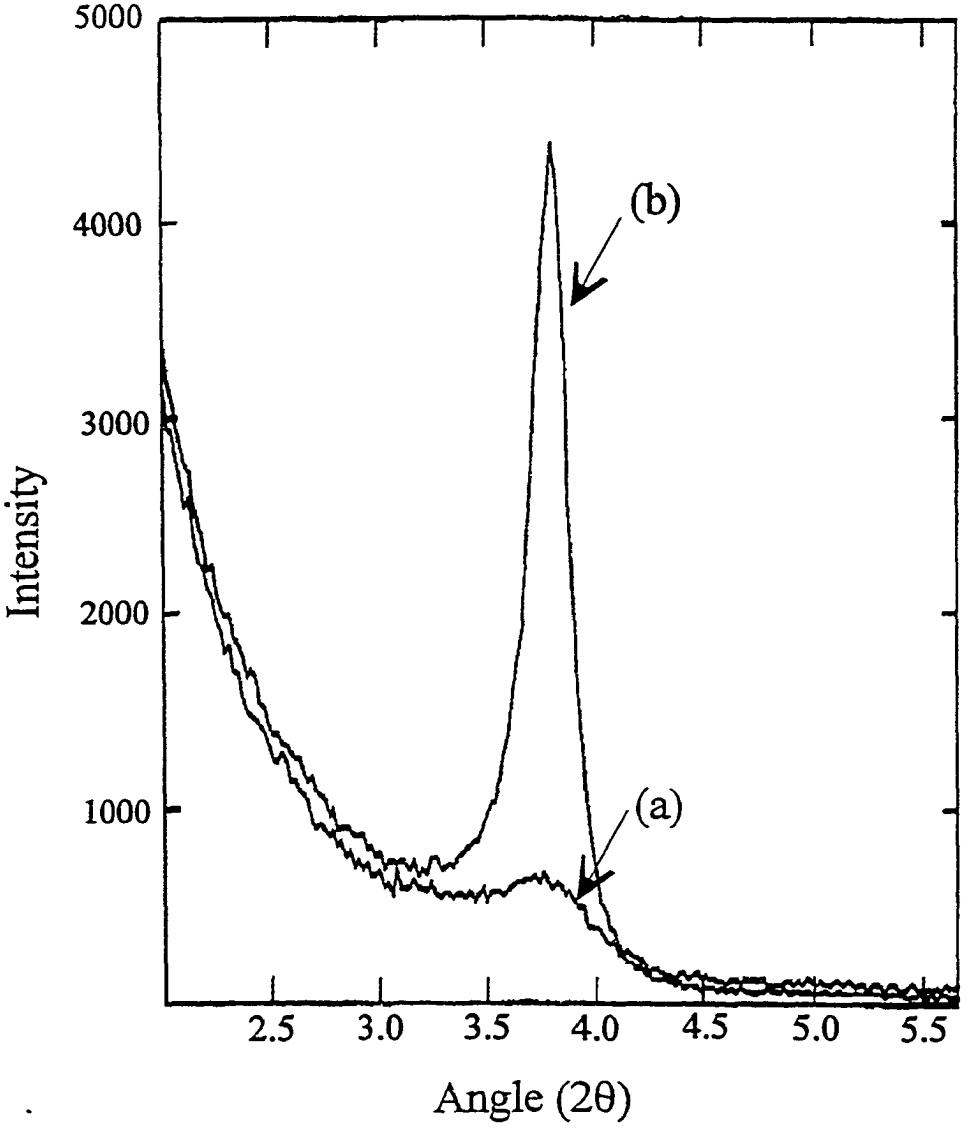

Figure 3.5, SAXS spectrum of a 15 bilayer thin film of $H_2Pc(OC_2OBz)_8$ on Si(100) before (a) and after (b) annealing for 2 hours at 100°C in air.

$H_2Pc(OC_2OBz)_8$ as discussed in the next section.

3.3.2 Effects of Annealing

The effects of annealing are great in both the $H_2Pc(OC_2OBz)_8$ and the $CuPc(OC_2OBz)_8$ thin films.

The small Bragg reflection observed in the $H_2Pc(OC_2OBz)_8$ thin films, increases in intensity markedly (Figure 3.5.b). The position of the main reflection changes minimally, 0.02° in 2θ, to 3.78 ° in 2θ. This corresponds with a d spacing of 23.4 Å. The peak width at half height was 0.223° in 2θ, determining a correlation length of 356 Å for a 15 bilayer film.

A Bragg reflection was observed for the annealed 15 bilayer of the $CuPc(OC_2OBz)_8$ thin films at 3.79° in 2θ (Figure 3.6). This corresponds with a d spacing of 23.3 Å. The coherence thickness of the film was calculated from the peak width at half height, 0.123° in 2θ, to be 647 Å.

The Bragg reflection of the annealed film is a narrower peak and it is also accompanied by what are known as Kiessig fringes which are a result of an increase in perfection of the interfaces that define the multi-layer structure. The low angle reflection seen in the un-annealed film is lost in the decay curve of the annealed sample. Upon annealing, the thin film must re-organize to a lower energy configuration that eradicates any bilayer constructs. The total thickness of the sample can be calculated by the periodicity of the Kiessig fringes (0.120° in 2θ) with respect to the Bragg law. The calculated film thickness is 735 Å for a 15 bilayer film.

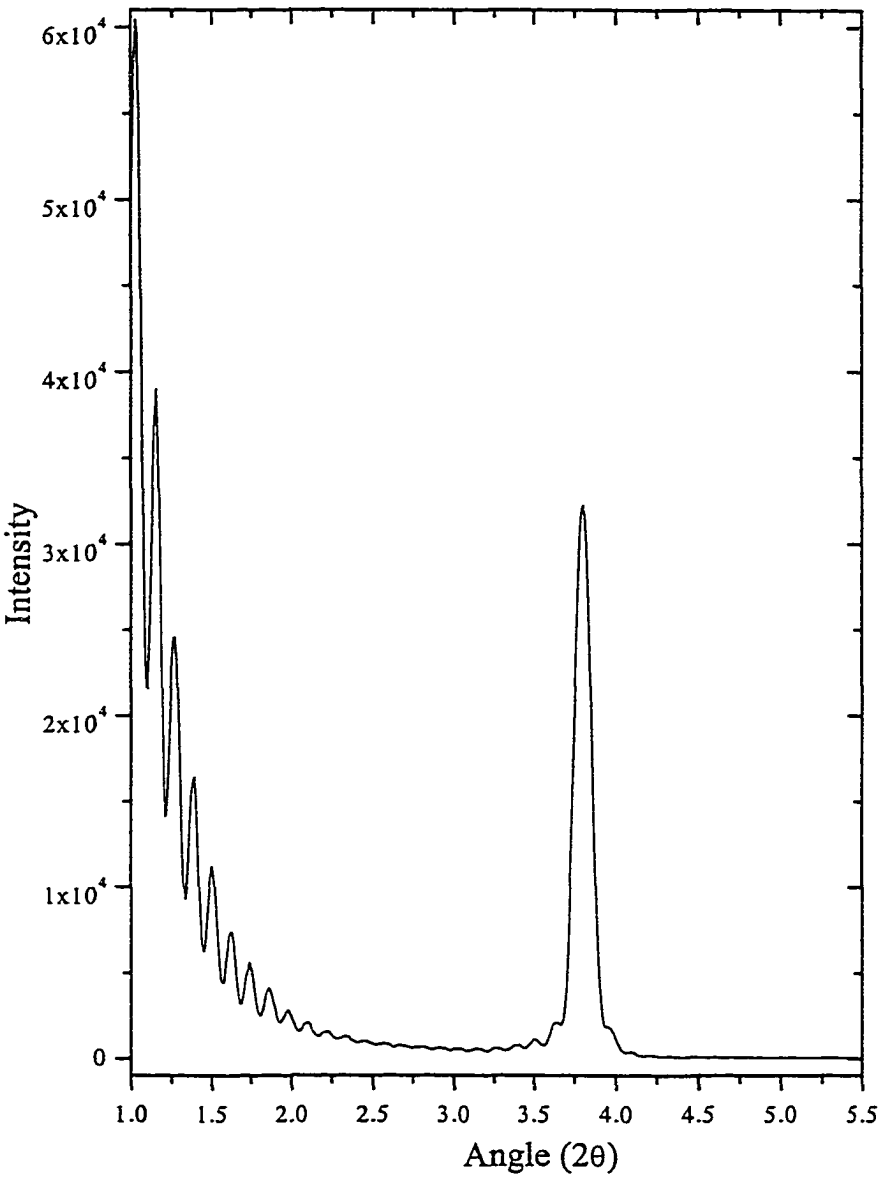

Figure 3.6, SAXS spectrum of a 15 bilayer thin film of $CuPc(OC_2OBz)_8$ on Si(100) after annealing for 2 hours at 100°C in air

3.3.3 Dimensional Information in Context of Molecular Ordering

There is little difference in the d spacing values for the un-annealed and the annealed films (23.6 Å and 23.3 Å respectively for the $CuPc(OC_2OBz)_8$ thin films and 23.5 Å and 23.4 Å respectively for the $H_2Pc(OC_2OBz)_8$ thin films). However, there is a great deal of difference in the clarity of the reflected intensities. The main reflection of the $H_2Pc(OC_2OBz)_8$ thin film increased dramatically with annealing. This suggests that there is little order in the un-annealed film, although the existence of monolayer structures are present. Upon annealing the junctions of the monolayer interfaces must become more defined, resulting in a stronger intensity Bragg reflection. Despite this increase, the $H_2Pc(OC_2OBz)_8$ thin films are not as organized as the $CuPc(OC_2OBz)_8$ thin films.

The d spacings found for the un-annealed and annealed films correspond to $CuPc(OC_2OBz)_8$ and $H_2Pc(OC_2OBz)_8$ column diameters of ca. 27 Å, found for a hexagonally close packed configuration. Because of the lack of change in these measurements before and after annealing, we can conclude that annealing tends to reorder the phthalocyanine columnar assemblies, but does not affect the interactions between the columns appreciably.

The appearance of pronounced Kiessig fringes supports this as they are an indicator of the definition between individual layers within the multilayered thin film. Kiessig fringes of this clarity have not been seen previously for thin films of $CuPc(OC_2OBz)_8$.[10,14] and correlate with the appearance of pronounced Kiessig fringes in

annealed films of an isomerically pure substituted phthalocyanine as reported by Nolte et al.[13]

3.4 Atomic Force Microscopy

Atomic Force Microscopy (AFM) is one of the scanning probe microscopies that provides visual information on a micro-nanoscopic scale. The basis of these microscopies is the detection of the interactions (ie. deflection, attraction, conductivity) of a tip in close proximity with the underlying surface. AFM used in the tapping mode, consists of an oscillating tip that is rastered over the surface. The change in amplitude of this oscillating tip due to attractive or repulsive forces from the underlying surface are detected as a function of lateral position. Mapping these changes in amplitude give an image of the underlying surface, with resolution reaching into the 10's of angstroms.

3.4.1 Considerations of using AFM as an Imaging Tool of Soft Materials

Direct images of soft materials with atomic force microscopy is subject to the stability of the sample. Many soft materials (ie. biological specimens, polymers, self-assemblies, and LB films) can be damaged by the adhesion force between the tip and sample. Manne et al. have been able to image ionic surfactant coated surfaces by imaging the double layer, or the effective repulsive force between a positively charged tip and surface.[22] Umemura et al. report that a lubricant coated-tip reduces the adhesion force between a silicon nitride tip and bacteria flagella, enabling the imaging of the biological specimen.[23] Therefore, the success of imaging a soft material is dependent on finding a set of conditions that allow the tip to float above the surface, modulated by repulsive

forces between the tip and the sample. Contact of the tip with a soft sample results in damage of the sample, and incomplete or damaged images.

We have found for these samples a completely hydrophilic silicon nitride tip is needed in order to image one bilayer LB films of $CuPc(OC_2OBz)_8$ and $H_2Pc(OC_2OBz)_8$ on Si(100). The force vs. distance curve for a partially hydrophobic tip in the presence of these samples is shown in Figure 3.7.a. On the approach to the surface there is no tip deflection until the tip is brought within ca. 45 nm of the surface, and then the deflection of the tip follows with its proximity to the surface. Upon retraction, the tip experiences a large attraction as it breaks away from the surface.

Looking now at the force distance curve for a completely hydrophilic tip (Figure 3.7.b), we see that as the tip approaches the surface there is a slight repulsive force experienced as the tip approaches within ca. 45 nm of the surface and the lack of the sudden negative deflection as the tip comes in contact with the surface. Upon retraction, the tip pulls away from the surface with no large deflection of the tip as a result of breaking the grip of any attractive forces between the tip and the sample. It is only with this tip behavior that reliable, accurate images could be obtained, especially in the case of the $H_2Pc(OC_2OBz)_8$ bilayer sample.

3.4.2 Images of Single Bilayer films of $CuPc(OC_2OBz)_8$ and $H_2Pc(OC_2OBz)_8$

Figure 3.8 shows long range ordering of $CuPc(OC_2OBz)_8$ columnar assemblies, with cohesion lengths varying from 100 - 1500 Å. The columns align themselves parallel to one another and are shown here to do so over a domain of $2.25x10^4$ nm^2 area, despite

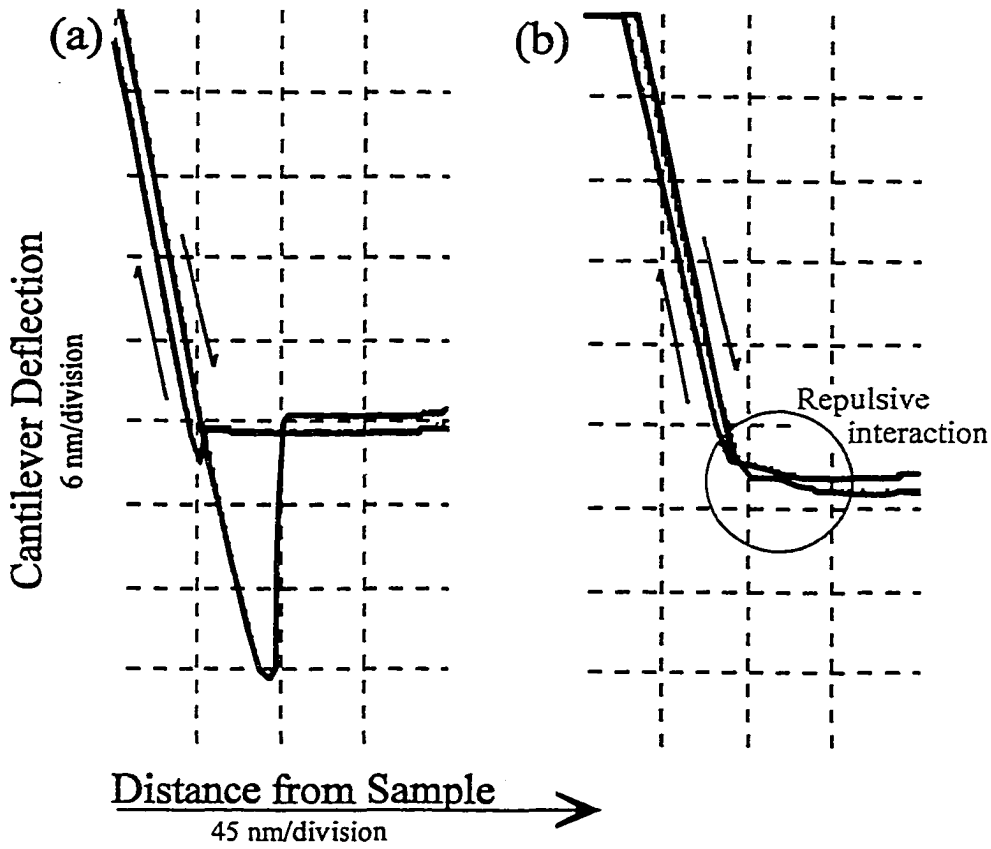

Figure 3.7, Force distance curves for a partially hydrophilic tip (a) and a fully hydrophilic tip (b).

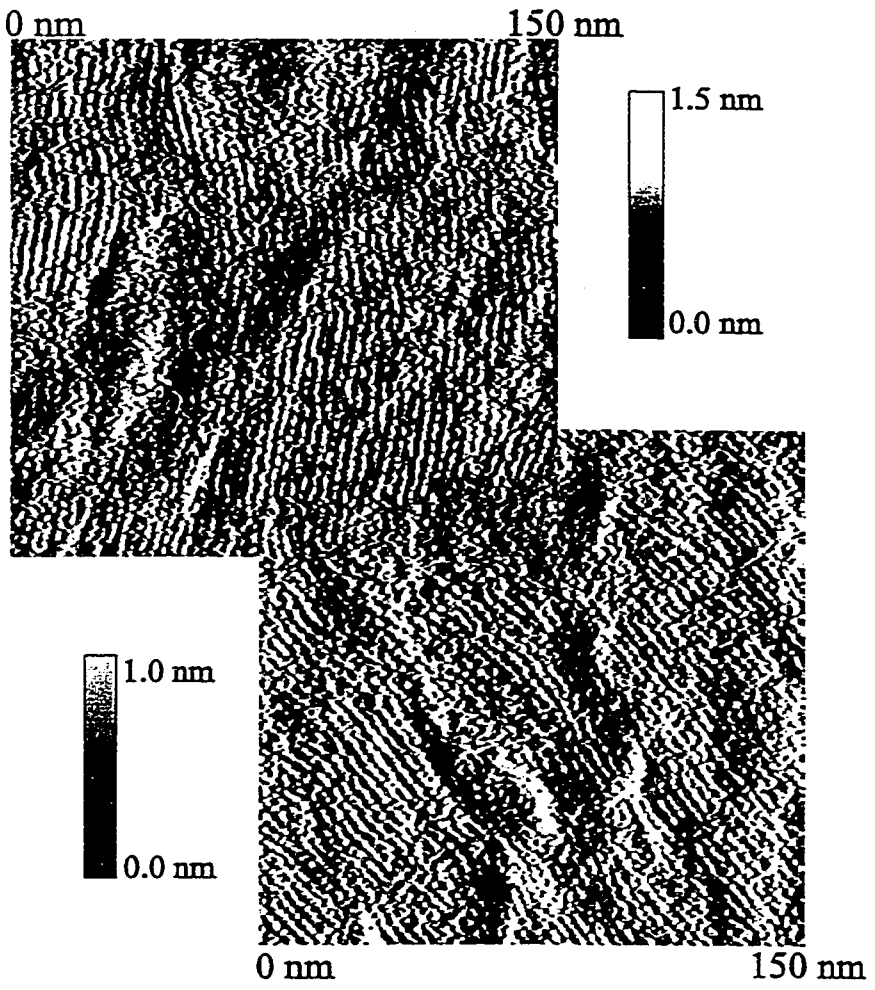

Figure 3.8, Tapping AFM images of a one bilayer LB thin film of $CuPc(OC_2OBz)_8$ showing long range ordering.

several underlying changes in surface morphology that would decrease this probability. The tendency for the Pc columns to "bend" around these defects may prove to be an essential factor in achieving long range coherence.

Looking at these $CuPc(OC_2OBz)_8$ columnar assemblies over short ranges, one can see the regularity of intercolumn distances, ca. 29 Å. This intercolumnar spacing, whether in an area of branching between different domains, or within a single domain (Figure 3.9.a and 3.9.b) is consistent with the SAXS data shown earlier and the WAXS data obtained for $CuPc(OC_2OBz)_8$ fiber bundles.

Images of one bilayer thickness $H_2Pc(OC_2OBz)_8$ films on Si(100) were much harder to acquire. It was essential that the silicon nitride tip be completely hydrophilic so that no attractive forces between the tip and the surface were present. Thin films of $H_2Pc(OC_2OBz)_8$ have proven to be more "soft" then films of $CuPc(OC_2OBz)_8$. This may be due to the absence of the metal core, which imparts a degree of stability in the columnar assemblies due to metal-Pc interactions in the $CuPc(OC_2OBz)_8$ systems. 50 nm^2 images of $H_2Pc(OC_2OBz)_8$ are seen in Figure 3.10. Again, the intercolumnar spacing is consistent with that found for thin films of $CuPc(OC_2OBz)_8$. The difficulty with which these images were obtained is seen with the poorer spatial definition, as compared with images of $CuPc(OC_2OBz)_8$ films.

An interesting area was found while imaging the $H_2Pc(OC_2OBz)_8$ material. Although found in the middle of the sample, it appeared to be the edge of a bilayer (Figure 3.11). Upon doing a bearing analysis, which determines the distribution of

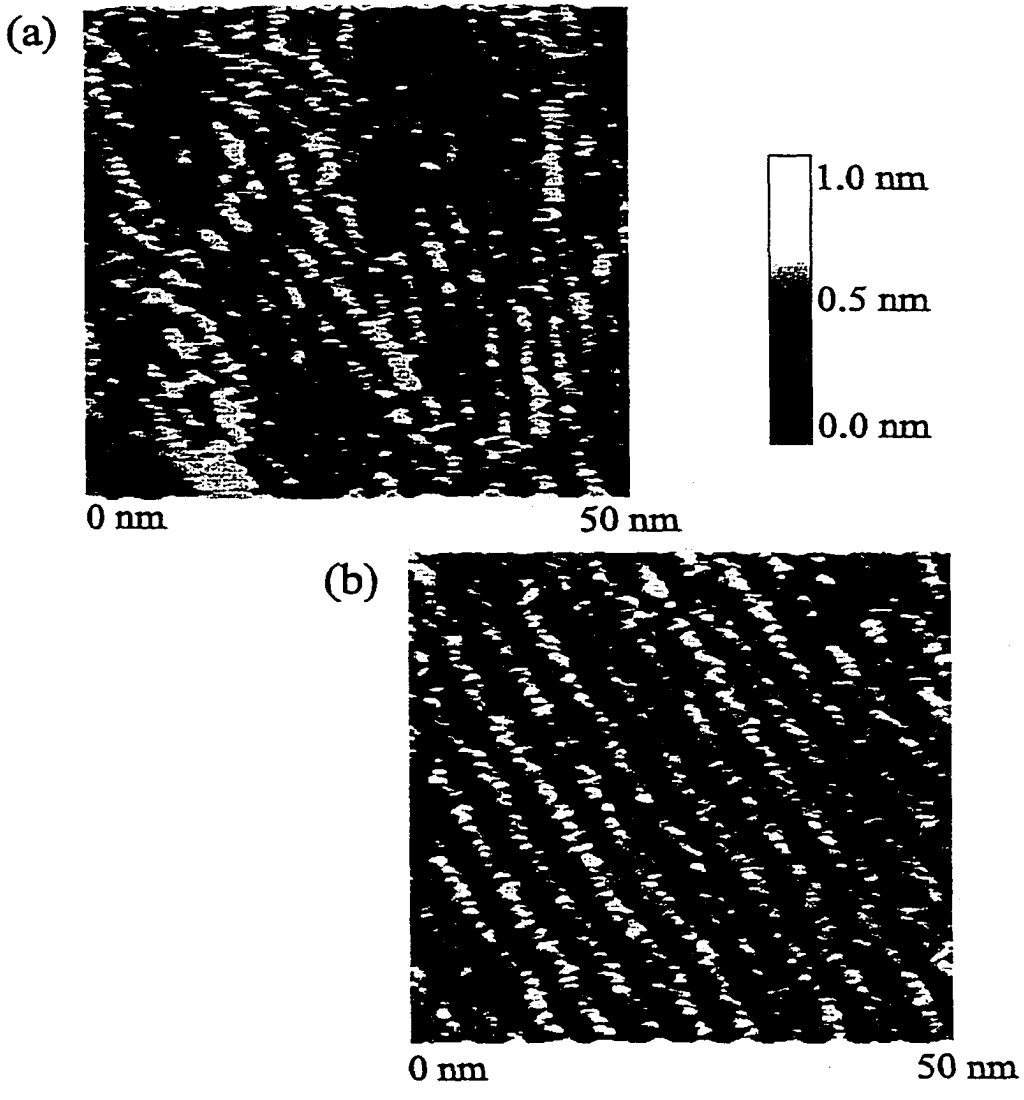

Figure 3.9, Tapping AFM images of a one bilayer LB thin film of $CuPc(OC_2OBz)_8$ showing short range ordering over 50 nm^2 (a) with areas of divergence of columns, and (b) highly organized parallel columns.

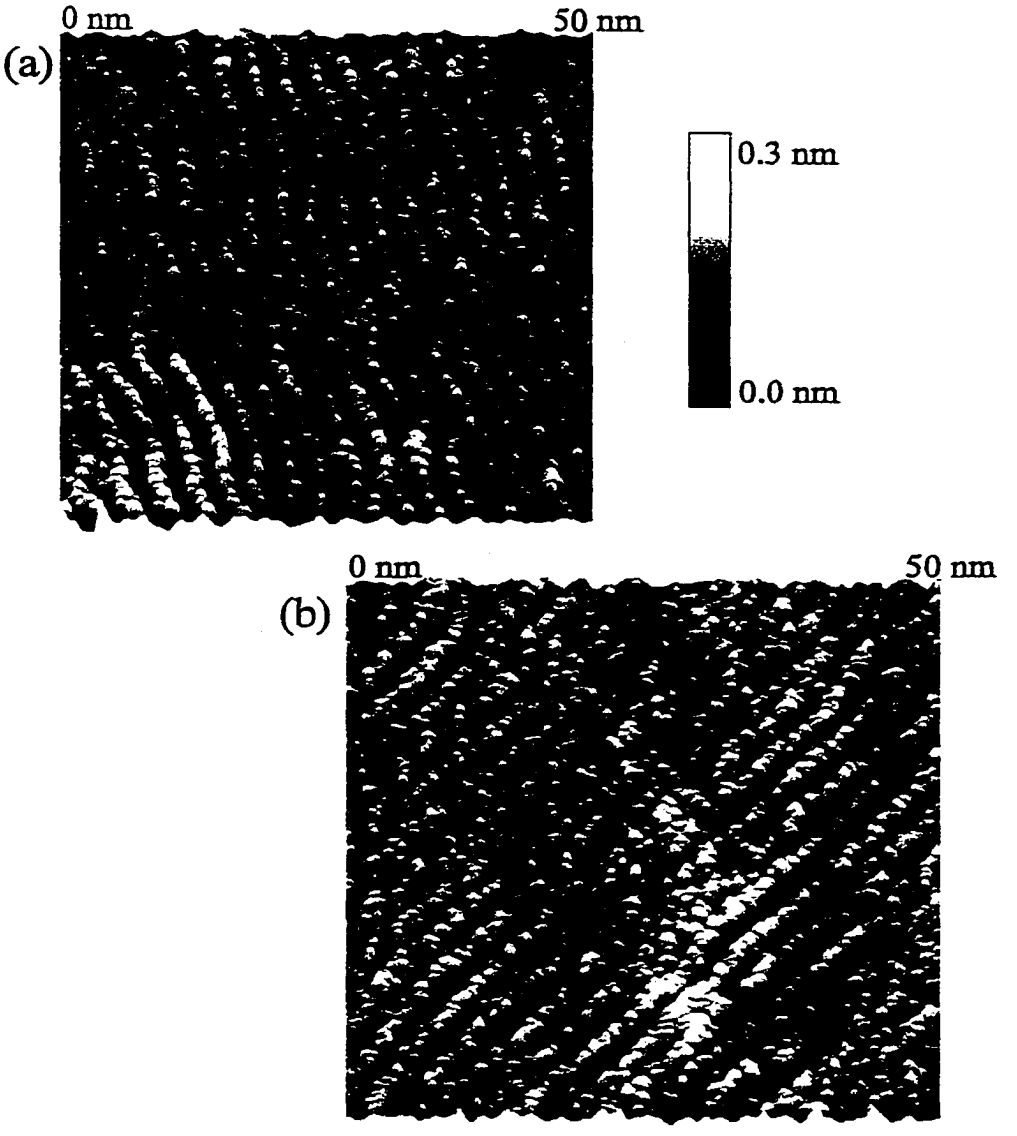

Figure 3.10, Tapping AFM images of 1 bilayer LB thin films of $H_2Pc(OC_2OBz)_8$ showing columnar order over 50 nm^2, scanning perpendicular (a) and off angle (b).

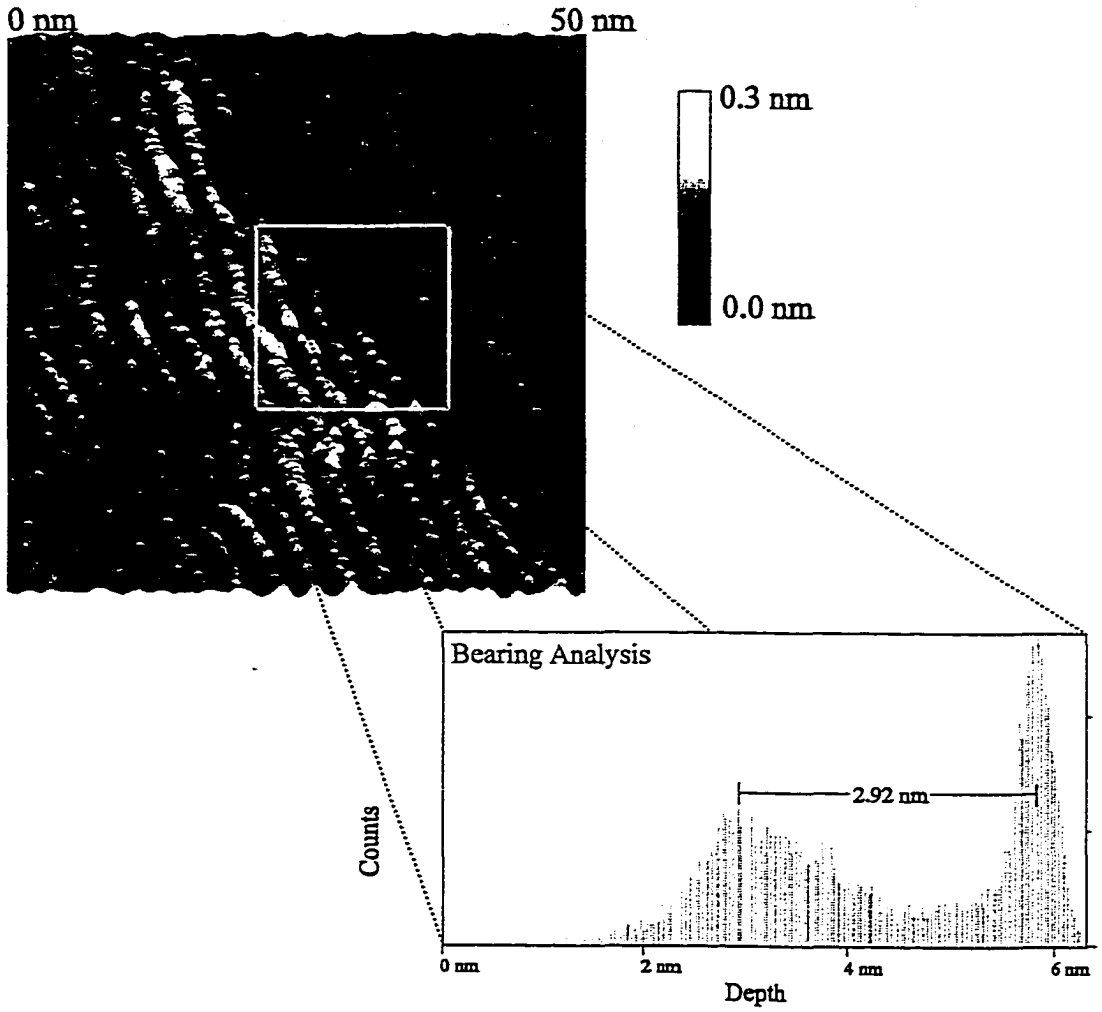

Figure 3.11, View of an edge of a $H_2Pc(OC_2OBz)_8$ monolayer within the center of an LB thin film sample.

heights found within a certain area of the image, it was determined that the edge was that of a monolayer. This is probably due to the presence of monolayer sections within the bilayer films. On the LB trough, as the monolayer is compressed into a bilayer, it could be expected that the overlaying monolayer does not form a complete second layer. Small pockets of the overlaying monolayer, dispersed throughout the film, would produce an image as seen in Figure 3.11. The ultimate proof of this would be successful imaging of the original monolayer to the right of the bilayer structure.

3.4.3 Comparison with SAXS Experiments

The intercolumn spacing of 29 Å found in the AFM images correlates well with that found from the SAXS data, 27 Å intercolumn spacing. The difference between the two measurements can be explained by the limitations of the AFM technique. The silicon nitride tip at its smallest point is ca. 5 μm, therefore, the lateral resolution in AFM imaging is limited by the ability of this microscopic tip to detect changes with nm resolution. Also, our reported coherence lengths for the $H_2Pc(OC_2OBz)_8$ and $CuPc(OC_2OBz)_8$ films are also conservative estimates, because our ability to measure them is limited by the ability to obtain an image over a large area. The SAXS experiment gives us much more quantitative information about the macroscopic ordering within the films, but that should not take away from the great accomplishment of being able to image these soft materials using tapping AFM in solution.

CHAPTER 4: MICROSCOPIC ORDERING DETERMINED BY IR SPECTROSCOPY

4.1 Overview of Experimental Parameters

Two experiments were conducted to determine the ordering of the molecules within the Pc columns by the interaction of specific vibrational transition moments with polarized electric fields. A transmission dichroism experiment using $\parallel$ and $\perp$ polarized light was used to probe seven bilayer LB films of $CuPc(OC_2OBz)_8$ and $H_2Pc(OC_2OBz)_8$ deposited on hydrophobized Si(100) wafers. Reflection absorption infrared spectroscopy (RAIRS) was used to probe one and three bilayer films of the same materials deposited on gold substrates. These two techniques are complementary (Figure 4.1). The transmission experiment probes those dipole moments parallel to the substrate surface at two orthogonal angles. The RAIRS experiment, because of the surface selection rules which are explained in Section 4.5.1, probes vibrations of dipole moment changes normal to the substrate surface. These two techniques allow for a three dimensional characterization of the Pc assembly.

4.2 Bulk Transmission IR Spectroscopy

The bulk IR transmission spectrum of $CuPc(OC_2OBz)_8$ has previously been assigned and reported, but is reproduced here in Figure 4.2.[11] Of the assigned bands in Table 4.1 there are several that become useful when determining the orientation of these molecules. The symmetric and asymmetric stretches of the Pc-O-C bonds at 1204 cm^{-1}

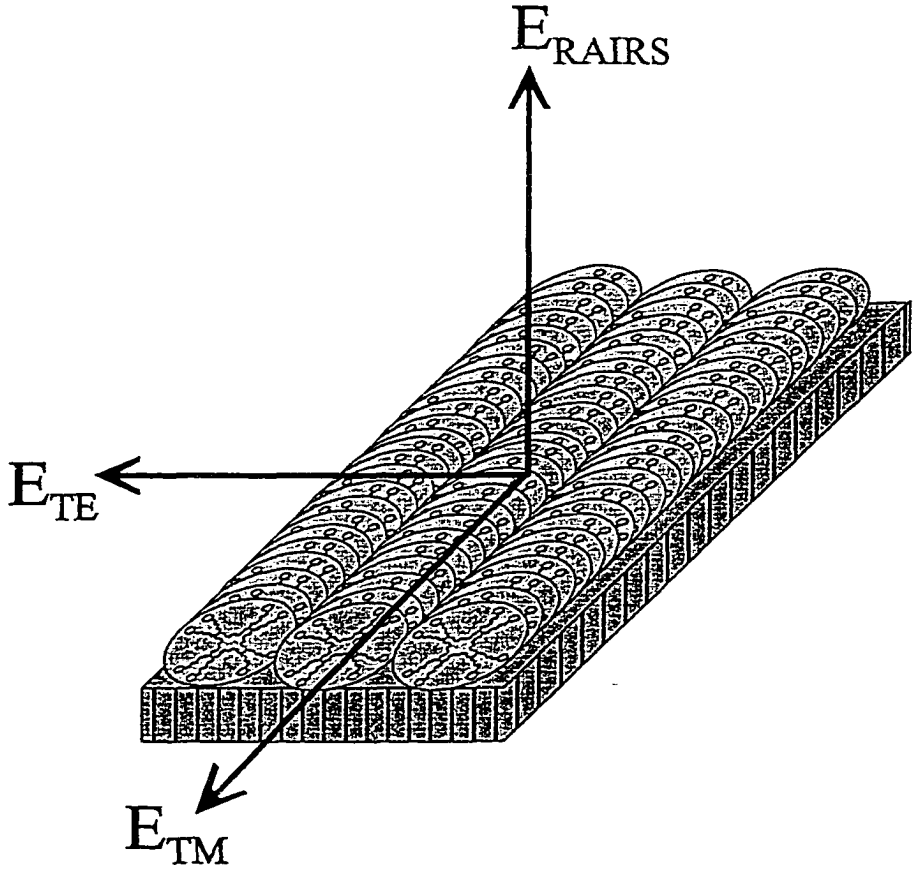

Figure 4.1, Geometric relation between the electric field vectors associated with RAIRS (E_{RAIRS}) and transmission (E_{TE} and E_{TM}) experiments.

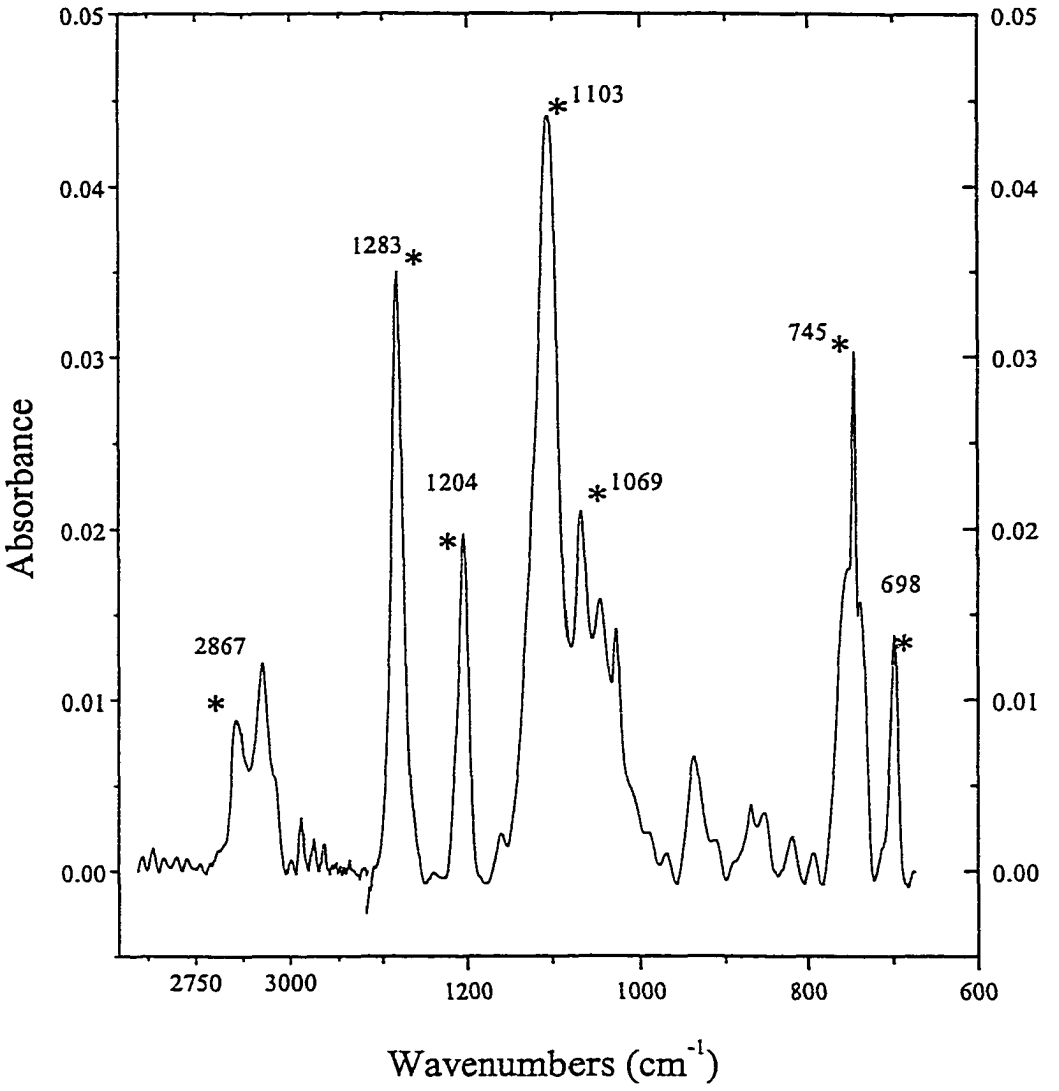

Figure 4.2, IR transmission spectrum of a KBr pressed pellet of $CuPc(OC_2OBz)_8$.

Table 4.1, Assignment of IR bands of $CuPc(OC_2OBz)_8$ in KBr pressed pellet.

Wavenumbers (cm^{-1})	Assignment	Absorbance
698	δ(ring C-H, op)	0.014
745	δ(ring C-H, op)	0.030
1069	ν(ring C-H, ip)	0.021
1103	ν_a(C-O-C)	0.044
1204	ν_s(Pc-O-C)	0.020
1283	ν_a(Pc-O-C)	0.035
2867	ν_s(-CH_2-)	0.009

and 1283 cm^{-1} respectively occur exclusively in the plane of the Pc macrocycle, likewise the out-of-plane-bend of the C-H groups on the Pc periphery occurs only out of the plane of the Pc macrocycle. Because of their known position in the Pc macrocycle, and their orthogonal nature to one another, these transitions were used in the transmission linear dichroism and RAIRS experiments.

A bulk IR transmission spectrum for $H_2Pc(OC_2OBz)_8$ has not been reported previously and is presented in Figure 4.3. Band assignments were based on those made for the $CuPc(OC_2OBz)_8$ molecule (Table 4.2), although there is quite a difference in the band shapes in the 1000-1300 wavenumber region. The smearing of bands in this region may simply be due to a less homogenous sample in the case of the $H_2Pc(OC_2OBz)_8$. The difference may also be due to a symmetry change in the molecule itself. When the core metal of a phthalocyanine is removed the symmetry of the molecule changes from D_{4h} to D_{2h} symmetry. This may cause a significant splitting in the C-O-C stretching region.

4.3 Transmission IR Spectroscopy with Polarized Excitation Source

4.3.1 Introduction

If a molecule of interest has a well defined geometry and is packed in an ordered film, then one would expect differences in the relative intensities of certain vibrational bands, comparing bulk (isotropic) spectra and spectra taken of thin films with polarized sources. Knowing the orientation of the subunits within the molecule, the orientation of the molecule can be determined by probing the subunits with at least two different polarizations of exciting radiation. Because of the great number of subunits that are

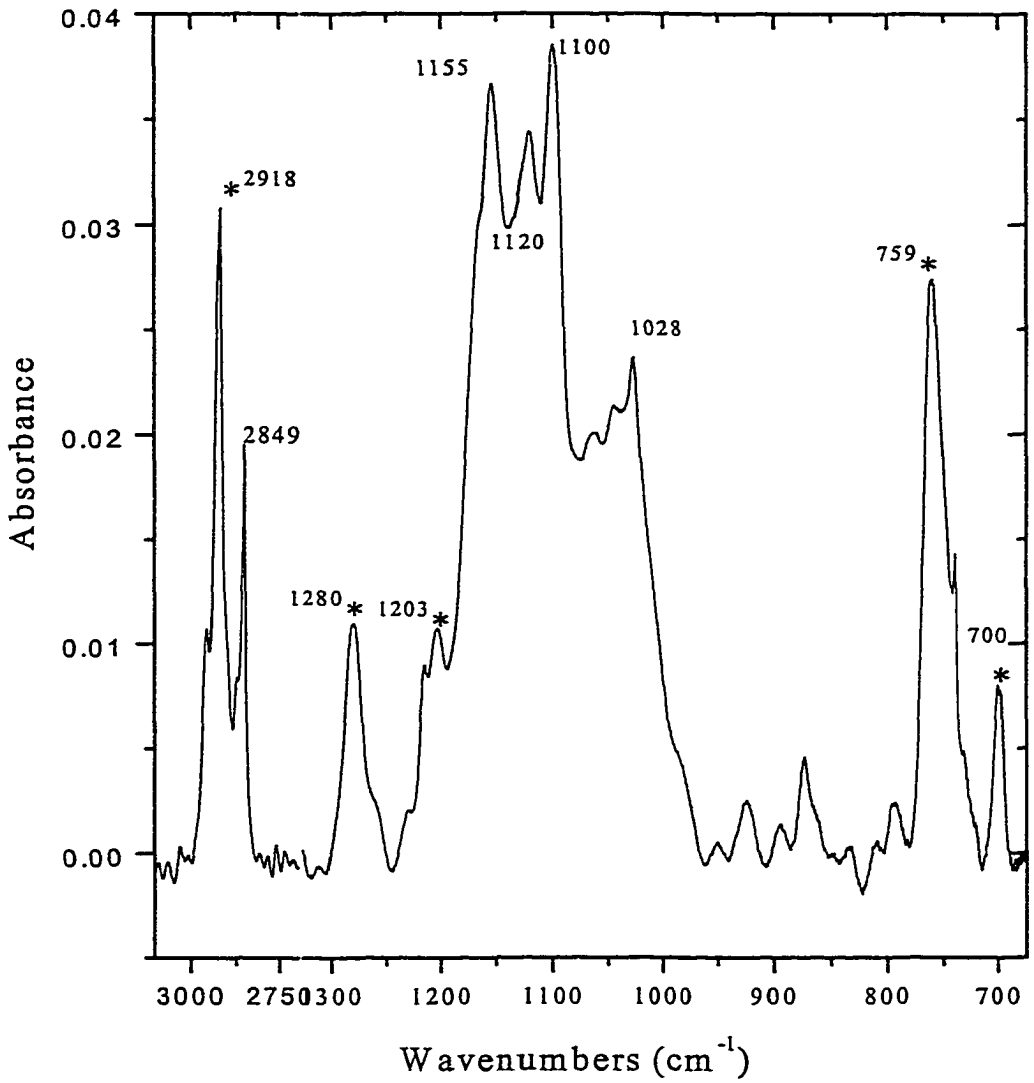

Figure 4.3, IR transmission spectrum of a KBr pressed pellet of $H_2Pc(OC_2OBz)_8$.

Table 4.2, Assignment of IR bands of $H_2Pc(OC_2OBz)_8$ in KBr pressed pellet.

Wavenumbers (cm^{-1})	Assignment	Absorbance
700	δ(ring C-H, op)	0.011
759	δ(ring C-H, op)	0.027
1028	ν(ring C-H, ip)	0.024
1100	ν_a(C-O-C)	0.038
1203	ν_s(Pc-O-C)	0.011
1280	ν_a(Pc-O-C)	0.011
2918	ν_s(-CH_2-)	0.031

present in the Pc molecules, there is more information available to base the orientation calculation upon.

4.3.2 Overview of the Experiment

A series of polarized IR spectra were taken of 7 bilayer LB films of both $CuPc(OC_2OBz)_8$ and $H_2Pc(OC_2OBz)_8$ on Si(100) substrates. The LB films were deposited by the Schaefer method, using the baffle as described in Section 1.2. The ultimate goal was to probe the molecular orientation within the films. Several variables were used and altered throughout the course of the experiment in an attempt to enhance the ordering as defined and evaluated in the following sections of this chapter. The variables that were altered were the water subphase temperature during the formation and deposition of the Langmuir layer, and the substrate surface modification as described in the previous chapter.

The subphase temperature was expected to affect the ordering of the Pc molecules on the air-water interface for two reasons. The first is that as a liquid crystalline material, the aggregation tendencies of the Pc molecules are greatly affected by temperature. Disc shaped liquid crystalline materials undergo phase changes from an anisotropic solid to a discotic phase to an isotropic liquid with an increase in temperature.[24] Although the specific phase changes have not been determined for these Pc materials, one may observe a variation of ordering within a Langmuir film over a ca. 30° temperature range.

The second effect of the subphase temperature is the change in surface tension of the water. The ridigity of the Langmuir film formed at the air-water interface is

dependent on the interactions of the probe molecules and the subphase. A decrease in the surface tension creates a situation of greater interaction between the subphase and the probe molecules. Perhaps even the probe molecules can "slip through" the water surface into the subphase. The surface tension of water changes ca. 5 dynes/cm over the temperature range used in this experiment. A temperature gradient of ca. 0°, 12°, 23°, and 30°C was used as the water subphase temperature, but only representative spectral data from the low and high extremes will be presented and discussed here. The surface tension of water is reported to be 70.71 dynes/cm at ca. 34.7°C, and extrapolated to be 76.08 dynes/cm at ca. 0.3° C.[25] These changes in surface tension are not negligible in the change in surface morphology of the Langmuir film.

The Si(100) substrate surfaces were modified with HMDS and DPTMDS as discussed in Chapter 3. In order to study the ordering and orientation of these Langmuir-Blodgett films, it is of great importance to try and achieve complete transfer with maintenance of the Langmuir layer ordering. We have found that hydrophobic substrate surfaces are needed for good transfer. A common way of hydrophobizing silicon surfaces is by silane chemistry.

HMDS was shown to coat the substrate surface successfully (Chapter 3) with a layer of methyl groups. DPTMDS was chosen as a second modifying reagent because it successfully coats the surface with a layer of primarily phenyl functional groups. It was supposed that van der Waals interactions between these phenyl groups and the benzyl groups on the periphery of the Pc molecules might impart better transfer and maintenance

of ordering in the Langmuir-Blodgett films.

4.3.3 Spectroscopic Results

Polarized IR spectra of 7 bilayer LB films of $CuPc(OC_2OBz)_8$ at the low and high temperature extremes and with the two different surface treatments are presented in Figures 4.4 and 4.5. Likewise, spectra of 7 bilayer LB films of $H_2Pc(OC_2OBz)_8$ for the same experimental conditions are presented in Figures 4.6 and 4.7. Absorbance values, dichroic ratios, R, order parameters, S_2, and tilt angles, ψ, (defined in the following sections) for the presented spectra are listed in Tables 4.3-4.10.

4.3.4 Definition and Evaluation of Semi-quantitative Parameters

Various groups have used IR spectroscopy with polarized sources to determine the orientation of thin films on metal and non-metal substrates.[8, 17, 26, 27] The Wegner group has used transmission IR spectroscopy to aid in determining the order of molecular assemblies of polymerized phthalocyaninato-polysiloxane.[28] These ordering calculations are based upon the linear dichroic ratio, R, of a particular band, defined below:

$$R = \frac{I(E \perp t)}{I(E \| t)} \qquad \text{(Eq. 4.1)}$$

The greater the dichroic ratio for those modes that are in the plane of the Pc, the greater anisotropy is present and vice versa for the out of plan mode δ(ring C-H, op). Comparing low verses high temperature deposition, it is obvious that the sample is more anisotropic when prepared at lower temperatures. At high temperature depositions a

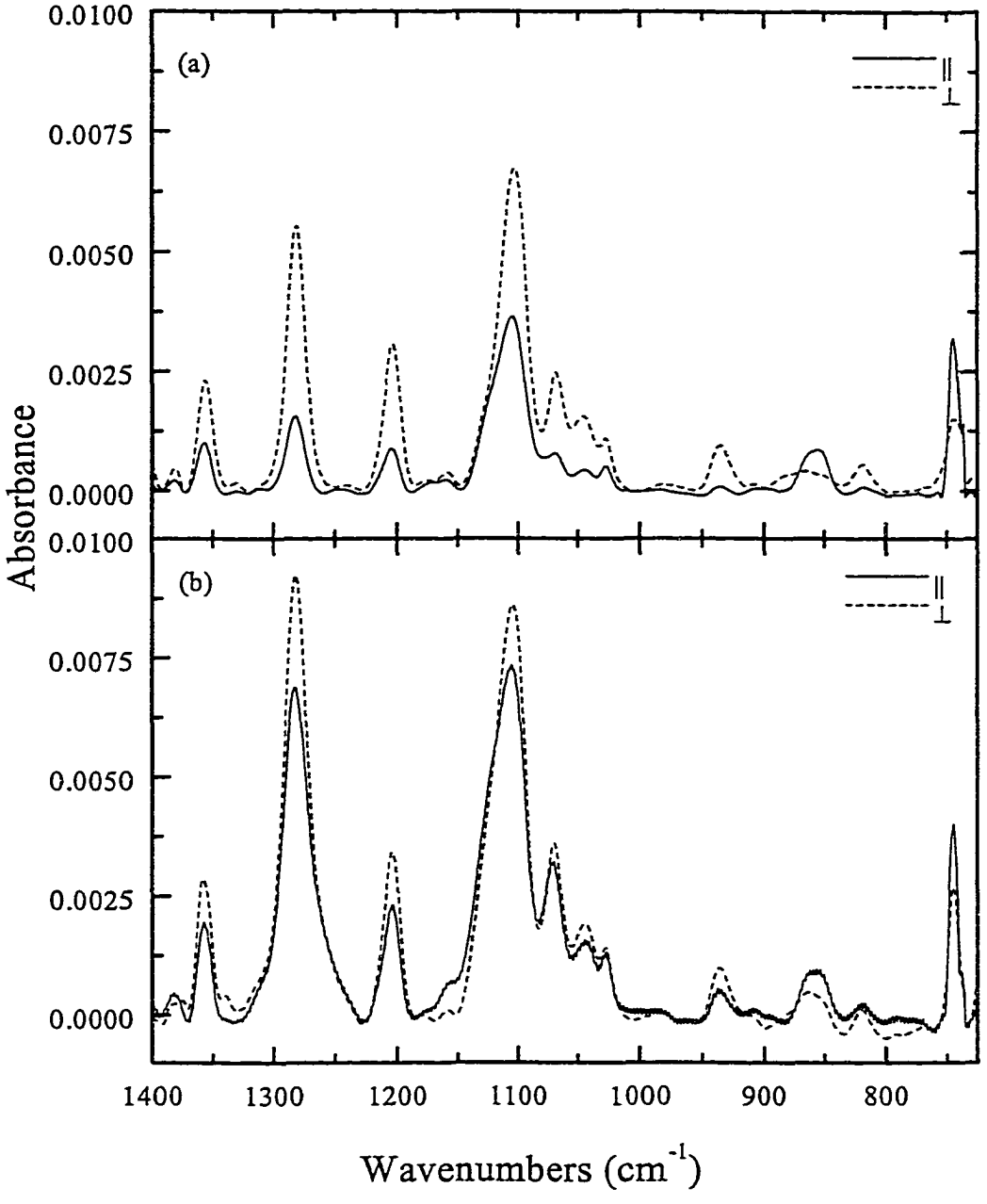

Figure 4.4, IR linear dichroism spectra of 7 bilayer films of $CuPc(OC_2OBz)_8$ on Si(100) modified with HMDS deposited at (a) 1.0°C and (b) 30.0°C.

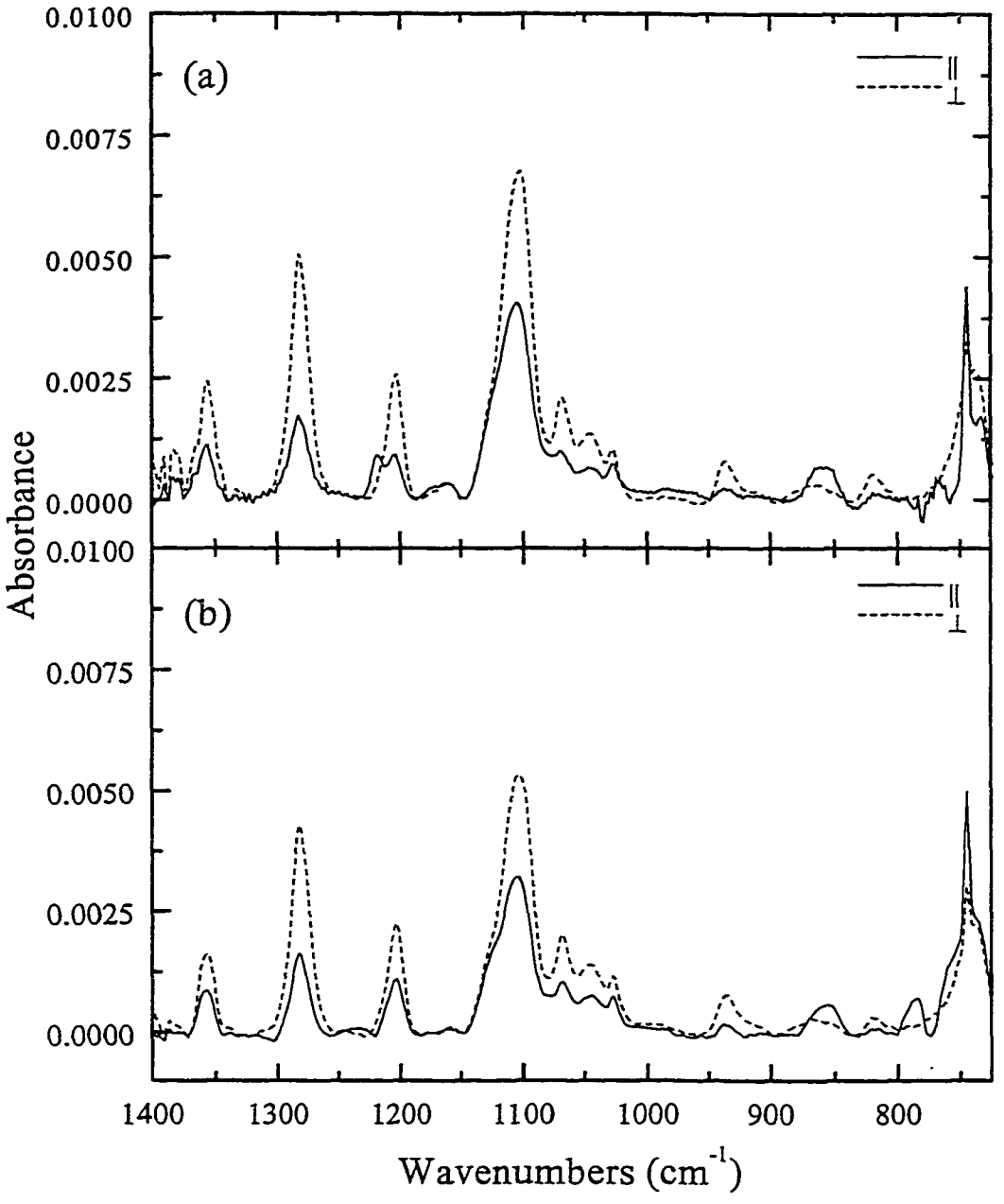

Figure 4.5, IR linear dichroism spectra of 7 bilayer films of $CuPc(OC_2OBz)_8$ on Si(100) modified with DPTMDS deposited at (a) 0.3 °C and (b) 30.0 °C.

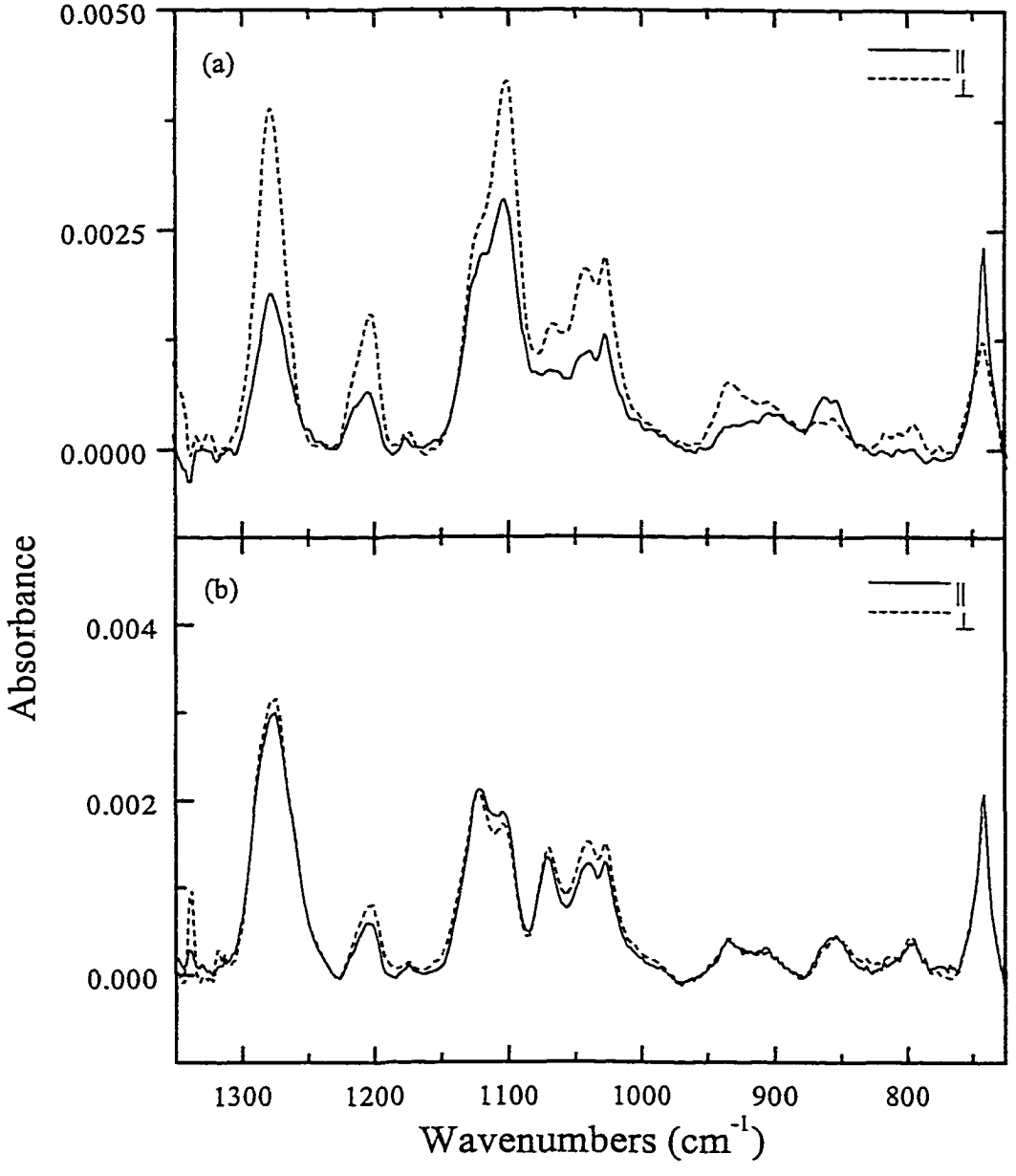

Figure 4.6, IR linear dichroism spectra of 7 bilayer films of $H_2Pc(OC_2OBz)_8$ on Si(100) modified with HMDS deposited at (a) 1.0°C and (b) 34.7°C.

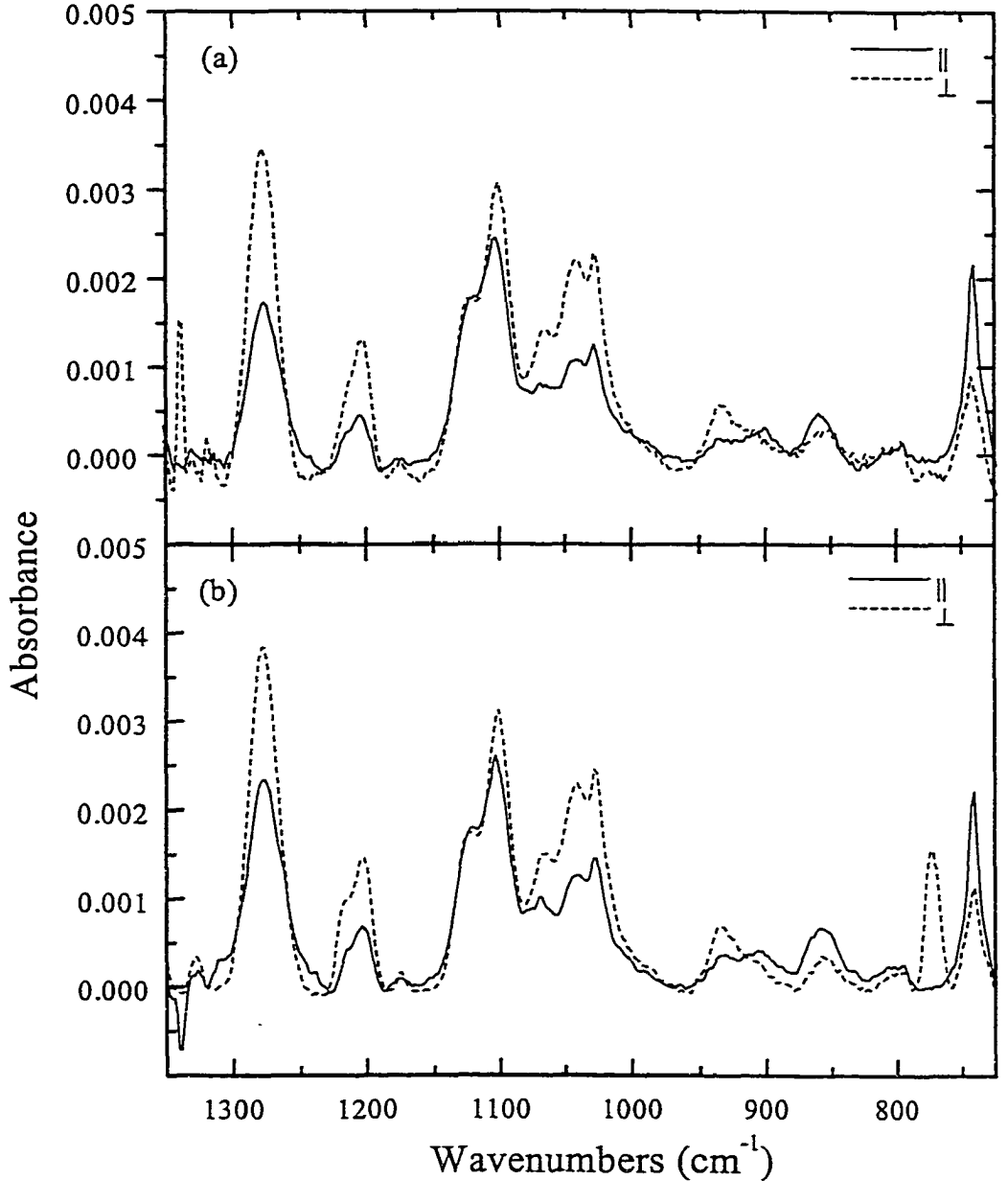

Figure 4.7, IR linear dichroism spectra of 7 bilayer films of $H_2Pc(OC_2OBz)_8$ on Si(100) modified with DPTMDS deposited at (a) 1.0°C and (b) 30.4°C.

Table 4.3, Absorbance intensities for 7 bilayer film of $CuPc(OC_2OBz)_8$ on Si(100) modified with HMDS at 1.0° C upon transfer.

Wavenumbers (cm^{-1})	Electric field ⊥ to Pc columns	Electric field ∥ to Pc columns	R	S_2	ψ°
745	0.00155	0.00320	0.48	0.35	35°
1069	0.00106	0.00027	3.93	0.59	27°
1103	0.00560	0.00289	1.94	0.32	36°
1204	0.00295	0.00086	3.43	0.55	28°
1283	0.00546	0.00156	3.50	0.56	28°
		Average	2.98	0.47	35°
		STD	0.91	0.13	12°

Table 4.4, Absorbance intensities for 7 bilayer film of $CuPc(OC_2OBz)_8$ on Si(100) modified with HMDS at 30.0° C upon transfer.

Wavenumbers (cm^{-1})	Electric field ⊥ to Pc columns	Electric field ∥ to Pc columns	R	S_2	ψ°
745	0.00276	0.00365	0.76	0.13	41°
1069	0.00201	0.00160	1.26	0.11	42°
1103	0.00645	0.00504	1.28	0.12	41°
1204	0.00339	0.00233	1.45	0.19	40°
1283	0.00920	0.00691	1.33	0.14	41°
		Average	1.33	0.14	43°
		STD	0.08	0.03	4°

Table 4.5, Absorbance intensities for 7 bilayer film of $CuPc(OC_2OBz)_8$ on Si(100) modified with DPTMDS at 0.3° C upon transfer.

Wavenumbers (cm^{-1})	Electric field ⊥ to Pc columns	Electric field ∥ to Pc columns	R	S_2	ψ°
745	0.00073	0.00326	0.22	0.62	25°
1069	0.00090	0.00018	5.00	0.67	24°
1103	0.00589	0.00315	1.87	0.30	36°
1204	0.00222	0.00066	3.36	0.54	29°
1283	0.00485	0.00136	3.57	0.56	28°
		Average	3.65	0.54	37°
		STD	1.20	0.14	17°

Table 4.6, Absorbance intensities for 7 bilayer film of $CuPc(OC_2OBz)_8$ on Si(100) modified with DPTMDS at 30.0° C upon transfer.

Wavenumbers (cm^{-1})	Electric field ⊥ to Pc columns	Electric field ∥ to Pc columns	R	S_2	ψ°
745	0.00093	0.00247	0.38	0.45	32°
1069	0.00085	0.00038	2.24	0.38	34°
1103	0.00461	0.00275	1.68	0.25	38°
1204	0.00218	0.00113	1.93	0.32	36°
1283	0.00419	0.00181	2.31	0.40	33°
		Average	2.16	0.36	40°
		STD	0.38	0.08	11°

Table 4.7, Absorbance intensities for 7 bilayer film of $H_2Pc(OC_2OBz)_8$ on Si(100) modified with HMDS at 1.0° C upon transfer.

Wavenumbers (cm^{-1})	Electric field ⊥ to Pc columns	Electric field ∥ to Pc columns	R	S_2	ψ°
745	0.00115	0.00288	0.40	0.43	32°
1069	0.00003	0.000005	6.00	0.71	22°
1103	0.00330	0.00206	1.60	0.23	38°
1204	0.00137	0.00056	2.45	0.42	33°
1283	0.00372	0.00170	2.19	0.37	34°
		Average	2.95	0.43	37°
		STD	1.74	0.18	13°

Table 4.8, Absorbance intensities for 7 bilayer film of $H_2Pc(OC_2OBz)_8$ on Si(100) modified with HMDS at 34.7° C upon transfer.

Wavenumbers (cm^{-1})	Electric field ⊥ to Pc columns	Electric field ∥ to Pc columns	R	S_2	ψ°
745	0.00202	0.00205	0.98	0.01	45°
1069	0.00080	0.00072	1.11	0.05	43°
1103	0.00143	0.00138	1.04	0.02	44°
1204	0.00074	0.00050	1.48	0.19	39°
1283	0.00314	0.00291	1.08	0.04	44°
		Average	1.14	0.06	43°
		STD	0.19	0.08	2°

Table 4.9, Absorbance intensities for 7 bilayer film of $H_2Pc(OC_2OBz)_8$ on Si(100) modified with DPTMDS at 1.0° C upon transfer.

Wavenumbers (cm^{-1})	Electric field ⊥ to Pc columns	Electric field ∥ to Pc columns	R	S_2	ψ°
745	0.00121	0.00212	0.57	0.27	37°
1069	0.00029	0.00027	1.07	0.04	44°
1103	0.00554	0.00189	2.93	0.49	30°
1204	0.00166	0.00063	2.63	0.45	32°
1283	0.00387	0.00187	2.07	0.35	35°
		Average	2.09	0.32	39°
		STD	0.73	0.18	10°

Table 4.10, Absorbance intensities for 7 bilayer film of $H_2Pc(OC_2OBz)_8$ on Si(100) modified with DPTMDS at 34.7° C upon transfer.

Wavenumbers (cm^{-1})	Electric field ⊥ to Pc columns	Electric field ∥ to Pc columns	R	S_2	ψ°
745	0.00137	0.00254	0.54	0.30	36°
1069	0.00029	0.00022	1.32	0.14	41°
1103	0.00254	0.00203	1.25	0.11	42°
1204	0.00153	0.00075	2.04	0.34	35°
1283	0.00317	0.00221	1.43	0.18	40°
		Average	1.58	0.21	42°
		STD	0.35	0.10	7°

nearly isotropic thin film is created. At both high and low temperature depositions, greater anisotropy is gained when the DPTMDS modified surface is used as the substrate.

An overall evaluation of the ordering of a system such as that investigated here or the PcPS system is the order parameter, S, as defined in the Wegner group.[28] The order parameter is based on the ratios of the intensities of a specific vibration in orthogonally polarized light. The order parameter concept is well known in the area of nematic liquid crystals. The nematic order parameter:

$$S = \langle P_2(\cos\theta)\rangle = \left\langle \tfrac{1}{3}\left(3\cos^2\theta - 1\right)\right\rangle \qquad \text{(Eq. 4.2)}$$

is the second moment of the orientation distribution function of the molecular symmetry axes in terms of Legendre polynomials, $P_i(\cos\theta)$. Considering the distribution function in only two dimensions we have:

$$S_2 = 2\langle\cos^2\psi\rangle - 1, \qquad \text{(Eq. 4.3)}$$

where ψ is defined in Figure 4.8. The order parameter is related to the dichroic ratio by:

$$S_2 = \frac{R-1}{R+1}\left(1 - 2\cos^2\alpha\right), \qquad \text{(Eq. 4.4)}$$

where α is the angle between a specific transition moment and the molecular symmetry axis. For the vibrations in and out of the plane of the Pc ring, $\alpha = 90°$ and $0°$ respectively.

The calculated values of S_2 (Tables 4.3 - 4.10) are very reasonable when

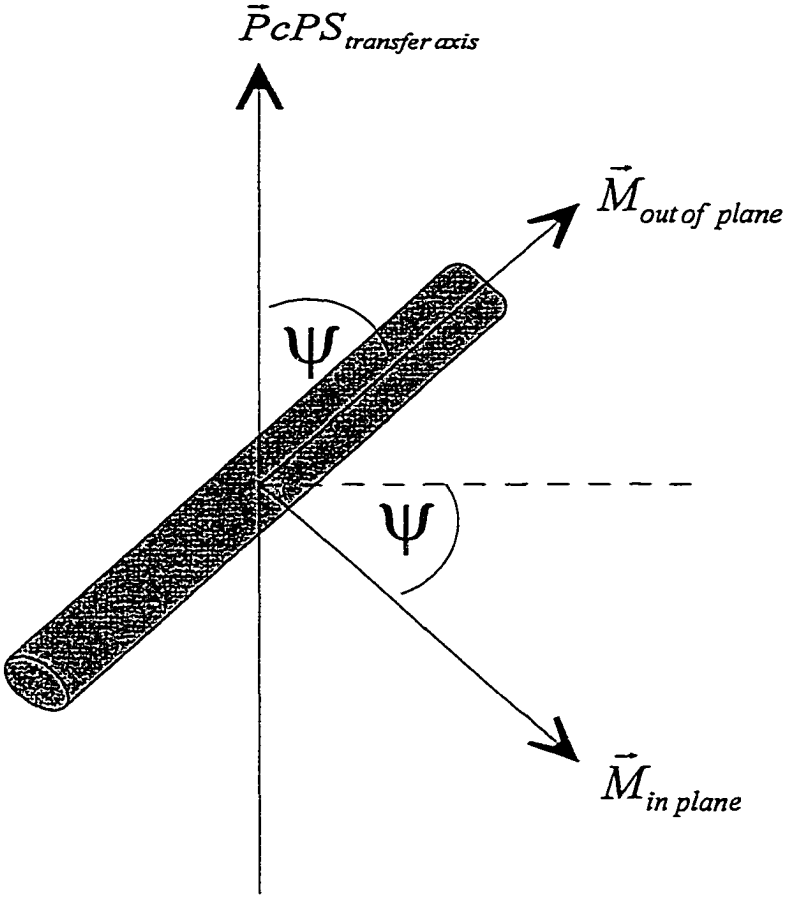

Figure 4.8, Definition of deviation angle, ψ, from the dipping direction based on dipole moments in the plane and out of the plane of the Pc molecule.

compared with that found for the Pc-PS system.[28] Sauer et al. report an average value of S_2 = ca. 0.35. The order parameters are generally higher for films deposited at low temperatures, and are greater on the DPTMDS modified surface for $CuPc(OC_2OBz)_8$ and on the HMDS modified surface for $H_2Pc(OC_2OBz)_8$. The highest order parameter reported for the $CuPc(OC_2OBz)_8$ film deposited at low temperature on a DPTMDS terminated surface (ca. 0.67) is substantially greater than that reported by Sauer et al.

We have shown previously that columnar assemblies of the Pc material align themselves parallel with the compression barriers of the LB trough using scanning probe microscopies.[14] Likewise, the PcPS system is reported to transfer parallel to the vertical dipping direction.[9]

Sauer et al. defined and determined the angle, ψ, that represents a deviation of the PcPS columns away from the dipping axis as defined in Figure 4.8. Unlike the PcPS system, where the Pc molecules are polymerized perpendicular to the main director axis, the phthalocyanine molecules of interest here are free to adopt a slip-stacked or angled stacking arrangement along the main director axis. We can still define a tilt angle, ψ, based on the interaction of a polarized electric field with a pair of orthogonal dipole moments in and out of the plane of the Pc core (Figure 4.9). The following relates equation 4.1 with the definition of ψ:[28]

$$R = \begin{cases} \dfrac{\langle \cos^2\psi \rangle}{\langle \sin^2\psi \rangle} = \dfrac{1-\langle \sin^2\psi \rangle}{\langle \sin^2\psi \rangle} & \textit{for in plane modes} \\ \dfrac{\langle \sin^2\psi \rangle}{\langle \cos^2\psi \rangle} = \dfrac{\langle \sin^2\psi \rangle}{1-\langle \sin^2\psi \rangle} & \textit{for out of plane modes} \end{cases} \qquad \text{(Eq. 4.5)}$$

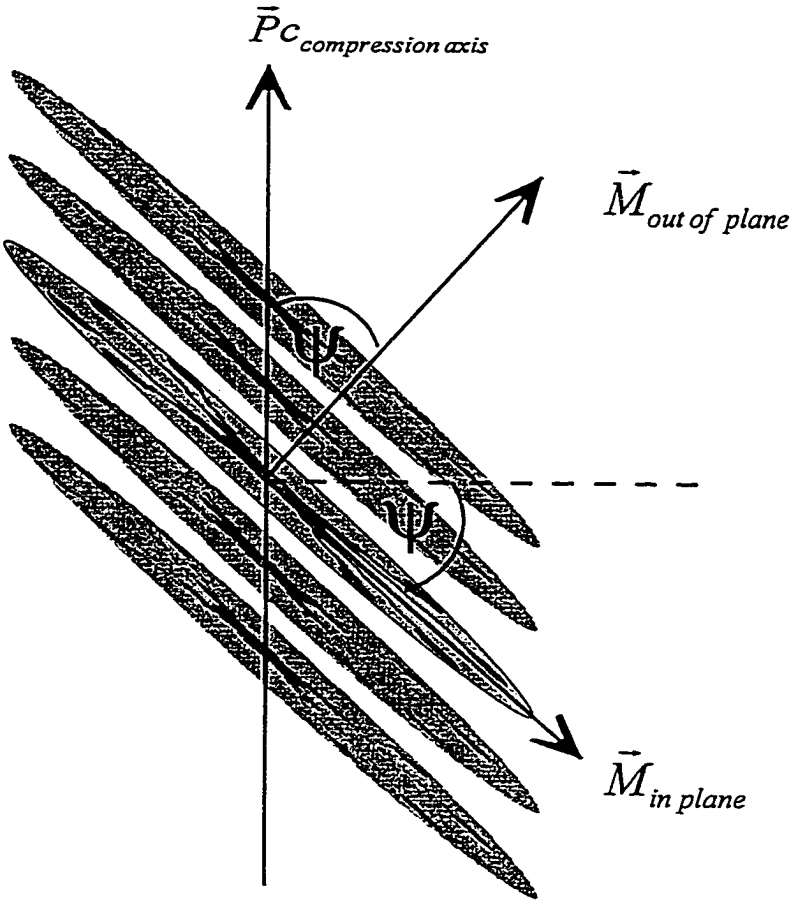

Figure 4.9, Definition of ψ for $CuPc(OC_2OBz)_8$ and $H_2Pc(OC_2OBz)_8$ Pc system.

This can then be simplified into:

$$\left\langle \sin^2 \psi \right\rangle = \begin{cases} \frac{1}{R+1} & \textit{for in plane modes} \\ \frac{R}{R+1} & \textit{for out of plane modes} \end{cases} \qquad \text{(Eq. 4.6)}$$

The sensitivity of Equation 4.6 to determine the tilt angle is dependant on the function plotted in Figure 4.10. At low dichroic ratios (< 1), there are large changes in tilt angle per unit change of dichroic ratio; at high dichroic ratios (> 7), there are gradual changes in tilt angle as the function approaches the x axis asymptotically. There are reasonable changes in ψ for the range of dichroic ratios found in these experiments.

Approximate values of ψ were found from the dichroic ratios and are listed for the eight cases (Tables 4.3 - 4.10). Previously reported tilt angles of $CuPc(OC_2OBz)_8$ were reported as ranging from 50° to 60°.[11] These angles are very close to the "magic angle" of 54.7° which is the angle found for a completely isotropic film. Clearly, the angles found under certain conditions for these films deviate significantly from the "magic angle."

The largest tilt angles are found for the least ordered films as defined by the order parameter, S_2, and were formed and transferred at elevated temperatures (Tables 4.4, 4.8, 4.10). Of the low temperature depositions, the smallest tilt angles are found for the $CuPc(OC_2OBz)_8$ film deposited on the DPTMDS modified surface (Table 4.5).

The tilt angles reported for the 745 cm^{-1} ring C-H out of plane bend and the 1204 cm^{-1}/1283 cm^{-1} Pc-O-C asymmetric/symmetric stretches should be of the same magnitude

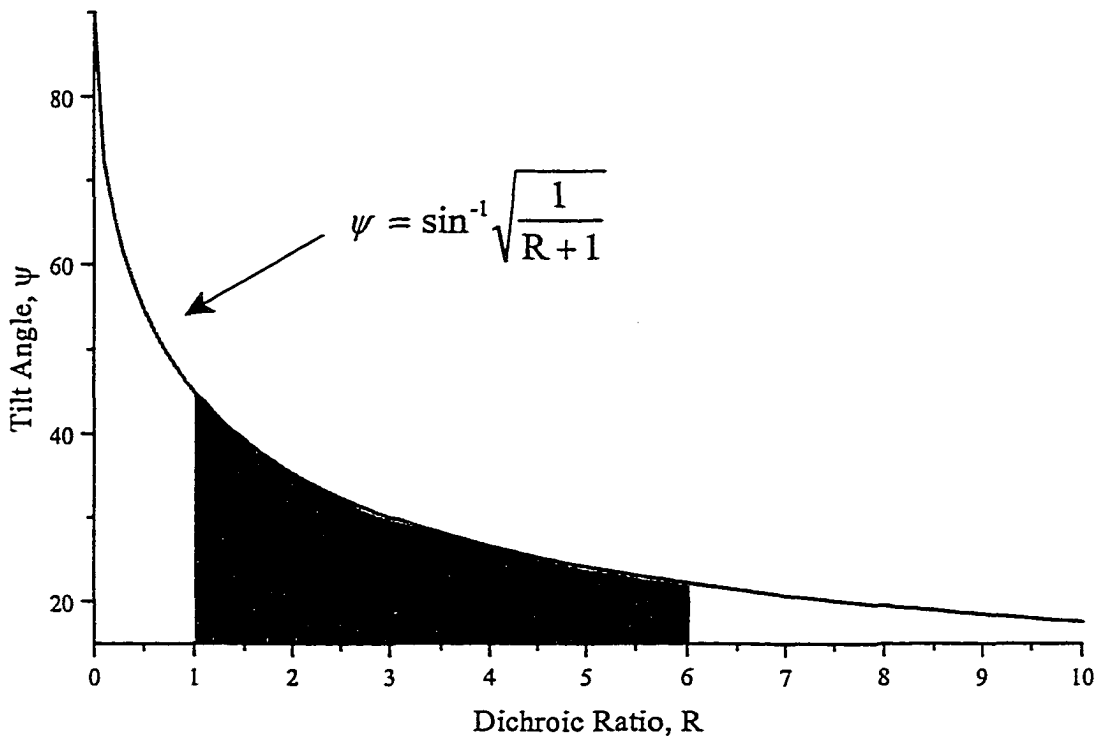

Figure 4.10, Plot of tilt angle, ψ, versus the dichroic ratio, R, showing large changes in tilt angle per unit change at low dichroic ratios and small changes in tilt angle per unit change at high dichroic ratios. Shaded region encompasses dichroic ratio range used to determine ψ in these experiments.

under the assumption that they are orthogonal vibrations. The agreement between the tilt angle magnitudes are fairly close throughout these experiments, but the tilt angle for the 745 cm^{-1} ring C-H out of plane bend is consistently higher.

The C-O-C asymmetric stretch, at 1103 cm^{-1}, indicates the tilt angle of the side chains. In a number of cases, this tilt angle is larger than that seen for the in plane asymmetric/symmetric stretches at 1204 cm^{-1} and 1283 cm^{-1}, respectively . Looking at the most ordered films, Table 4.5 for $CuPc(OC_2OBz)_8$ and Table 4.7 for $H_2Pc(OC_2OBz)_8$, The tilt angle indicated by the 1103 cm^{-1} stretch is ca. 6° greater than the tilt angle determined by the 1204 cm^{-1}/1283 cm^{-1} stretches for the Pc macrocycle (Figure 4.11.a). The increase in tilt angle may be an indication of disorder, or a real measure of the conformation of the side chains with respect to the Pc macrocycle.

Previously reported WAXS data recorded for fibers of $CuPc(OC_2OBz)_8$ show broad reflections at large angles which may be due to various molecular lattice spacings of side chains and Pc macrocycles within the columnar assemblies.[10] Further WAXS studies of these new well ordered films should indicate whether there are at least two different lattice spacings from reflections at large angles due to differences in tilt angle of the side chains versus the Pc macrocycle (Figure 4.11.b)

The significance of the tilt angles reported here will become more apparent when they are compared with another tilt angle measurement derived for the RAIRS experiment as discussed in Section 4.5.

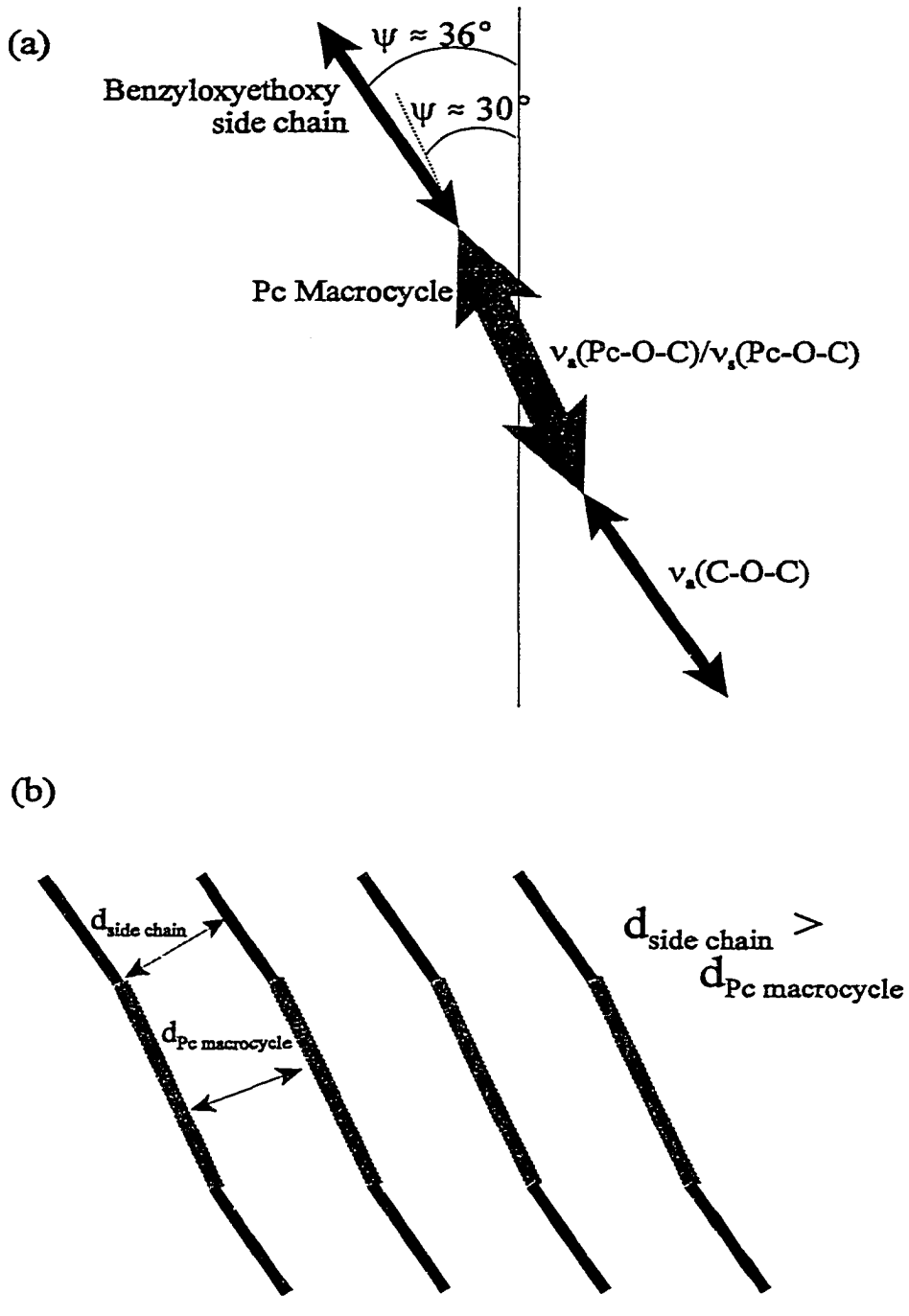

Figure 4.11, The difference in tilt angles, ψ, as indicated by the side chain and Pc macrocycle vibrations of $CuPc(OC_2OBz)_8$ (a). The difference in tilt angles may be quantitatively determined by WAXS reflections from the corresponding differences in lattice spacings (b).

4.4 Transmission Polarized IR Spectroscopy of Annealed films

There has been previous evidence that annealing of LB deposited thin films increases their anisotropy.[13, 28] Polarized IR spectra of a 7 bilayer film of $CuPc(OC_2OBz)_8$ on Si(100) were taken before and after annealing in air for 2 hours at 100° C. As seen in Figure 4.12, the intensities of the modes in the plane of the Pc molecule increase with polarized light perpendicular to the Pc column axis and the intensity of the out of plane mode increases with polarized light parallel to the Pc column axis. Note that an improvement of the overall ordering in the unannealed sample has increased as well, putting to use some of the findings discussed in the previous section (Table 4.13). The net result is an increase in the dichroic ratios upon annealing as listed in Table 4.14.

Calculated values of ψ and S_2, also in Tables 4.13 - 4.14, show that there is an overall decrease in the tilt angle and an increase in the order parameter upon annealing. The tilt angle of the side chains, as indicated by the 1103 cm^{-1} ν_a(C-O-C) vibration, is tilted ca. 9° from the tilt angle of the Pc macrocycle. Further WAXS studies on these annealed well ordered films should confirm this.

The specific effects of annealing at the microscopic level are unknown, but are supposed to be due to rearrangement of the molecules into a lower energy configuration. Several events may occur simultaneously: the Pc columns may incorporate stray "monomers" into the columnar array, a larger fraction of the Pc columns likely move into the close packed hexagonal array, and the elimination of excess water of hydration in the film may also occur, which has been seen previously.[14]

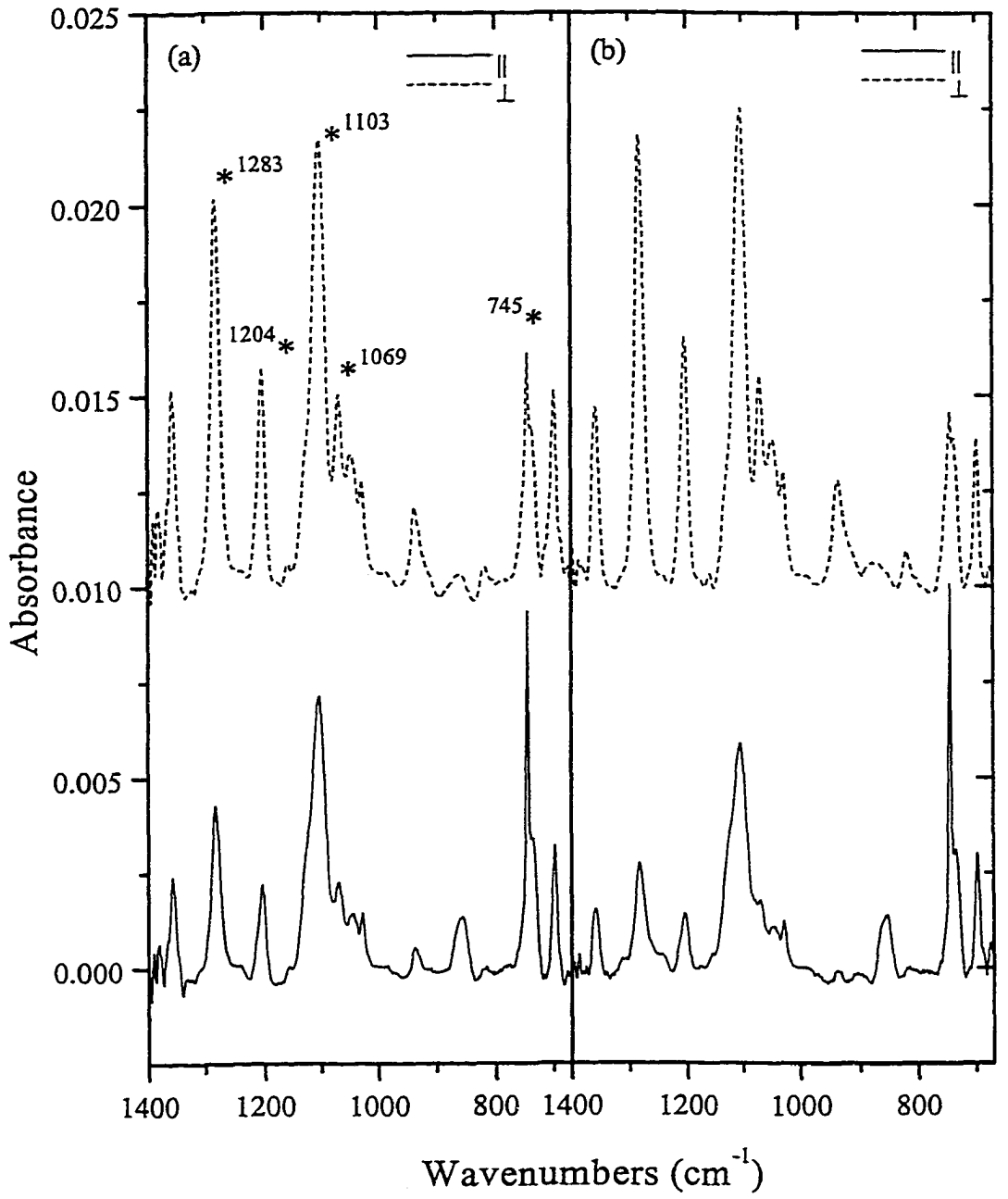

Figure 4.11, IR linear dichroism spectra of 7 bilayer films of $CuPc(OC_2OBz)_8$ (a) before and (b) after annealing for 2 hours at 100° C in air.

Table 4.13, Absorbance intensities for un-annealed 7 bilayer film of $CuPc(OC_2OBz)_8$ on Si(100) modified with HMDS at 23.4° C upon transfer.

Wavenumbers (cm^{-1})	Electric field ⊥ to Pc columns	Electric field ∥ to Pc columns	R	S_2	ψ
745	0.00651	0.00935	0.70	0.18	39.8°
1069	0.00543	0.00227	2.40	0.41	32.9°
1103	0.01213	0.00713	1.70	0.26	37.5°
1204	0.00617	0.00220	2.80	0.47	30.9°
1283	0.01058	0.00429	2.47	0.42	32.5°
		Average	2.16	0.35	37°
		STD	0.57	0.12	8°

Table 4.14, Absorbance intensities for annealed 7 bilayer film of $CuPc(OC_2OBz)_8$ on Si(100) modified with HMDS at 23.4° C upon transfer.

Wavenumbers (cm^{-1})	Electric field ⊥ to Pc columns	Electric field ∥ to Pc columns	R	S_2	ψ
745	0.00467	0.01004	0.46	0.37	34.3°
1069	0.00562	0.00178	3.15	0.52	29.4°
1103	0.01258	0.00588	2.14	0.36	34.4°
1204	0.00662	0.00143	4.64	0.65	24.9°
1283	0.01191	0.00276	4.31	0.62	25.7°
		Average	3.28	0.32	34°
		STD	1.17	0.21	13°

4.5 Reflection Absorption Infrared Spectroscopy (RAIRS)

Reflection absorption infrared spectroscopy is used primarily in two different areas of research; the study of the vibrational properties of adsorbed molecules in ultra high vacuum, and the study of organic layers deposited onto a metal substrate.[26] We are concerned with the later.

RAIRS spectroscopy has an inherent surface selection rule that makes it a very useful technique for studying the orientation of organic molecules at a reflective surface such has been done to determine the average tilt angle of self-assembled monolayers on gold surfaces.[17] An advantage of determining the orientation of a more complicated molecule is the greater amount of functional groups which can be probed by vibrational spectroscopy. If the location of a certain vibration is known with respect to others within a molecule and with respect to a laboratory coordinate system, then the orientation of the molecule can be determined.

4.5.1 RAIRS Theory

Because of the grazing angle of incidence associated with the RAIRS experiment there are certain selection rules that make this technique uniquely sensitive to the orientation of transition dipoles relative to the reflective surface.

The configuration of the RAIRS experiment is shown in Figure 4.13. The incident beam, composed of its TE and TM components, strikes the metal surface at some angle, θ. The TE component will be referred to as the s-wave component (parallel with the incident surface) and the TM component will be referred to as the p-wave component

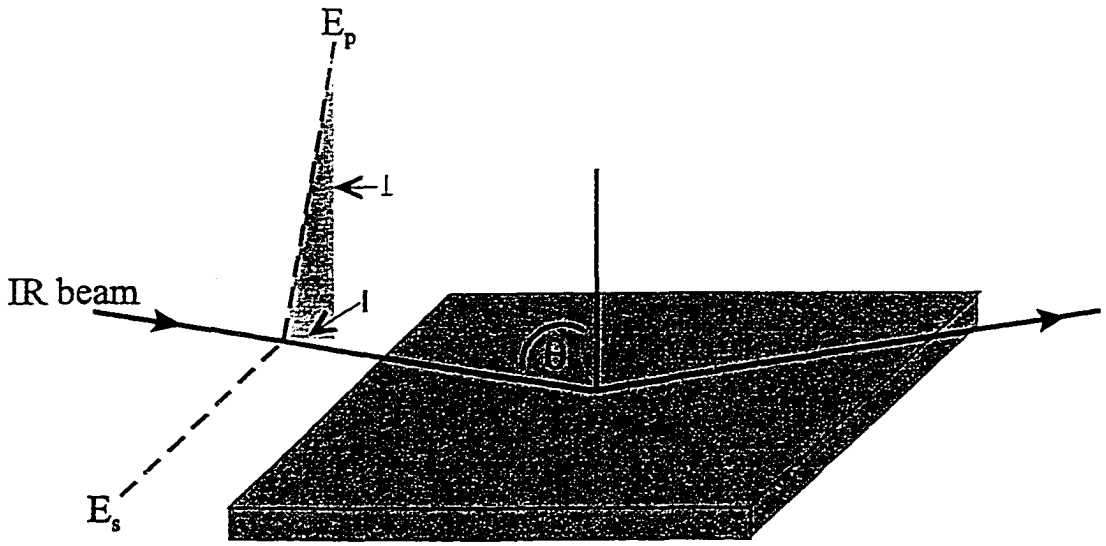

Figure 4.13, Configuration of RAIRS experiment at grazing incidence. The p-polarized IR standing wave has perpendicular and parallel components with respect to the surface, whereas the s-polarized light has components both parallel to the surface.

(perpendicular to the incident surface). At an incident grazing angle the s-wave component remains parallel to the surface, but the p-wave component has surface normal ($\perp$) and surface parallel ($\parallel$) components.

As the incident beam is reflected, there is a phase shift at the interface. The magnitude and direction of the field at the interface is dependent on the phase shift. The phase shift for s-wave components, including the surface parallel component of the p-wave is ca. 180° for all angles.[26] This results in a very small field parallel to the surface at the probing region. Conversely, the surface normal component of the p- wave phase shift is very dependent on the incident angle and reaches a phase shift of $-\frac{\pi}{2}$ at ca. 88°, which results in nearly doubling the field normal to the surface at the probing area.

It is known that the IR absorption intensity is dependent on the square of the electric field vector, E. Therefore, with grazing angle incidence, the absorption intensity associated with $E_{p\perp}$ is dependent on the angle of incidence, and can be nearly twice that of $E_{p\parallel}$, or E_s field components.[26] Because of these surface selection rules, RAIRS is specifically targeted to probe transition dipoles having components aligned perpendicular to the reflective surface.

By defining a coordinate system with respect to the plane of reflection, and defining a coordinate system with respect to specific dipole transitions within a molecule, one can relate the two and determine a relative orientation of the molecules with respect to the surface. This strategy, and the theory behind it has been explained by a number of researchers.[8, 40] The work of M. K. Debe has been chosen for the discussion here.[26, 27]

4.5.2 Debe Theory on Determination of Molecular Orientation

Debe's treatment requires that there be two or more vibrational modes within a molecule that are mutually orthogonal and can be used to define a plane with respect to the molecule. For our purposes vibrations in and out of Pc macrocycle core were chosen to define the molecular plane. The ν(Pc-O-C) symmetric and asymmetric stretches at 1204cm^{-1} and 1283cm^{-1} respectively are in the plane of the Pc ring and the δ(ring C-H,op) bend at 745cm^{-1} is out of the plane. Therefore, **the molecular plane is orthogonal to the plane of the Pc macrocycle** (Figure 4.14).

The orientation of the molecular plane can be determined by a set of simple equations that relate the molecular plane to the surface coordinates via Euler angles. Following is an account of Debe's derivation in the context of the molecules of interest here. One should refer to the original publications for a full derivation.

The Euler angles, ψ_{Debe} and θ, are defined in relation to the molecular plane coordinates (x', y', z') and the surface coordinates (x, y, z) in Figure 4.15. The two sets of coordinates are related by a transformation matrix:

$$\begin{pmatrix} x' \\ y' \\ z' \end{pmatrix} = \begin{pmatrix} \cos\psi_{Debe} & \cos\theta\sin\psi_{Debe} & \sin\psi_{Debe}\sin\theta \\ -\sin\psi_{Debe} & \cos\theta\cos\psi_{Debe} & \cos\psi_{Debe}\sin\theta \\ 0 & -\sin\theta & \cos\theta \end{pmatrix} \begin{pmatrix} x \\ y \\ z \end{pmatrix} \quad \text{(Eq. 4.7)}$$

We let $I^t_{i,o}$ represent the intensity of the ith vibrational band of an out of plane vibration of the Pc molecule and $I^t_{i,i}$ represent the intensity of the ith vibrational band in the plane of

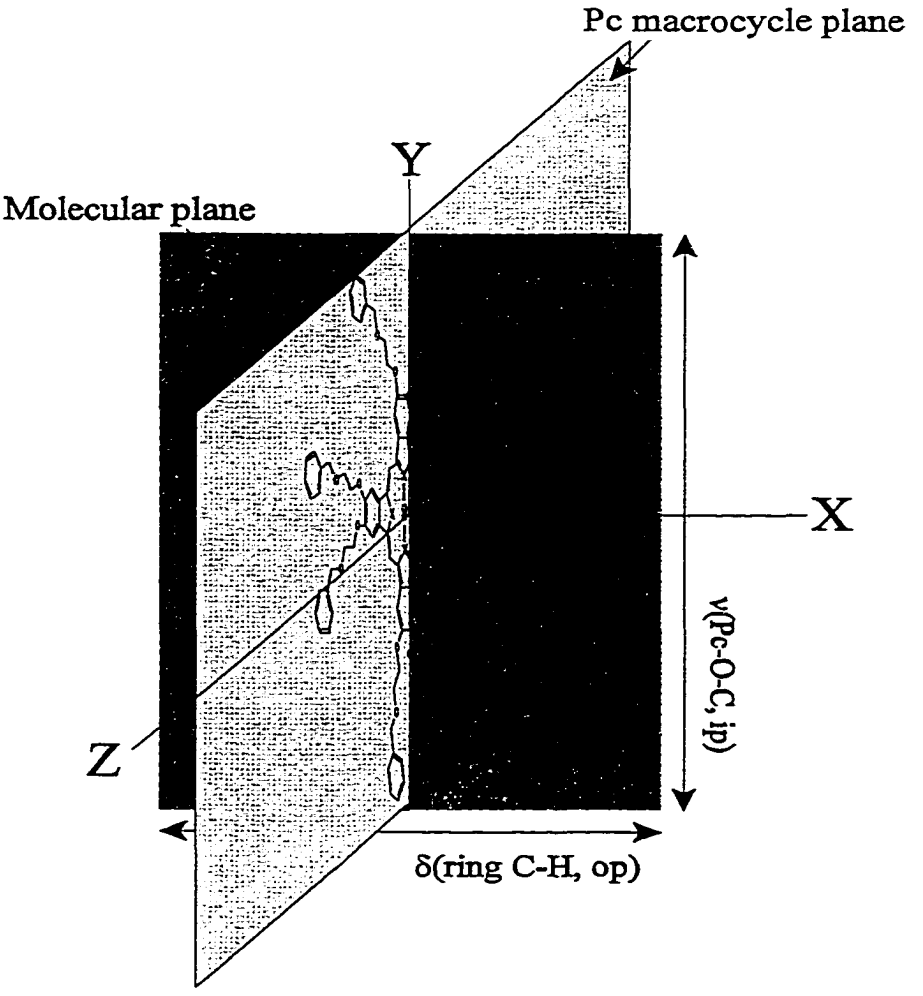

Figure 4.14, The molecular plane, defined by the orthogonal vibration pair, is perpendicular to the Pc macrocycle plane.

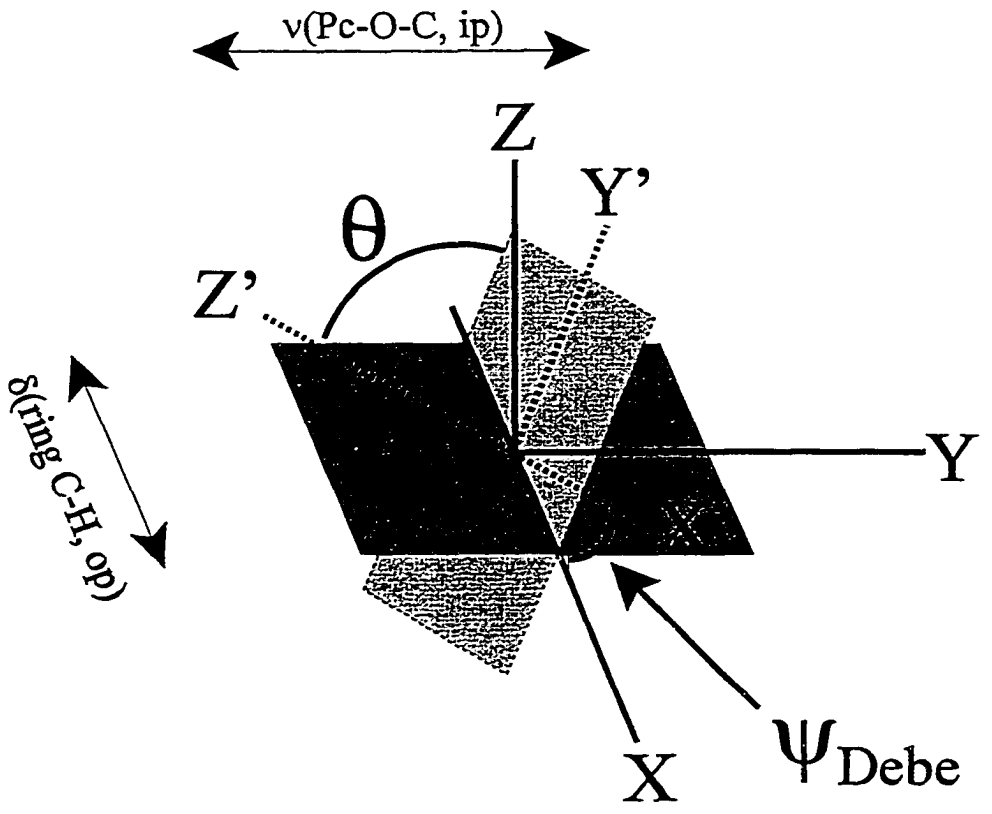

Figure 4.15, Definition of Euler angles, ψ_{Debe} and θ, with respect to the molecular plane defined by IR active vibrations in and out of the plane of the phthalocyanine molecule.

the Pc molecule (both intensities represented as thin film intensities by the superscript t). Recall that the intensity of a band is proportional to the square of the dipole moment, M_i, and the electric field vector, E $\therefore$ $I_i \propto |M \cdot E|^2$. We assign the out- of plane moment to be parallel to x' and the in plane moment be parallel to y'. From the transformation matrix we see that:

$$M_{i,i} = |M_{i,i}|\hat{y}' \& M_{i,o} = |M_{i,o}|\hat{x}'. \qquad \text{(Eq. 4.8)}$$

Taking into account that the only portion of the dipole moment that is probed is parallel to the surface normal we can write:

$$\begin{aligned} M_{i,i} \cdot \hat{z} &= |M_{i,i}|\hat{y}' \cdot \hat{z} = |M_{i,i}|\cos\psi_{Debe}\sin\theta \\ M_{i,o} \cdot \hat{z} &= |M_{i,o}|\hat{x}' \cdot \hat{z} = |M_{i,o}|\sin\psi_{Debe}\sin\theta \end{aligned} \qquad \text{(Eq. 4.9)}$$

The resultant intensities of the orthogonal mode pair can then be written:

$$\begin{aligned} I^t_{i,i} &\propto |M_{i,i}|^2 |E|^2 \cos^2\psi_{Debe}\sin^2\theta \\ I^t_{i,o} &\propto |M_{i,o}|^2 |E|^2 \sin^2\psi_{Debe}\sin^2\theta \end{aligned} \qquad \text{(Eq. 4.10)}$$

Debe defined a fractional change, δ, in the relative absorbance between an isotropic bulk spectrum and that of a thin film spectrum:

$$\delta_i \equiv \frac{I^t_i - I^b_i}{I^b_i} = \frac{I^t_i - \frac{1}{3}I_i}{\frac{1}{3}I_i} = 3\frac{I^t_i}{I_i} - 1 \qquad \text{(Eq. 4.11)}$$

where I_i is the maximum intensity possible, which corresponds to $M_i \| E$. The maximum intensities are again proportional to the square of the dipole moment and electric field vector:

$$I_{i,i} \propto \left|M_{i,i}\right|^2 |E|^2 \;\&\; I_{i,o} \propto \left|M_{i,o}\right|^2 |E|^2 . \qquad \text{(Eq. 4.12)}$$

Combining equations 4.10, 4.11, and 4.12 we are left with two simple equations relating the Euler angles to the change in measured absorption of two orthogonal bands within the molecule:

$$\begin{aligned} \delta_{i,i} &= 3\cos^2\psi_{Debe}\sin^2\theta - 1 \\ \delta_{i,o} &= 3\sin^2\psi_{Debe}\sin^2\theta - 1 \end{aligned} \qquad \text{(Eq. 4.13)}$$

Looking back to the definition of δ, we can simplify equation 4.13 in terms of the measured intensities:

$$\begin{aligned} \frac{I^t_{i,i}}{I^b_{i,i}} &= 3\cos^2\psi_{Debe}\sin^2\theta \\ \frac{I^t_{i,o}}{I^b_{i,o}} &= 3\sin^2\psi_{Debe}\sin^2\theta \end{aligned} \qquad \text{(Eq. 4.14)}$$

Solving these equations simultaneously we can determine ψ_{Debe} by

$$\frac{I^t_{i,o}}{I^b_{i,o}} \times \frac{I^b_{i,i}}{I^t_{i,i}} = \tan^2\psi_{Debe} \text{ or } \frac{I^t_{i,o}}{I^t_{i,i}} \times \frac{I^b_{i,i}}{I^b_{i,o}} = \tan^2\psi_{Debe} \text{ and } \theta \text{ by } \frac{I^t_{i,o}}{3I^b_{i,o}\sin^2\psi_{Debe}} = \sin^2\theta$$

$$\text{or } \frac{I^t_{i,i}}{3I^b_{i,i}cos^2\psi_{Debe}} = \sin^2\theta .$$

4.5.3 Qualitative Evaluation of Spectroscopic Results

A priori, we expect that the Pc molecules would be at some angle with respect to the surface. This expectation is based on previously reported x-ray reflection data and molecular modeling.[11] Snow, et al. have recently shown that substituted Pc molecules that are vacuum deposited on Au can be sitting perpendicular to the surface; they base this on the absence of an out-of-plane absorption peak in the RAIRS spectrum they report.[32] For any vibration to be absent, it has to be absolutely parallel to the surface of reflection. Since the δ(ring C-H,op) bend is perpendicular to the Pc macrocyle plane it must be oriented orthogonal to the surface.

Figure 4.16.c shows the spectrum of a single bilayer film of $CuPc(OC_2OBz)_8$ on a Au surface that was modified with 1-benzyloxyethanethiol. It can be seen that there is an absorption band present at 745 cm^{-1}, indicating that our Pc molecules are not standing on end, orthogonal to the surface, but are at some determinable angle. The same can be seen for the case of $H_2Pc(OC_2OBz)_8$ in Figure 4.17.c.

Different modifications of the Au surface were chosen to investigate whether the Pc Langmuir film would interact preferentially with a surface functionalized with 1-benzyloxyethanethiol over a surface functionalized with an alkane thiol of approximately the same chain length. The hypothesis was that the substituent arms on the Pc have a great deal of influence over the packing of the Pc columnar assemblies. A surface functionalized with 1-benzyloxyethanethiol would look like a sheet of next neighboring Pc columns to the Pc column in the Langmuir film, and would pack on that layer as it

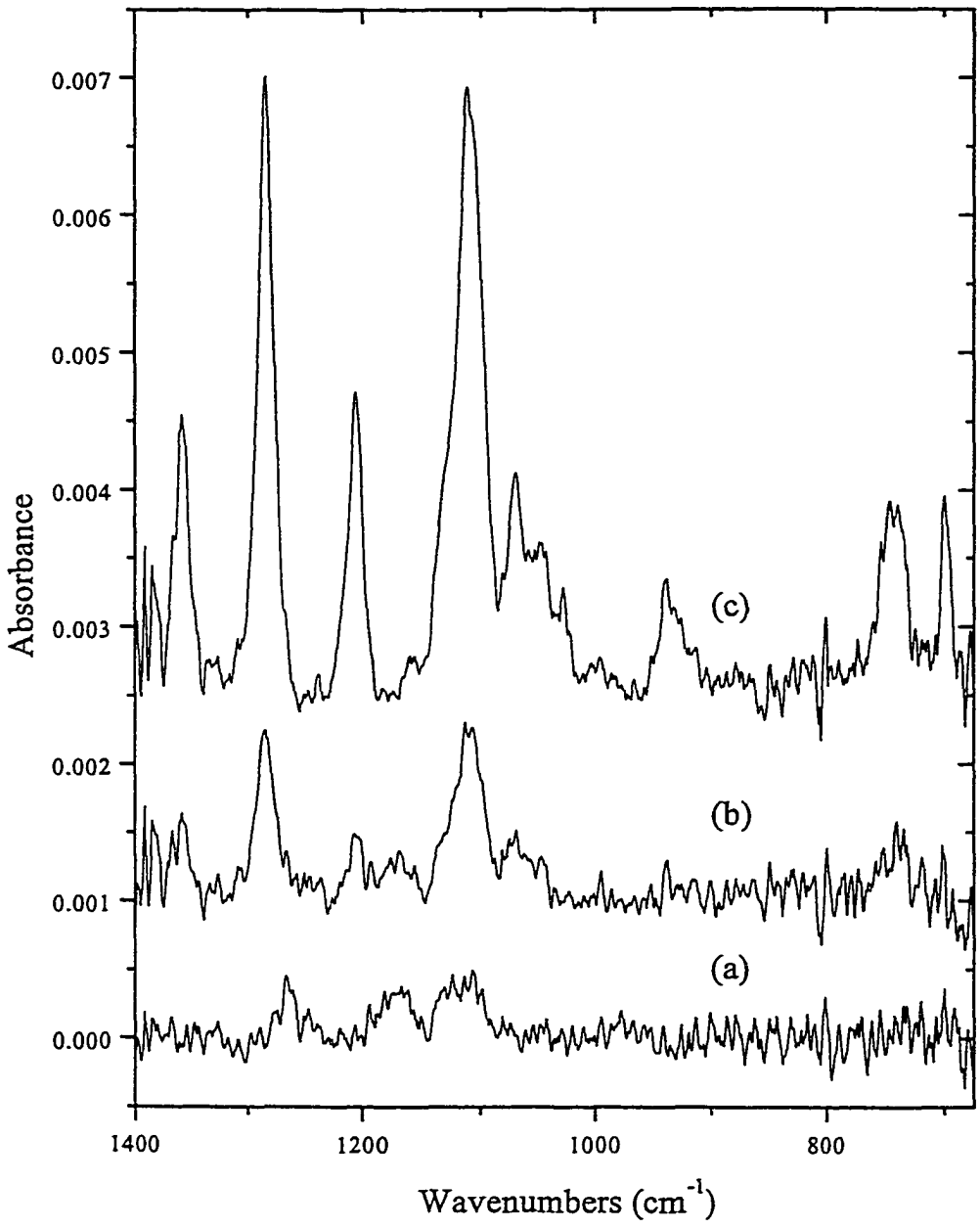

Figure 4.16, RAIRS spectra of 1 bilayer films of $CuPc(OC_2OBz)_8$ deposited on Au (a) un-modified, (b) modified with octanethiol, and (c) modified with benzyloxyethanethiol.

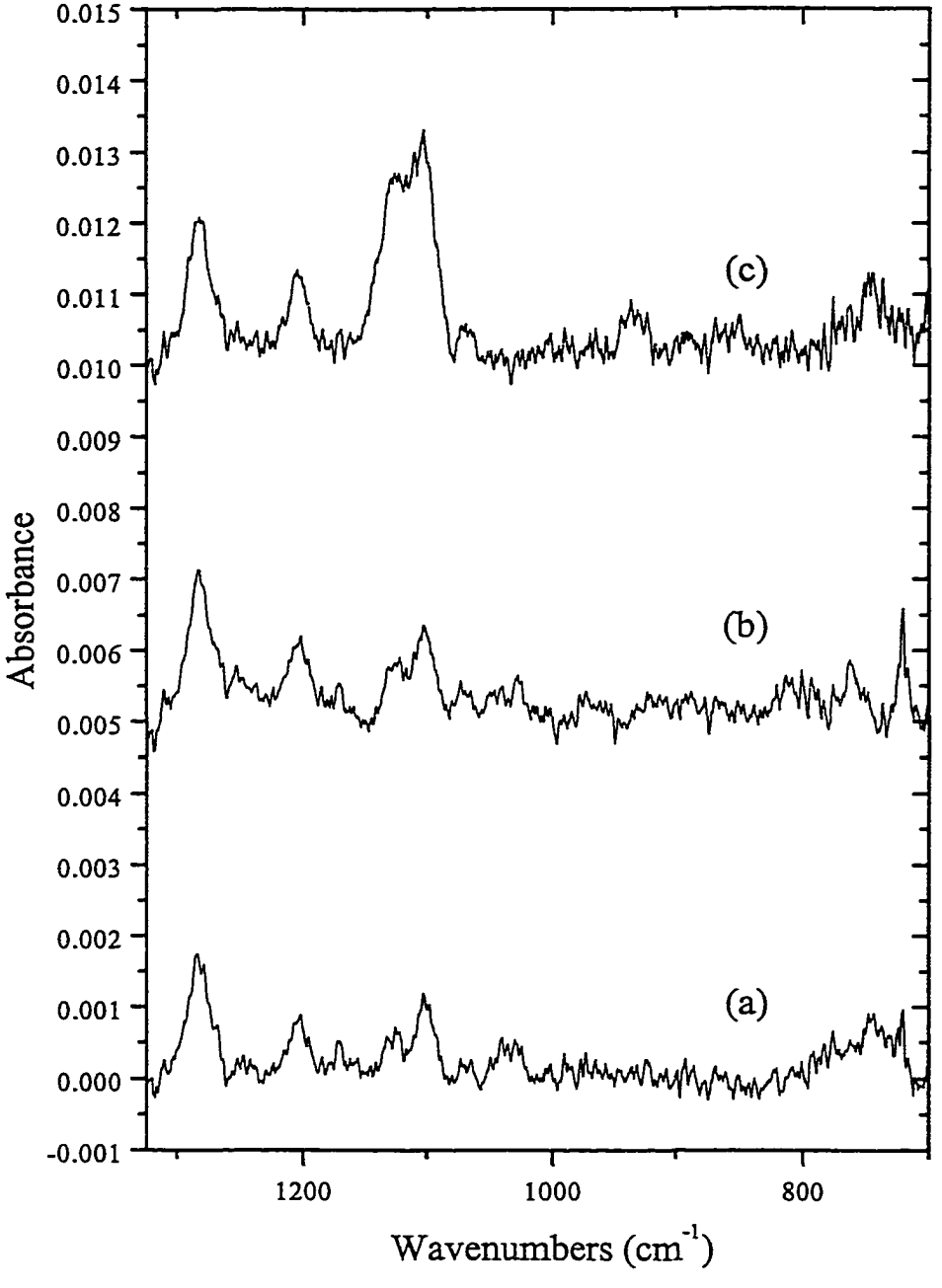

Figure 4.17, RAIRS spectra of 1 bilayer films of $H_2Pc(OC_2OBz)_8$ deposited on Au (a) un-modified, (b) modified with octanethiol, and (c) modified with benzyloxyethanethiol.

does in multilayer Langmuir-Blodgett films.

Looking at the spectra in Figure 4.16 and 4.17, it is apparent that the LB deposited thin films of $CuPc(OC_2OBz)_8$ and $H_2Pc(OC_2OBz)_8$ interact more effectively with the 1-benzyloxyethanethiol modified surface (c) than that modified with 1-octanethiol (b), and much more than a bare gold surface (a). The gold surface modified with the 1-benzyloxyethanethiol better approximates the next closest bilayer film and minimizes orientational deformations due to the impingement of the substrate surface. Therefore, our imminent determination of orientation angles with respect to the surface can be extended as an approximation of orientation angles of the Pc molecules in multilayer films as determined from these data.

The small magnitude of intensities seen in parts a and b of Figures 4.16 and 4.17 indicate that the transfer of $CuPc(OC_2OBz)_8$ and $H_2Pc(OC_2OBz)_8$ films to the bare gold and 1-octanethiol surfaces are not as efficient as to the benzyloxyethanethiol modified surface, and/or the bare gold and 1-octanethiol surfaces impart deformation of the self-assembly, perhaps rearranging the Pc molecules more parallel with the surface.

The implications of either of these processes is precluded by the subsequent transfer of ordered films. Figures 14.18 and 14.19 show three bilayer films of $CuPc(OC_2OBz)_8$ and $H_2Pc(OC_2OBz)_8$ on the same series of substrates. The maximum intensities vary little between the three spectra; therefore, the effects of an inefficient or disordered base transfer layer are not seen in a multilayer film.

The spectra of one and three bilayer LB deposited films of $H_2Pc(OC_2OBz)_8$ reflect

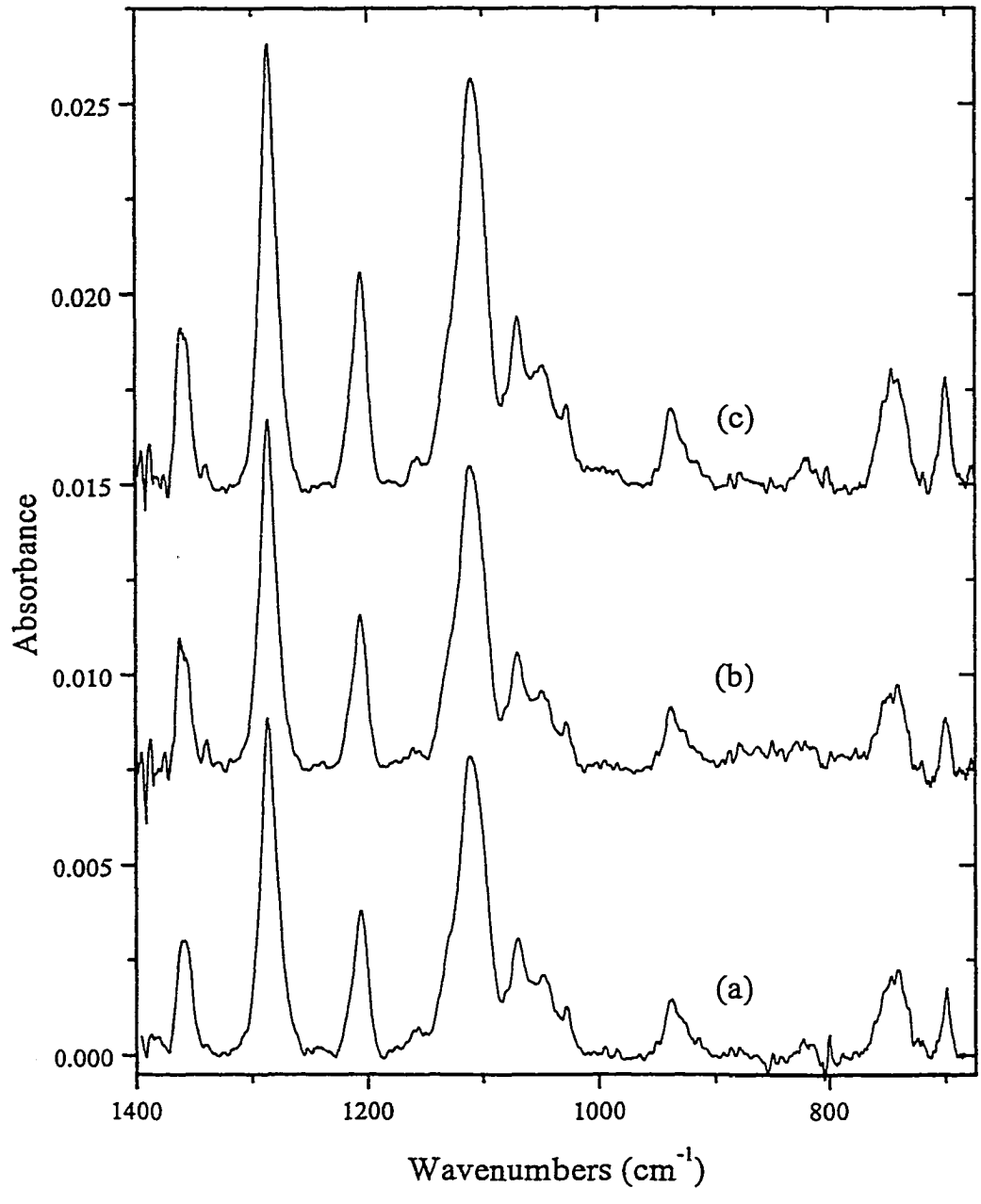

Figure 4.18, RAIRS spectra of 3 bilayer films of $CuPc(OC_2OBz)_8$ deposited on Au (a) un-modified, (b) modified with octanethiol, and (c) modified with benzyloxyethanethiol.

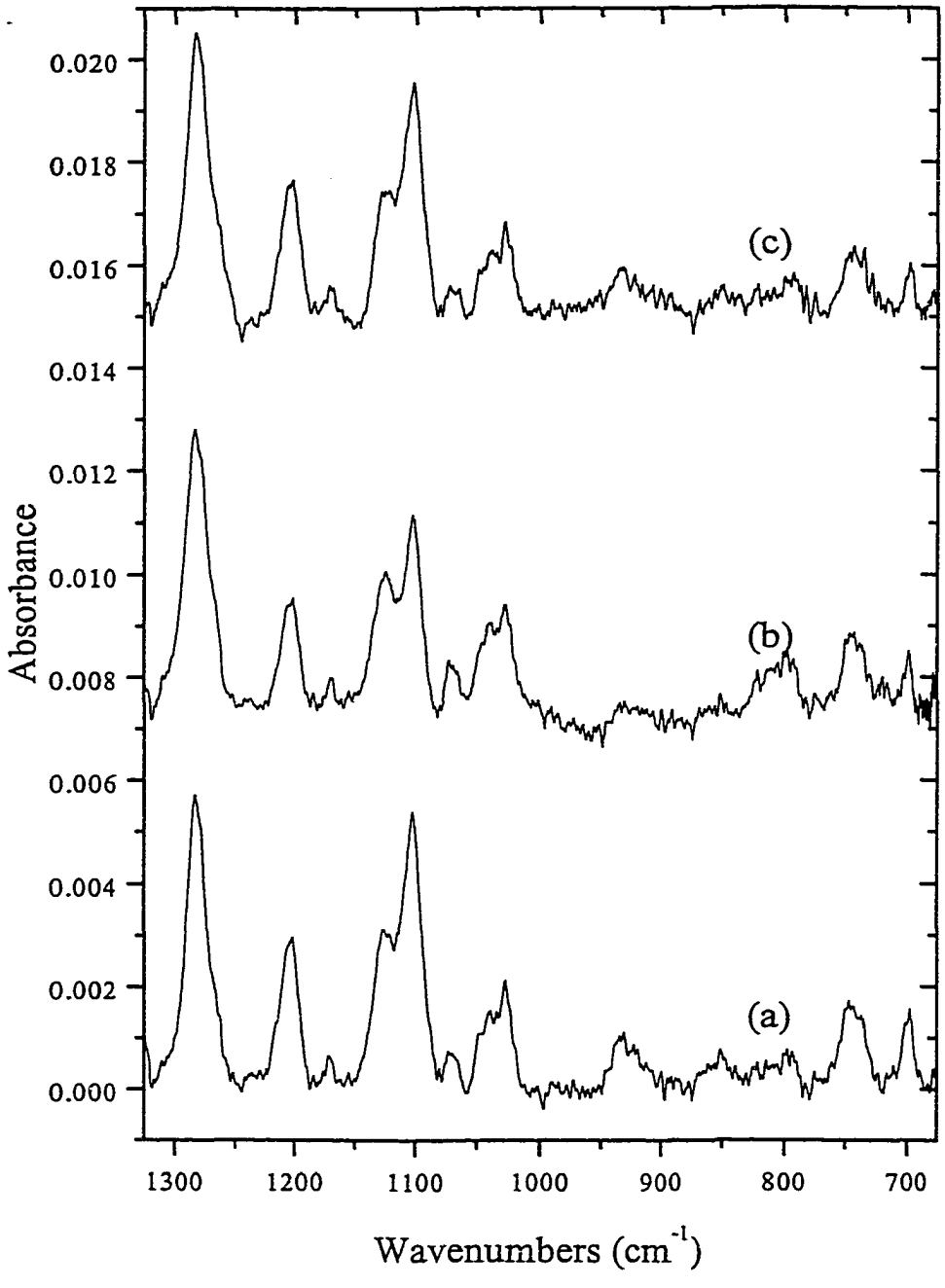

Figure 4.19, RAIRS spectra of 3 bilayer films of $H_2Pc(OC_2OBz)_8$ deposited on Au (a) un-modified, (b) modified with octanethiol, and (c) modifiedwith benzyloxyethanethiol.

those results found for the $CuPc(OC_2OBz)_8$ thin films. There appears to be greater transfer effectiveness of the Langmuir films to 1-benzyloxyethanethiol modified Au surfaces, although the effects are not as pronounced as in the $CuPc(OC_2OBz)_8$ case.

The exclusive transfer of ordered films to the benzyloxyethanethiol modified Au surface may lead to future micro patterning of these films.

4.5.4 Quantitative Analysis: Evaluation of Debe Theory

As was derived previously, Debe's treatment relates the position of a plane defined with respect to the molecule, the molecular plane, to the surface plane by Euler angles, ψ_{Debe} and θ. The molecular plane was defined by two orthogonal vibrations, the ν(Pc-O-C) symmetric and asymmetric stretches at $1204cm^{-1}$ and $1283cm^{-1}$ and the δ(ring C-H,op) bend at $745cm^{-1}$. The ν(Pc-O-C) symmetric and asymmetric stretches are located in the plane of the Pc macrocyle and the δ(ring C-H,op) bend at $745cm^{-1}$ is located out of the plane. Two vibrations within the plane of the Pc where chosen because they were available, and because it allows for a confirmation of calculated orientation angles. Again, the plane defined by the ν(Pc-O-C) stretch and the δ(ring C-H, op) bend is orthogonal to the Pc macrocyle as shown in Figure 4.14. The conformational effects of rotating through the Euler angles specific to the $CuPc(OC_2OBz)_8$ and $H_2Pc(OC_2OBz)_8$ systems are defined in Figure 4.20 with respect to the molecular plane and in Figure 4.21 with respect to the Pc macrocycle.

Representative absorbances of the wavelengths of interest are tabulated for bulk , one, and three bilayer spectra of $CuPc(OC_2OBz)_8$ LB thin films in Table 4.15.

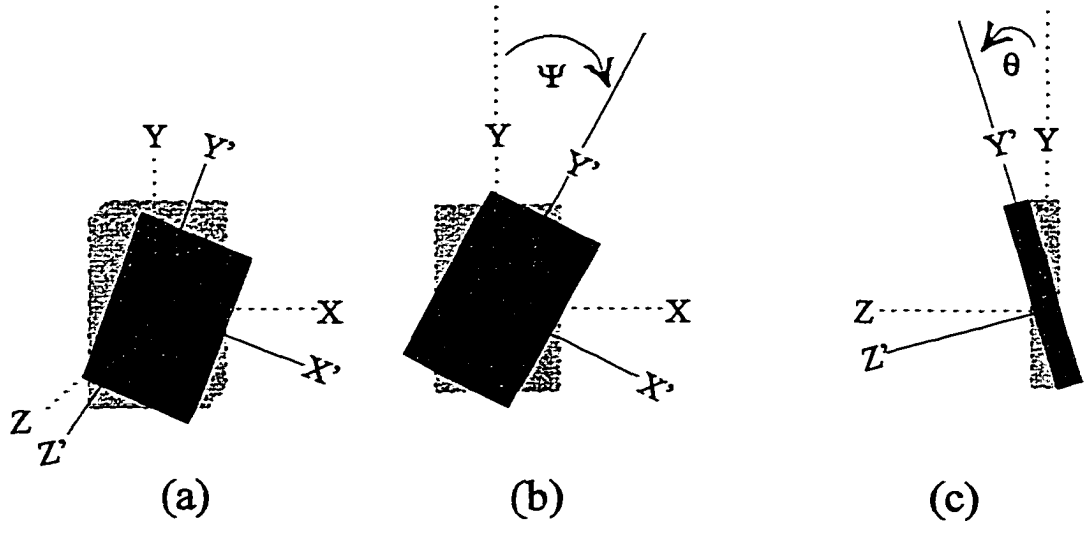

Figure 4.20, Molecular plane with respect to the surface coordinate x, y, z and with respect to orientation coordinates x', y', z' in (a) three dimensional perspective, (b) along the z axis, and (c) along the x axis.

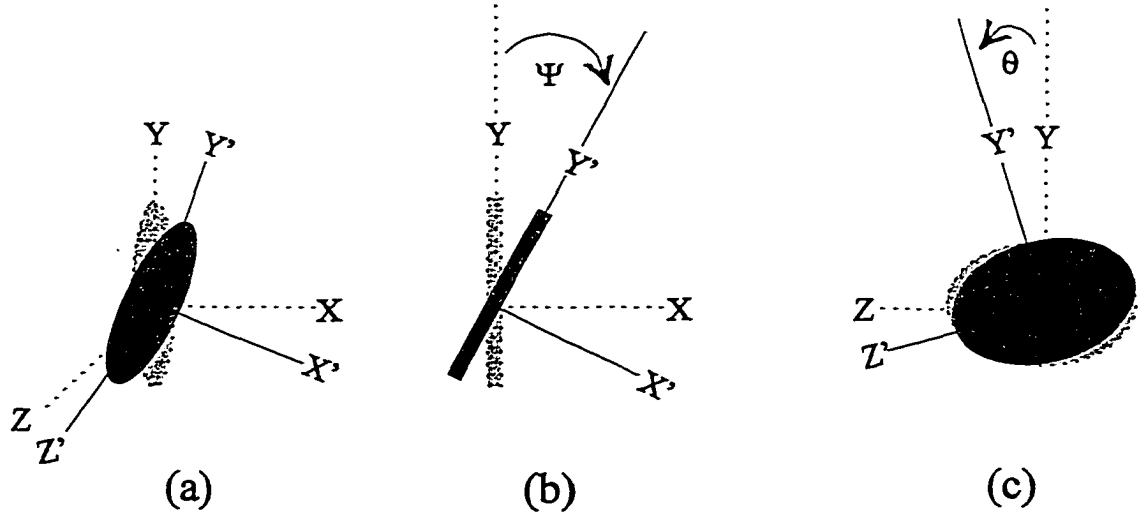

Figure 4.21, Pc macrocycle plane with respect to the surface coordinate x, y, z and with respect to orientation coordinates x', y', z' in (a) three dimensional perspective, (b) along the z axis, and (c) along the x axis.

Table 4.15, Absorbances of $CuPc(OC_2OBz)_8$ orthogonal mode pairs used to define the molecular plane.

	745 cm^{-1}	1204 cm^{-1}	1283 cm^{-1}
Bulk	0.0303	0.0197	0.0349
1 Bilayer	0.0015	0.0020	0.0047
3 Bilayers	0.0025	0.0038	0.008

Table 4.16, Absorbances of $H_2Pc(OC_2OBz)_8$ orthogonal mode pairs used to define the molecular plane.

	745 cm^{-1}	1283 cm^{-1}
Bulk	0.0274	0.0109
1 Bilayer	0.0009	0.0019
3 Bilayers	0.0012	0.0055

Using these absorbances and Equations 4.13 and 4.14 the Euler angles were determined. For the one bilayer film of $CuPc(OC_2OBz)_8$, $\psi_{Debe} = 32.5°$ and $\theta = 13.5°$. For the three bilayer film of $CuPc(OC_2OBz)_8$, $\psi_{Debe} = 30.2°$ and $\theta = 19.4°$. There is no statistical difference between the angles of ψ_{Debe} for the one and three bilayer films, although there is a significant difference between the angles of θ. This may be due to a reordering of the Pc molecules beyond the first bilayer transfer.

Representative absorbances for the $H_2Pc(OC_2OBz)_8$ LB thin films are listed in Table 4.16. There was not a well defined peak at 1204 cm^{-1} therefore, only one in plane vibration was used, the asymmetric stretch at 1283cm^{-1}. Euler angles were again determined using Equations 4.13 and 4.14. The one bilayer film of $H_2Pc(OC_2OBz)_8$ showed $\psi_{Debe} = 23.9°$ and $\theta = 15.7°$, and the three bilayer film of $H_2Pc(OC_2OBz)_8$ showed $\psi_{Debe} = 25.2°$ and $\theta = 16.2°$.

There is a marked decrease in ψ_{Debe}, the tilt angle in the xy plane rotated around the z axis for $H_2Pc(OC_2OBz)_8$. This would indicate that the phthalocyanine molecules are more edge normal to the surface. Molecular modeling calculations for un-substituted Pcs suggest that the metal center in one molecule is positioned above the bridging nitrogen in an adjacent molecule, known as a β polymorph.[11] This positioning imparts a "tilt" of the molecules with respect to the substrate surface. The tilt angle of this β polymorph is 45°, and would be expected to change due to influences from side chain substitution. Without the metal center, the $H_2Pc(OC_2OBz)_8$ molecules are oriented closer to the substrate surface normal.

4.6 Summary of IR Results

The transmission spectra of the bulk and thin films, along with the RAIRS spectra indicate the microscopic arrangements of the $CuPc(OC_2OBz)_8$ and $H_2Pc(OC_2OBz)_8$ molecules within the LB thin films as well as within the columnar assemblies.

The most generalized evaluation of the ordering within the films is given by the two dimensional order parameter, S_2, with 1.0 indicating a perfectly organized solid. Order parameters were calculated for LB thin films $CuPc(OC_2OBz)_8$ based on UV-Vis spectroscopic data and reported as $S_2 = 0.43$. We have shown that this order parameter measurement can be improved by using a baffle to segment the Langmuir film into isolated sections, using lower water subphase temperatures, and tailoring the surface of the substrate to include phenyl moieties that induced better transfer of an intact Langmuir film. The average order parameter value, $S_2 = 0.54 \pm 0.14$ under these conditions, is a marked improvement and has been observed to be as high as 0.65.

We have shown in Section 5.2.2 that the thin film ordering is increased upon annealing. This is supported by the increase in dichroic ratios and order parameters as discussed in Section 4.4. Wegner et al. reported a 50% increase in dichroic ratio upon annealing 15 monolayer films of PcPS;[28] Nolte et al. has more recently reported a 75% increase in dichroic ratio upon annealing 20 bilayer films of an stereoisomerically pure branched alkane substituted Pc.[13] The increase in dichroic ratios reported here for LB thin films of $CuPc(OC_2OBz)_8$ is very similar with percentage increases ranging from 30-75%.

Dichroic ratios and order parameters reported for the PcPs system by Wegner et al. and for thin films of $CuPc(OC_2OBz)_8$ by Smolenyak et al. were based upon the anisotropy found in UV-Vis spectra taken with perpendicular polarization of light. The use of infrared spectroscopy to probe the anisotropy of individual vibrational bands within the phthalocyanine columnar assemblies can lead to determination of molecular orientation within these assemblies, especially with regards to the RAIRS experiment.

A tilt angle, ψ, of the $CuPc(OC_2OBz)_8$ and $H_2Pc(OC_2OBz)_8$ macrocycle within the thin films defined as the deviation angle by Sauer et al., was calculated from the transmission IR spectra using polarized incident radiation. Larger tilt angles, closer to the "magic angle" of 54.7 ° for an isotropic film, were found for less ordered films formed and transferred at elevated temperatures. The tilt angle of the $CuPc(OC_2OBz)_8$ macrocycle, in the most ordered thin film formed and transferred at low temperatures onto a DPTMDS modified surface, is ca. 30 °and the side chain tilt angle is about 36 °. The conformation of the side chain tilt angle, relative to that of the Pc macrocycle, may be elucidated by WAXS experiments on these highly ordered thin films.

The RAIRS data are uniquely valuable because of the surface selection rules as discussed in Section 4.5.1. The average tilt angle as determined in the transmission experiments is actually the combination of two angles, ψ_{Debe} and θ, describing the rotation of the phthalocyanine molecule through two defined orthogonal planes with relation to specific vibrational transition moments within the molecule. To picture these rotations through ψ_{Debe} and θ is a feat of mental gymnastics. Figure 4.22 is presented as an aid in

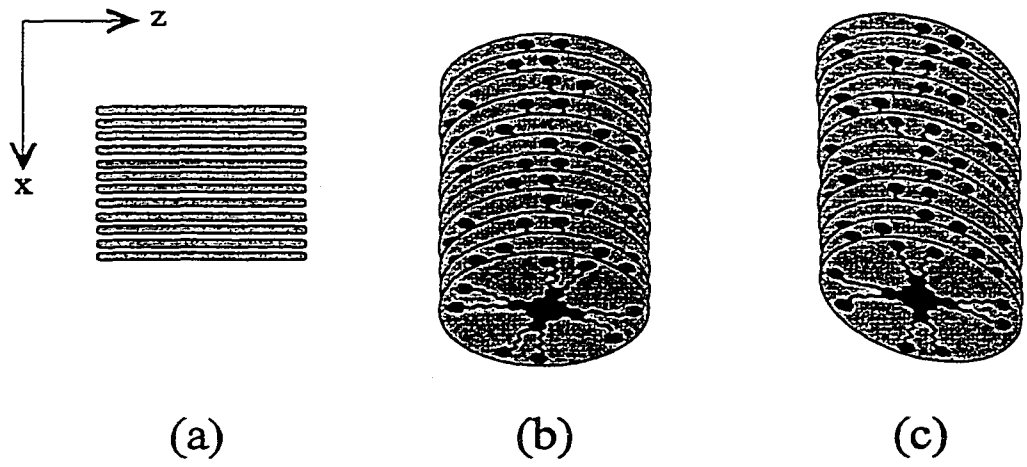

Figure 4.22, Top view of columnar assemblies viewed along y axis (a) before any rotation, (b) after rotation through ψ_{Debe}, and (c) after rotation through θ.

this process. Figure 4.22.a is a top view of a columnar assembly where each line represents a single phthalocyanine molecule. After rotation through ψ_{Debe}, the view from the top reveals the front face of the molecules, and flattening of the columns (Figure 4.22.b). Rotation through θ further deforms the flattened columns into elliptical assemblies (Figure 4.22.c).

Note that the rotational orientation of the Pc molecules within these elliptical assemblies are depicted as random in Figure 4.22. Energy minimization calculations of the $CuPc(OC_2OBz)_8$ molecules were reported by Osburn et al.[11] Two low energy confirmations of $CuPc(OC_2OBz)_8$ were found with the eight side chains distributed equally around the Pc core, and with adjacent side chains close to each other to maximize van der Waal interactions. Various propositions as to the packing of the $CuPc(OC_2OBz)_8$ molecules based on these calculations and other factors have been discussed in detail.[11]

Molecular modeling results suggest a β polymorph stacking configuration of the $CuPc(OC_2OBz)_8$ molecules, in which the metal center of one molecule is above the bridging nitrogen of an adjacent molecule. This configuration predicts a molecular tilt angle ca. 30°.[11] This corresponds well with the tilt angles found using the RAIRS data and Debe treatment, although column-column interactions were not taken into consideration in the initial molecular models.

The IR spectroscopic data, SAXS data, and AFM images give a nearly complete picture as to the organization of the $CuPc(OC_2OBz)_8$ and $H_2Pc(OC_2OBz)_8$ molecules as an elliptical columnar assembly composed of off-axis cofacial stacking of said molecules.

The column-column interactions are still unclear.

Future WAXS data, taken of these highly ordered films, may indicate regularities in the side chain positions with a different periodicity than seen in the Pc-Pc ring spacing, which could indicate the role of the side chains in overall ordering. The amount of hydration in the thin films may indicate to what degree the side chains are solvated by water molecules on the LB trough and in multilayer thin films. Molecular energetic calculations could predict a space filling model of a hexagonally arranged group of these Pc molecules, that could be compared with the column-to-column distances found by AFM and SAXS to determine whether the side chains are overlapping between the columns.

CHAPTER 5: CHARGE MOBILITIES AND DOPING EFFECTS IN LB THIN FILMS OF $CuPc(OC_2OBz)_8$

The search for electronically conducting organic materials has been increasing over the last twenty years. The promise of low cost, high efficiency flat-panel-displays, flexible low power integrated circuits, and other such devices has driven research in this area to new levels. Effective electroactive organic materials would offer competitive electronics with reduced cost and complexity of processing required by the semiconductor materials used presently.

The most promising organic semiconductor materials are based on linear thiophenes. Charge transport mobilities for these materials range from $10x10^{-2}$ to $10x10^{-1}$ $cm^2V^{-1}s^{-1}$, with on/off ratios of up to $10x10^6$.[6] These thiophene materials still require delicate syntheses and vacuum desposition techniques in order to produce highly ordered, crystalline solids. The search for an electroactive organic molecule that can be organized into a well ordered solid by a simple method, such as the Langmuir-Blodgett technique, is still under investigation. The phthalocyanine molecules have shown some promise in filling this role.

5.1 $CuPc(OC_2OBz)_8$ as a Thin Film Transistor Semiconducting Material

Phthalocyanines were probably the first reported and most studied organic semiconductor materials.[6] Reported field-effect mobilities for un-substituted Pcs range from 1.0×10^{-4} to 1.0×10^{-2} $cm^2V^{-1}s^{-1}$.[30,31] Most Pc semiconducting layers have been

vacuum deposited thin films of un-substituted Pcs with varying metal centers (ie. Cu, Fe, Ni, Pt, or Sn). Although a fair amount of research has been done to determine conductivities in LB thin films of substituted Pcs,[13, 32, 33] little research has been devoted to determine the performance of these thin films in a thin film transistor (TFT) configuration.

In traditional inorganic and metal semiconductors, charge transport occurs in delocalized states facilitated by phonons, or thermally induced lattice deformations. There are several charge transport models for the case of organic materials .[6] Charge is described as "hopping" within a semiconductor between deformation sites. A polaron is one type of deformation that is a charge induced deformation of a conjugated chain. In well ordered organic materials, the band theory can be applied to conductivity observed within a coherent length of the organic material, like that observed in a PcPS polymerized chain.[29]

Bässler et al. have developed a model describing charge transport mobilities in amorphous materials.[34] The Bässler model describes charge transport as a hopping of charge between localized states within a material. These localized states are subject to a Gaussian distribution of molecular orientations, relative distances, and site energies.[35] The dependence on these Guassian distributions may be shown by a directional dependance of charge transfer in an anisotropically orientated material.

LB bilayers of $CuPc(OC_2OBz)_8$ are composed of an anisotropic arrangement of columnar assemblies. Closer proximal distances between $CuPc(OC_2OBz)_8$ molecules

within the columns are found than in between the columns. This would suggest that charge mobility, if any, would be better facilitated along the long axis of the columns than across columns. In order to probe this, LB films with thicknesses of 3 and 6 bilayers were deposited perpendicular and parallel to Au channel walls of the TFT substrate (Figure 5.1) as described in Section 2.9.

5.2 Determination of Charge Mobilities

In the characterization of a new organic semiconducting material in the channel region, it is standard practice to obtain a series of current vs. drain-source voltage curves for different gate voltages applied. Using a well behaved p-type semiconducting material in a thin film transistor, a series of curves as shown in Figure 5.2 are obtained. The current behavior is classified into two regimes. At low drain-source voltages the current varies linearly with drain-source voltage and is governed by Equation 5.1.

$$I_d = \frac{Z}{L}\mu C_i\left(V_g - V_t - \frac{V_d}{2}\right)V_d \qquad \text{(Eq. 5.1)}$$

Where Z is the channel width, L is the channel length, C_i is the capacitance density of the dielectric layer, and V_t is the threshold voltage which was approximated as the voltage at which the organic layer behaved as a p-type semiconductor. At high drain-source voltages, the current reaches a saturation regime which is governed by Equation 5.2.

$$I_{d,sat} = \frac{Z}{2L}\mu C_i\left(V_g - V_t\right)^2 \qquad \text{(Eq. 5.2)}$$

Using either of these two equations, the mobility and sign of the majority charge carrier

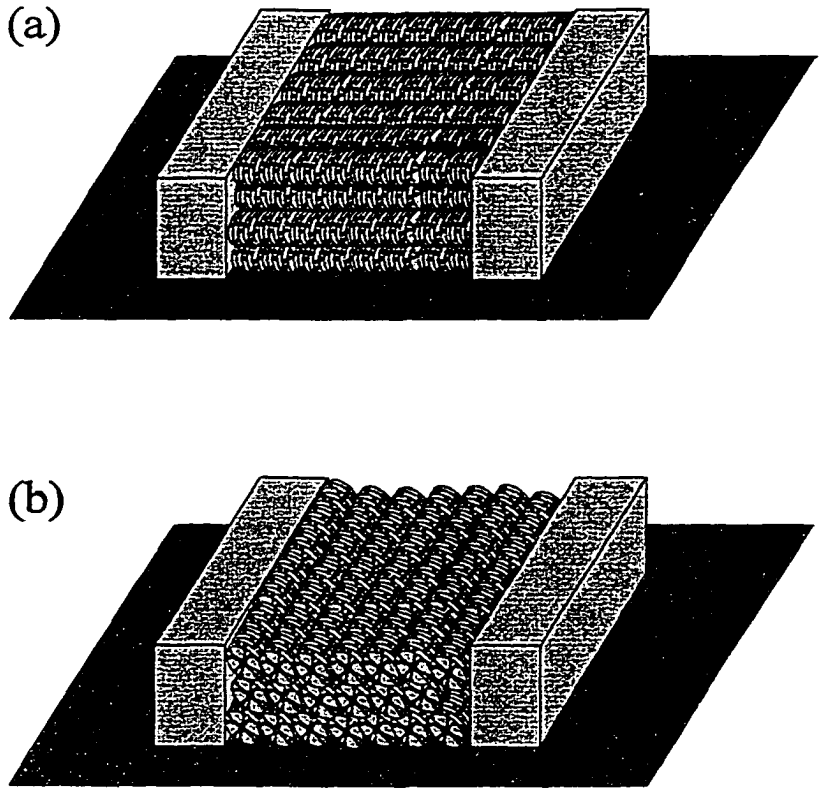

Figure 5.1, Directional transfer of LB films of $CuPc(OC_2OBz)_8$ (a) perpendicular ($\perp$), and (b) parallel ($\parallel$) with respect to the channel walls.

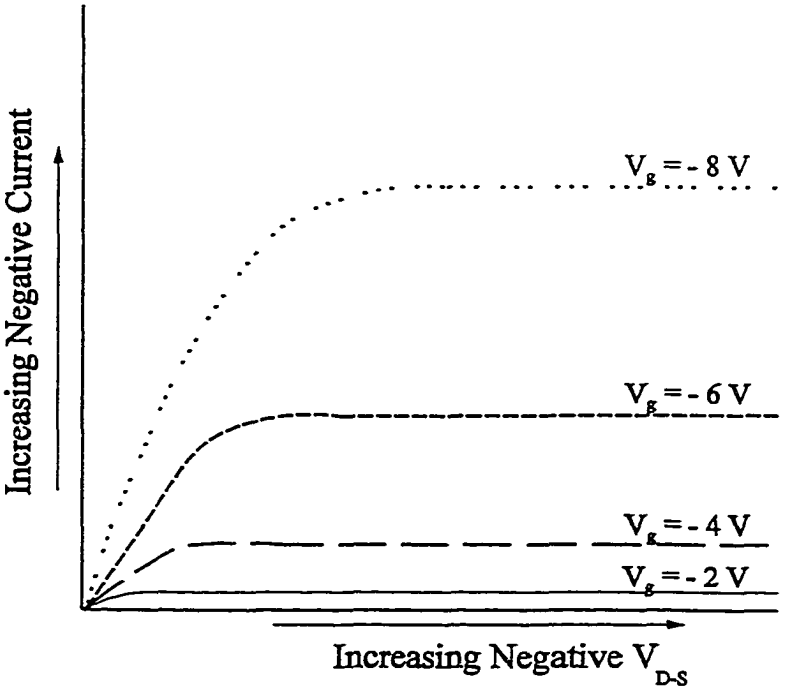

Figure 5.2, Typical current-voltage curves for a field-effect transistor with a p-type semiconducting layer at varying gate voltages, (V_g).

of the semiconducting layer can be found.

5.1.3 Evaluation of $CuPc(OC_2OBz)_8$ as a Semi-Conduction Material in TFT's

A series of current vs. drain-source voltage curves were obtained for different gate voltages applied. The curves for the 3 bilayer OFET are shown in Figure 5.3, and those for the 6 bilayer OFET are shown in Figure 5.4. Neither show the typical current vs. drain-source voltage response, meaning that there is no saturation regime over the gate voltage tested. Therefore, mobilities were found using Equation 1, for the linear regime. There is no indication from these measurements that there would not be a region of saturation at more negative gate voltages.

Mobilities for the four current voltage curves are listed in Table 5.1. There is a significant increase in absolute current passed and mobilities from the three bilayer case to the six bilayer case. This is primarily due to the doubling of available semiconducting material. There is also an increase in mobility between the parallel and perpendicular cases, shown in the calculation of the ratio of $\mu_{\perp}/\mu_{\parallel}$. This increase can be explained by the anisotropy of the thin films.

Charge transport is better facilitated along the $CuPc(OC_2OBz)_8$ columnar assemblies, versus across column interfaces. The anisotropy in the mobilities are comparable to similar degrees of anisotropy found in conductivity measurements made previously in our group of LB deposited thin films of $CuPc(OC_2OBz)_8$, and PcPs system.[14, 15]

The mobilities found for thin films of the $CuPc(OC_2OBz)_8$ are reasonable for a LB

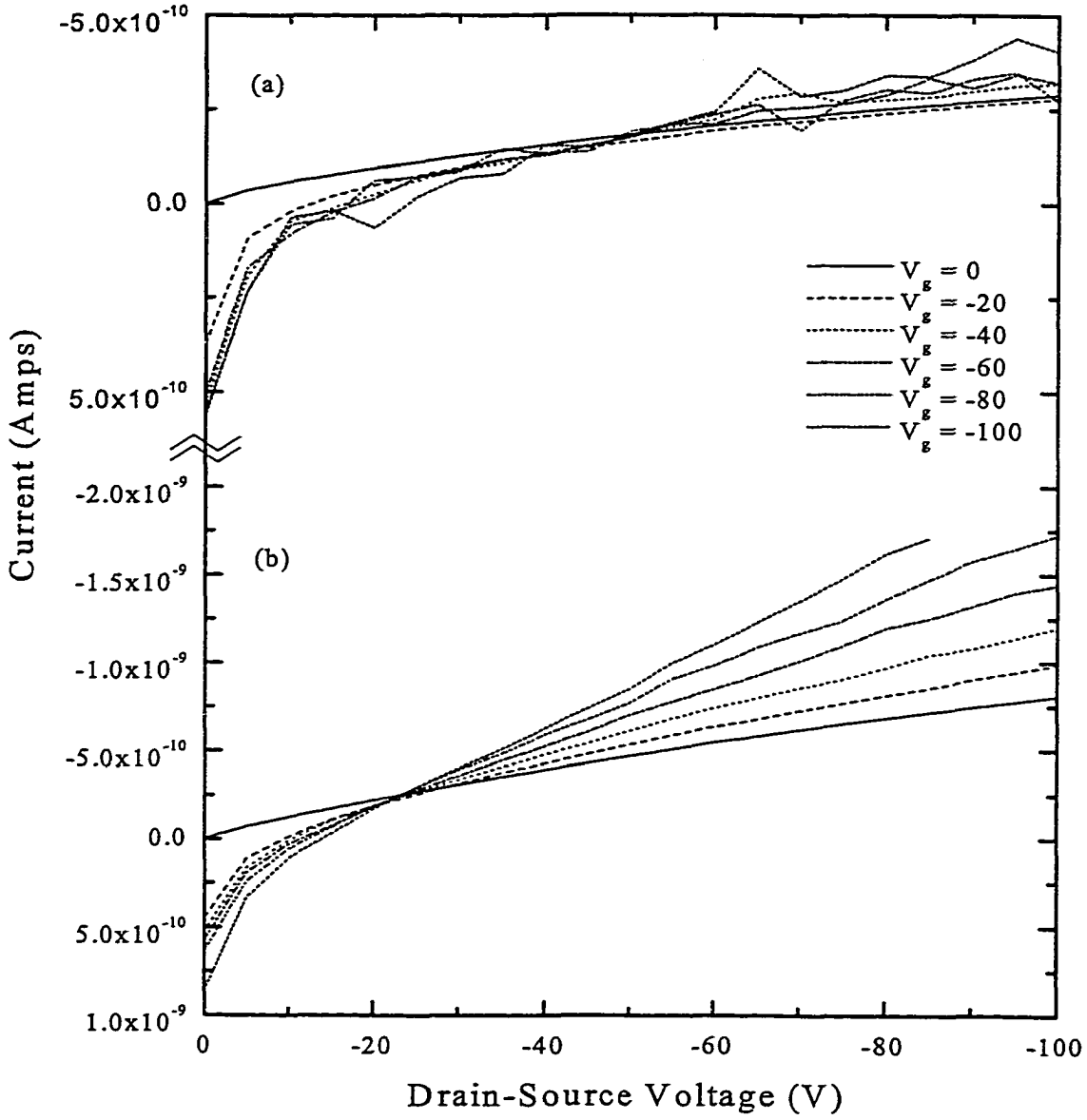

Figure 5.3, Current - Voltage curves for 3 bilayer films of $CuPc(OC_2OBz)_8$ deposited (a) parallel with and (b) perpendicular with the channel walls of the TFT substrate.

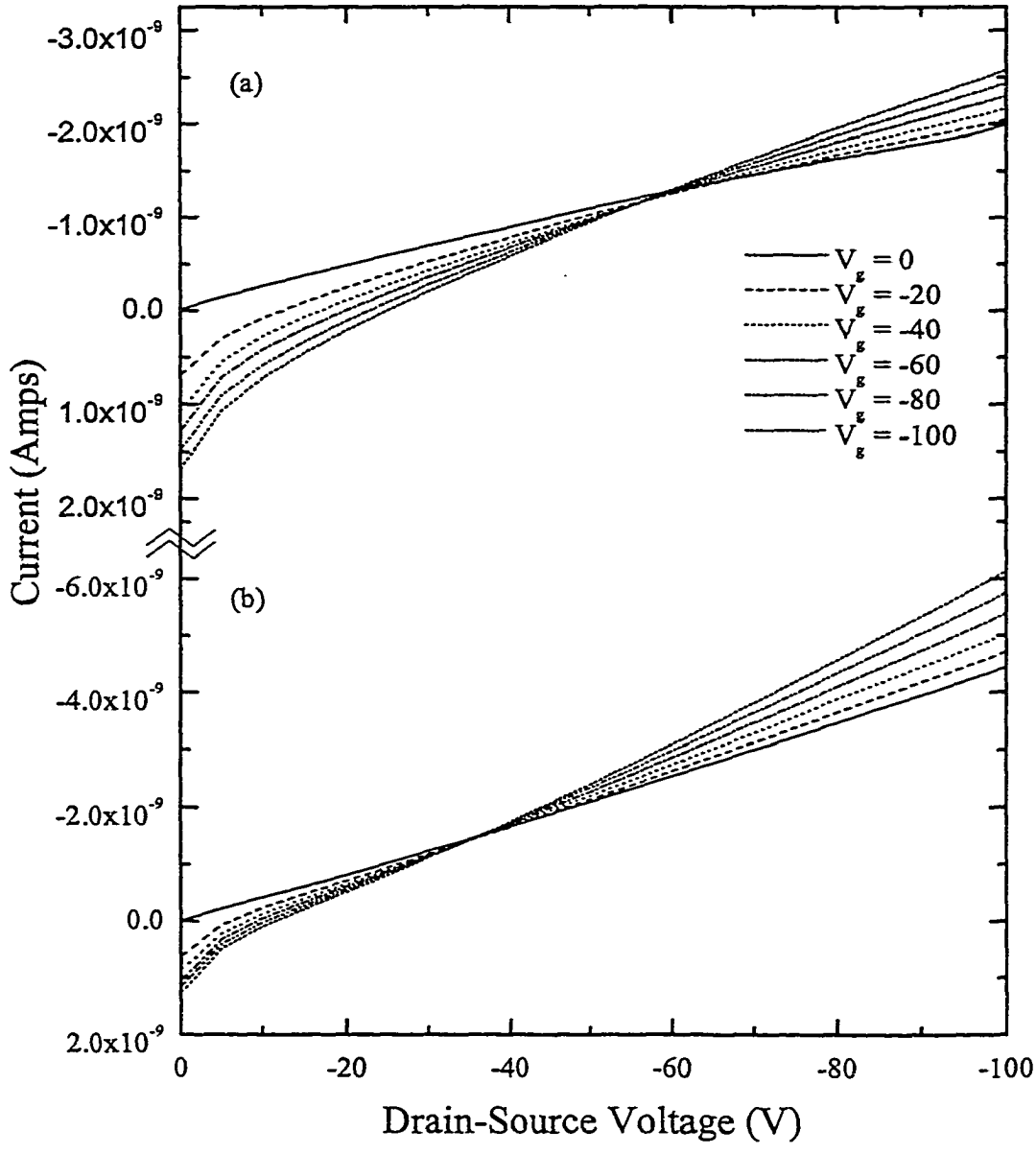

Figure 5.4, Current - Voltage curves for 6 bilayer films of $CuPc(OC_2OBz)_8$ deposited (a) parallel with and (b) perpendicular with the channel walls of the TFT substrate.

Table 5.1, Threshold voltages and field-effect mobilities for LB films of $CuPc(OC_2OBz)_8$

No. of Bilayers	Orientation	V_T (V)	μ ($cm^2V^{-1}s^{-1}$)	$\mu_\perp/\mu_\parallel$
3	$\perp$	-45	3.14E-5	3.72
3	$\parallel$	-22	8.44E-6	
6	$\perp$	-57	1.32E-4	2.74
6	$\parallel$	-35	4.82E-5	

deposited film of a substituted phthalocyanine layer. Although the mobilities are not impressive from a practical standpoint, there is still room for improvement. There is evidence that annealing of these films should increase the mobilities even more. Anisotropy ratios of conductivity measurements, reported by Wegner et al., increased as much as four times for annealed LB thin film samples of PcPs.

The IR linear dichroism data (Section 4.4) and the SAXS data (Section 3.3.2) indicate a significant increase in ordering within these films as well. We should expect similar increases in anisotropy ratios verses the PcPS system after annealing of the sample. Further experiments are needed to confirm this and to evaluate whether LB thin films of $CuPc(OC_2OBz)_8$ are a practical material for use in an organic field effect transistor.

5.2 Electrochemical Doping of $CuPc(OC_2OBz)_8$ Thin Films with the ClO_4^- Anion

5.2.1 Theoretical Effects of Doping an Organic Thin Film

It has been shown that some organic solids can be oxidized to their radical cation state, counter balanced by the introduction of an anion into the solid. The interest in such doping processes stems from the observations that appropriately oxidized materials exhibit a relatively high degree of electronic conductivity, and have been termed "synthetic metals."[29, 36] The oxidation and insertion of anions into phthalocyanine films have been studied by a number of groups.[29, 36, 37, 38] Most of the work in this area has been on vacuum deposited un-substituted phthalocyanine molecules with various metal centers (ie. Fe, Co, Ni, Cu, and Zn), although anion insertion into polymerizable Si-Pc-O type

assemblies have been investigated as well.[9] The extent of insertion, defined by the ratio of anion species to phthalocyanine molecule or monomer unit, varies from 0.3 to 0.5 for the studies referred to above.

Preliminary studies of the degree of insertion of the ClO_4^- anion into LB bilayer films of $CuPc(OC_2OBz)_8$ have been completed. Fifteen bilayer films on ITO of said molecule were electrochemically oxidized in the presence of aqueous 0.1 M $LiClO_4^-$. The redox behavior of LB films of this molecule in the presents of various electrolytes has been previously reported.[12, 14] The redox behavior of un-annealed and annealed films of $CuPc(OC_2OBz)_8$ with 0.1 M $LiClO_4^-$ as the supporting electrolyte is reproduced here in Figure 5.5.

The un-annealed film exhibits two oxidation processes followed by one reduction peak. The behavior is best explained in context of the findings of Jansen and Beck, who reported several anodic processes for vacuum deposited films of CuPc also using 0.1 M $LiClO_4^-$ as the supporting electrolyte.[38] They hypothesized that the first oxidation wave is due to anion insertion that is an intrinsic redox process. The second oxidation wave may be due to forced insertion of anions into the film that may result in dissolution of the first few layers of the film. The single reduction peak represents the reduction of Pc molecules limited by the ability of the anions to migrate back out into solution.

The annealed film shows similar oxidation and reduction potentials, but only one oxidation peak is observed. We can assume that the insertion mechanism has been

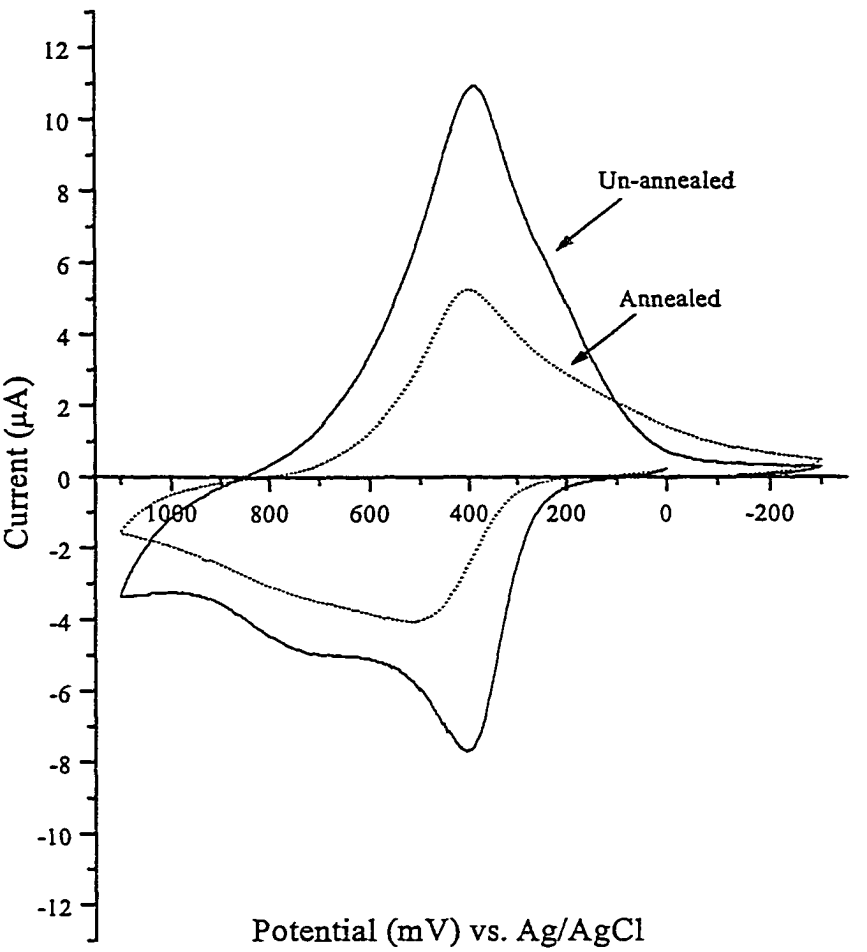

Figure 5.5, Cyclic voltammetry of un-annealed and annealed 15 bilayer films of $CuPc(OC_2OBz)_8$ on ITO in the presence of 0.1 M $LiClO_4$ as the supporting electrolyte.

hindered by the more ordered film (Section 4.4 and Section 3.3.2) resulting in a shift of the oxidation peak to more positive potentials. Again, we see one reduction peak as the potential is swept back negative.

CuPc films were doped just past the first oxidation wave, and then removed from solution under potential control to investigate the amount of detectible insertion, if any, that occurred during the non-destructive anion insertion process. The amount of charge passed during the potential sweep to 400 mV in the un-annealed film was determined to be ca. 1×10^{-4} C. Using a density approximation, determined from the LB isotherm of 110 $Å^2$ / molecule, and approximating the surface area of the "electrochemical cell" as determined by the electrolyte drop diameter, the charge passed is equivalent to the oxidation of the first 9 monolayers of the 15 bilayer . An equivalent calculation was done for the annealed film, showing that less charge is passed as the potential is swept to 500 mV, and is equivalent to the oxidation of the first 6 monolayers of the annealed 15 bilayer film. Therefore, 30% of the molecules in the un-annealed film and 20% of the molecules in the annealed film have been oxidized in the doping process.

5.2.2 Quantitation of the Extent of Doping by XPS

X-ray photoelectron spectroscopy has been used to estimate the extent of anion doping into thin films.[9] Although exact quantitation of dopant concentration is not realiable by this analysis, relative atomic ratios are available and indicate the relative amount of anion doping into these films.

Ideally the intensity of emitted photoelectrons would be proportional to the

number of atoms in a sample. The reality is that there are a number of factors that influence the intensity of the photoelectron signal. The intensity is proportional to a variety of terms which include: $I^o \equiv$ incident X-ray flux, $T \equiv$ transmission efficiency of the analyzer, $D \equiv$ detector efficiency, $\sigma \equiv$ photoionization cross section, $N \equiv$ number of atoms in the sample, and $\lambda \equiv$ inelastic mean free path. Using a relative atomic ratio approach, a number of the above terms are eliminated, and assumptions about T, D, and λ are eliminated due to an inverse relationship between their respective functions over the kinetic energy window of interest.

The expression used here to determine the relative atomic ratios of atoms A and B, Equation 5.3, relates the number of atoms to the intensity and to the photoionization cross-section that has been determined and reported by Scofield.[39]

$$N_A / N_B = I_A \sigma_B / I_B \sigma_A \qquad \text{(Equation 5.3)}$$

High resolution photoelectron emission spectra of four elements (C, N, Cl, and Cu) are combined in Figure 5.6. Figure 5.6.a and 5.6.b show the similarity in photoelectron emission spectra of the C 1s line of the plain CuPc film and a doped film. One can see that the peak areas appear to remain unchanged for the N 1s (c) and (d), and the Cu $2p_{1/2}/2p_{3/2}$ (g) and (h) as well. Previous to doping, there is no Cl 2p signal (Figure 5.6.e), but after doping there is a well defined Cl 2p peak that was used to determine the relative atomic ratio of the ClO_4^- anion to CuPc molecule.

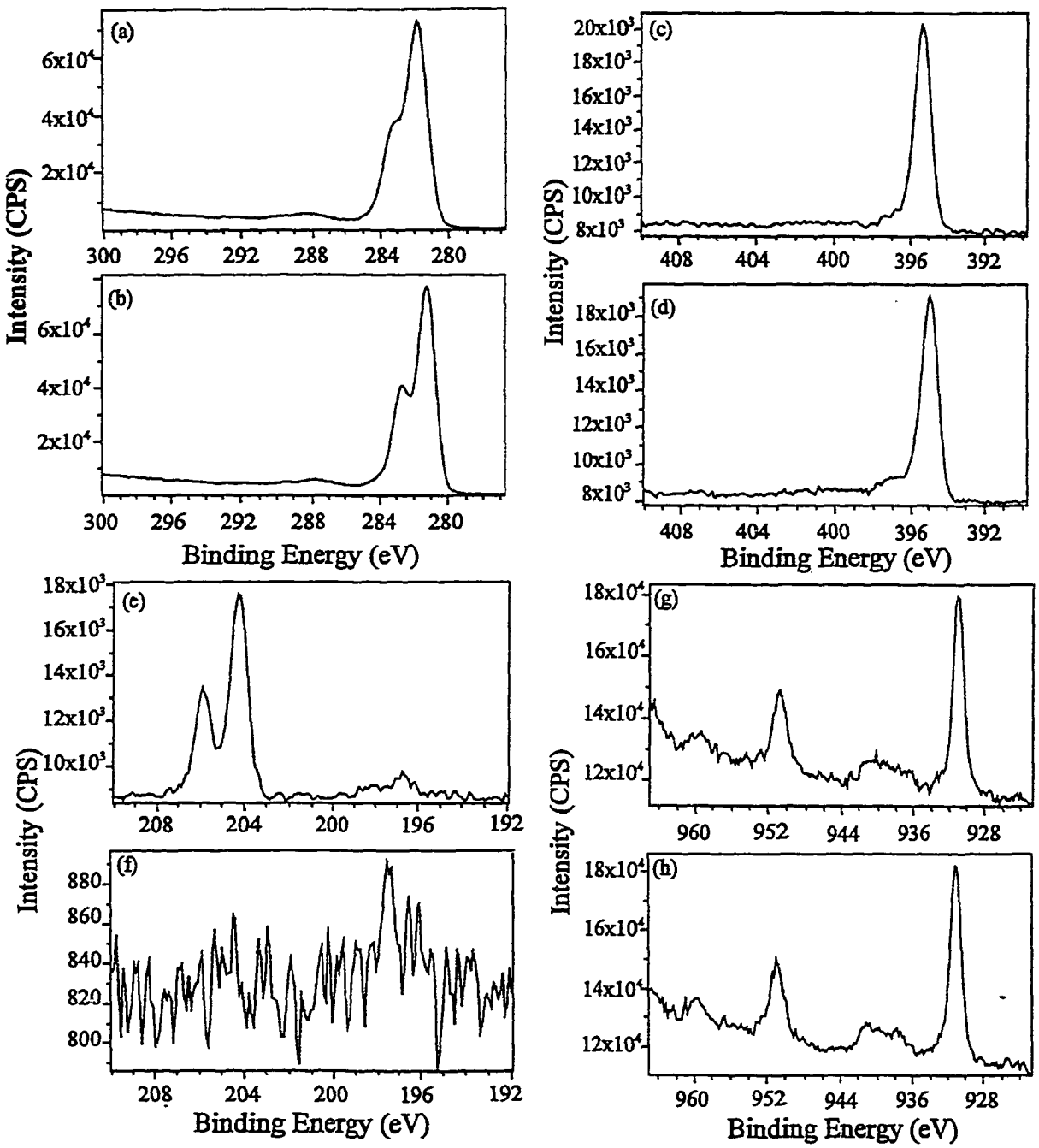

Figure 5.6, Photoelectron Spectra of C 1s (a) and (b), N 1s (c) and (d), Cl 2p (e) and (f) and Cu 2p (g) and (h) peaks of doped and undoped films respectively.

Raw peak areas, corrected peak areas, and relative atomic ratios are summarized in Tables 5.2 and 5.3. It would appear that the relative atomic ratio of ClO_4^- anions to CuPc molecules, as indicated by the Cl/Cu ratio, is high relative to the previously reported ratios of 0.3-0.5, but it is reasonable that every CuPc molecule has been oxidized within the sampling depth of the XPS experiment. The validity of the assumptions made to produce Equation 5.3 seem reasonable based on the stoichiometrically correct atomic ratios found for N/Cu, despite the wide kinetic energy gap between the N 1s and the Cu 2p peaks.

5.2.3 Hypotheses on the Interactions of ClO_4^- Anions in these Pc Thin Films

One hypothesis as to the high efficiency of doping out to the first oxidation peak is based on possible solubility effects. The ethyloxy linked side arms of the Pc may solubilize the anions. The would create a situation of not only electrochemical doping, but osmotic doping as well. If this hypothesis proves true in further studies, there is a possibility for four anions to incorporate around one CuPc molecule. The possibility of such incorporation is supported by the work of Gaudiello and Marks who measured the x-ray powder diffraction spectra of doped Si(Pc)O systems.[37] Their data suggests that an orthorhombic lattic of Pc molecules can incorporate anions by the deformation of the orthorhombic structure into a tetrahedral structure where each Si(Pc)O is surrounded by four anions and vice versa.

Further x-ray and possibly AFM studies will reveal if structural changes occur

Table 5.2, XPS data from undoped films of $CuPc(OC_2OBz)_8$

Raw Intensity	C 1s	N 1s	Cl 2p	Cu 2p
	110268	17022	NA	23704
Scoffied cross-sections	1.000	2.281	1.800	25.390
Corrected Intensity	110268	7463	NA	934
Relative Atomic Ratios	C/N	C/Cu	N/Cu	
	15	118	8	

Table 5.3, XPS data from ClO_4^- doped films of $CuPc(OC_2OBz)_8$

Raw Intensity	C 1s	N 1s	Cl 2p	Cu 2p
	109548	14535	1623	20989
Scoffied cross-sections	1.000	2.281	1.800	25.390
Corrected Intensity	109548	6372	902	827

Relative Atomic	C/N	C/Cu	N/Cu	Cl/Cu	N/Cl
Ratios	17	128	8	1	7

when anions, such as ClO_4^- are introduced into the columnar CuPc assemblies. The electronic effects of doping are also of interest. Conductivity measurements have been previously made in our group using micrometer Au comb electrode configurations, and will give some indication of the performance one would expect in a TFT configuration after doping with a suitable anion.

CHAPTER 6: CONCLUSIONS

6.1 Summary of Results

The experiments and data presented in the preceding chapters explains the ways in which the previously observed ordering in LB thin films of $CuPc(OC_2OBz)_8$ and $H_2Pc(OC_2OBz)_8$ can be enhanced. The variables investigated were the macroscopic and microscopic organizational effects of using a baffle in the LB trough, annealing the films, varying the subphase temperature, and using different substrate surface pretreatments. Each of these variables has a significant effect on the resulting LB multi-layered films.

The Schaefer (horizontal) method of LB transfer is a superior method of transfer for Langmuir films of $CuPc(OC_2OBz)_8$ and $H_2Pc(OC_2OBz)_8$ because of the conservation of order achieved at the air-water interface. The incorporation of a baffle into the transfer method does not lead to better transfer of the initial film, but rather disrupts the deterioration of the Langmuir film as sections of it are pulled away by the substrate. The baffle, in effect, makes it possible to make high quality multilayer film transfers out of one Langmuir film. The effects of this may be seen in automated production of LB films of these and other related materials for use in organoelectronic applications.

The impact of using the baffle in constructing multilayer films can be seen in the comparison of previously obtained SAXS[14] and WAXS[10] data with the SAXS data shown here, and also in the degree of spectroscopic dichroism found in these films, as compared with less ordered films of these same materials.[11, 12]

The degree of ordering in these films was found to increase dramatically upon

annealing of the films. Annealing has proven to reorganize LB films of the PcPS system,[28] and the stereoisomerically pure Pc system used by Nolte et al.[13] into more ordered arrays of columnar assemblies. The material investigated here is no different. The appearance of Kiessig fringes in the SAXS data of the $CuPc(OC_2OBz)_8$ and the increase in dichroism in the IR data (up to 75%) show increased ordering within the films.

Although the composition of the subphase has been varied previously,[11] there has been no investigation of the effects of the subphase temperature on the ordering within the film. Although a room temperature water subphase was the accepted procedure, more highly ordered films are transferred at lower temperatures. The formation of a more "crystalline" structure at lower temperatures fits with the model phases of discotic liquid crystals as reviewed by Ringsdorf.[24] As the temperature decreases, the arrangement of discotic liquid crystal molecules transform from a completely isotropic arrangement, to an anisotropic arrangement to a crystalline solid arrangement. The specific phase transition temperatures for $CuPc(OC_2OBz)_8$ and $H_2Pc(OC_2OBz)_8$ have not yet been determined.

The substrate surface pretreatments gave some of the most interesting results. Higher IR dichroic ratios were found for multilayer films deposited onto a phenyl terminated surface. The significance of this is most drastically seen in the exclusive conservation of order upon transfer of one bilayer films of $CuPc(OC_2OBz)_8$ and $H_2Pc(OC_2OBz)_8$ onto benzyloxyethanethiol modified Au surfaces. This could prove to be

a stepping point for micropatterning deposition of these films, although it was shown in the RAIRS spectra that after three bilayers were transferred, there was no significant difference in the amount of material transferred subsequent to the first partial or first bilayer transferred.

Microscopic organization was probed using RAIRS. Euler tilt angles were found for the $CuPc(OC_2OBz)_8$ and $H_2Pc(OC_2OBz)_8$ molecules within a multilayer assembly. These angles predict a ca. 15° to 30° degree tilt of the macrocyle plane away from the surface normal and a ca. 15° to 20° rotation around the Pc column axis, resulting in an elliptical array of these molecules.

Bragg peaks found at low angles in previously reported WAXS data indicated a hexagonal columnar D_h phase for fibers of $CuPc(OC_2OBz)_8$. This assumption was used in determining the column-to-column spacing from the lattice parameters of the SAXS data presented in Section 2.5 as well. There is some question as to how elliptical array of molecules predicted by the Debe treatment of the RAIRS data can adopt a hexagonal close packed assembly. Several possible arrangements are shown in Figure 6.1.

A deformed hexagonal packing occurs when a second layer of $CuPc(OC_2OBz)_8$ or $H_2Pc(OC_2OBz)_8$ lays commenserate with the column troughs of the layer below. This configuration is more accurately described by a orthorhombic arrangement as seen in Figure 6.1.a. If the elliptical array of columns were to adopt a hexagonal close packed arrangement, there would be overlap of the side chains on the periphery of the Pc molecule (Figure 6.1.b). The side chains would have to intercalate or adopt a different

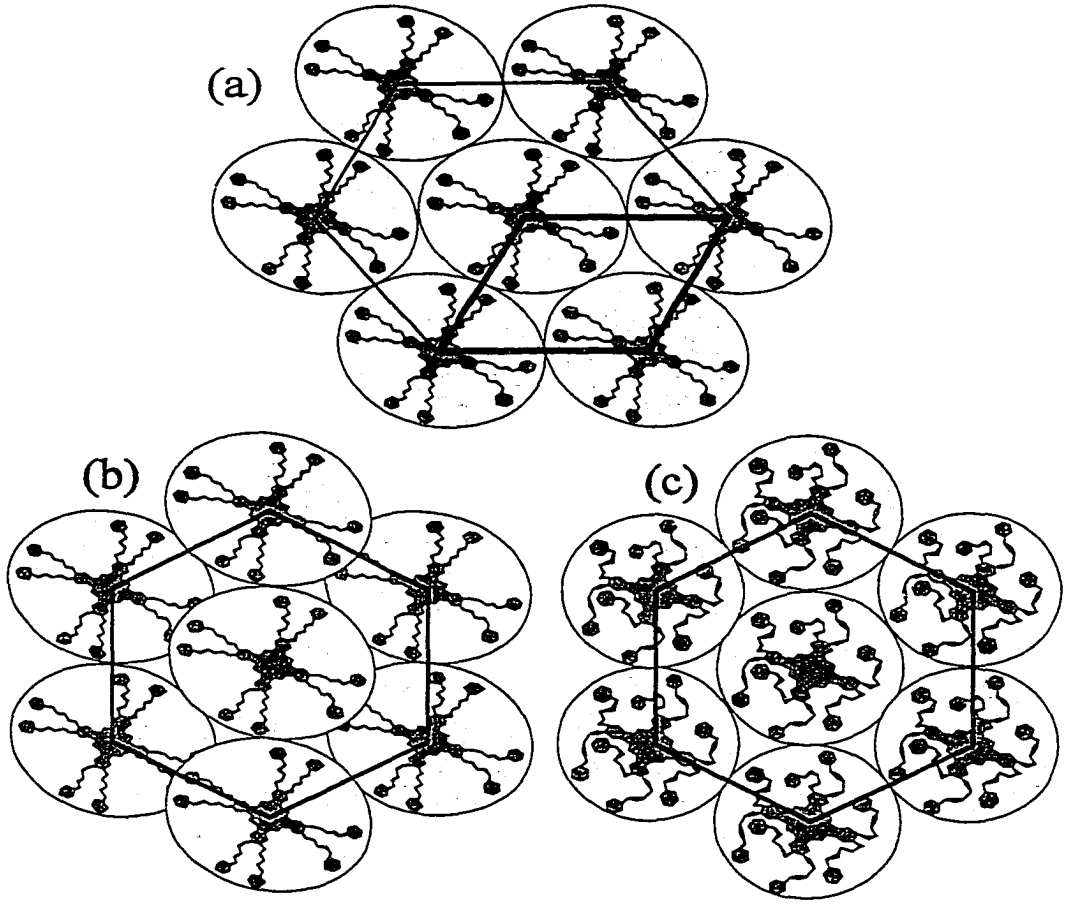

Figure 6.1, Possible packing arrangements of elliptical $CuPc(OC_2OBz)_8$ and $H_2Pc(OC_2OBz)_8$ molecules: (a) rombehedral packing of columnar layer on top of columnar layer, (b) overlap of elliptical projections in hexagonal close packing, (c) deformation of Pc substituents, creating a possible hexagonal close packing, while maintaining the elliptical projection of the Pc macrocyle core.

geometry, so that the outside perimeter would be circular, but the elliptical projection of the Pc macrocycle, as calculated from the RAIRS data would be preserved (Figure 6.1.c). WAXS data of these new, well ordered films may indicate which of these packings is most accurate.

6.2 Future directions

The ability to make LB thin films with the degree of ordering and coherence found through the preceding experiments leads to several future directions. The first is a detailed examination of the photocurrent properties of these well ordered films. Fox et al., have found significant short circuit photocurrents for a similar porphyrin molecule.[42] A sandwich cell design would be used to monitor any current generated when the cell is exposed to excitation radiation.

Another type of sandwich cell composed of a multilayer film on one piece of ITO, and a doped mulitlayer film on the other piece of ITO fused together by annealing, may behave as a diode. One could imagine the doped multilayer film as an n-type material with respect to the un-doped film. Investigating the diode behavior, if any, of this configuration is another possible future direction.

We have proven that charge mobilities within the multilayer thin films is anisotropic. Our ability to control the orientation of the colmunar assemblies with respect to a laboratory coordinate system will allow us to make multilayered thin films of various orientations within the layers. This would allow us to make a conductive thin film, with any variety of directional response based on the direction of transfer onto the substrate.

Micro patterning is another possible future direction because of the nearly exclusive transfer of $CuPc(OC_2OBz)_8$ and $H_2Pc(OC_2OBz)_8$ Au substrates functionalized with benzyloxyethanethiol.

These new directions are based on our ability to make directionally ordered thin films of $CuPc(OC_2OBz)_8$ and $H_2Pc(OC_2OBz)_8$, and our ability to understand what the chemical nature of the thin films are. The experiments and results presented in this thesis outline a new procedure of making highly ordered thin films for use in further investigations of the possible uses of these materials in organoelectronic devices.

REFERENCES

1. Grieg, R., Personal Account, *2nd Internaltional Symposium on Pthalocyanines: Seventy Years of Scientific Progress*, The Royal Society of Chemistry, Sept. 21-23, 1998

2. Moser, F. H.; Thomas, A. L., The Phthalocyanines I: Properties, CRC Press. Boca Raton, FA, 1983, 1-2

3. Separovic, D.; Mann, K. J.; Oleinick, N. L., J. *Inorg. Chem.* **1998** 68, 101-109

4. Wohrle, D.; Meissner, D., *Adv. Mater.* **1991** 3, 129-138

5. Agbabiaka, A. A.; Mukhopadhyay, S.; Mukherjee, D.; Thorpe, S. C., *Supramol. Sci.* **1997** 4, 185-109

6. Horowitz, G., *Adv. Mater.* **1998** 10 365-377 and references therein

7. Baker, S.; Petty, M. C.; Roberts, G. G.; Twigg, M. V., *Thin Solid Films* **1983** 99, 53

8. Chesters, M. A.; Cook, M. J.; Gallivan, S. L.; Simmons, J. M.; Slater, D. A., *Thin Solid Films* **1992** 210/211, 538-541.

9. Ferencz, A.; Armstrong, N. R.; Wegner, G., *Macromolecules* **1994** 27, 1517-1528

10. Osburn, E. J. ; Schmidt, A.; Chau, L.-K.; Chen, S.-Y.; Smolenyak, P.; Armstrong, N. R.; O'Brien, D. F., *Adv. Mater.* **1996** 8, 926-928.

11. Osburn, E. J. ; Chau, L.-K.; Chen, S.-Y.;Collins, N.; O'Brien, D. F.; Armstrong, N. R., *Langmuir* **1996** 12, 4784-4796.

12. Smolenyak, P. E.; Osburn E. J.; Chen, S.-Y.; Chau, L.-K.; O'Brien, D. F.; Armstrong, N. R., *Langmuir* **1997** 13, 6568-6576

13. van Nostrum, C. F.; Bosman, A. W.; Gelinck, G. H.; Schouten, P. G.; Warman, J. M.; Kentgens, A. P. M.; Devillers, M. A. C.; Meijerink, A.; Picken, S. J.; Sohling, U.; Schouten, A.-J.; Nolte, R. J. M., *Chem. Eur. J.* **1995** 1, 171-182

14. Smolenyak, P. E. *Ph. D. Dissertation*, The University of Arizona, 1998

15. Smolenyak, P. E.; Peterson, R. A.; Töerker, M.; O'Brien, D. F.; Armstrong, N. R., Manuscript in Preparation

REFERENCES - Continued

16. Ulman, Al., *An Introduction to Ultrathin Organic Films from Langmuir-Blodgett to Self-Assembly*, Academic Press, Inc.: San Diego, 1991.

17. Porter, M. D.; Bright, T. B.; Allara, D. L.; Chidsey, C. E. D., *J. Am. Chem. Soc.* **1987** 109, 3559-3568

18. Zisman, W. A.; *Contact Angle Wettability and Adhesion American Chemical Society*, Washington, D. C. 1964

19. Watanabe, S.; Nakayama, N.; Ito, T., *Appl. Phys. Lett.* **1991** 59, 1458

20. Warren, B. E. *X-ray Diffraction*, Addison-Wesley Publishing Co. Inc., Reading, MA: 1969

21. Guinier, A., *Small-Angle Scattering of X-rays*, John Wiley & Sons, Inc., London, 1955

22. Manne, S.; Cleveland, J. P.; Gaub, H. E.; Stucky, G. D.; Hansma, P. K., *Langmuir* **1994** 10, 4409-4413

23. Umemura, S.; Igarashi, M.; Andoh, Y.; Noguchi, K.; Dekura, T.; Toda, A., *J. Vac. Sci. Technol. B* **1998** 16, 38-42

24. Ringsdorf, H.; Schlarb, B.; Venzmer, J., et al., *Angew. Chem., Int. Ed. Eng.* **1988** 27, 113-158.

25. Gittens, G. J., *Journal of Colloid and Interface Science* **1969** 30, 406-412

26. Debe, M. K., *Optical Probes of Organic Thin Films*, 1989

27. Debe, M. K., *Applications of Surface Science* **1982-83** 14, 1-40

28. Sauer, T.; Arndt, T.; Batchelder, D. N.; Kalachev, A. A.; Wegner, G., *Thin Solid Films* **1990** 187, 357-374

29. Gaudiello, J. G.; Almeida, M.; Marks, T. J.; McCarthy, W. J.; Butler, J. C.; Kannewurf, C. R., *J. Phys. Chem.* **1986** 90, 4917-4920

30. Bao, Z.; Lovinger, A. J.; Dodabalapur, A., *Appl. Phys. Lett.* **1996** 69, 3066-3068

REFERENCES - Continued

31. Bao, Z.; Loveinger, A. J.; Dodabalpur, A., *Adv. Mater.* **1997** 9, 42-44

32. Kutzler, F. W.; Barger, W. R.; Snow, A. W.; Wohltjen, H., *Thin Solid Films* **1987** 155, 1-16

33. H. Rengel, Gattinger, P.; Silerova, R.; Neher, D., In Press

34. Bässler, H. *Phys. Status Solidi* **1993** B175, 16

35. Ioannidis, A.; Dodelet, J. P., *J. Phys. Chem. B* **1997** 101, 5100-5107

36. Marks, T. J., *Science* **1985** 227, 881-889

37. Gaudiello, J. G.; Kellogg, G. E.; Tetrick, S. M.; Marks, T. J., *J. Am. Chem. Soc.* **1989** 111, 5259-5271

38. Jansen, R.; Beck, F., *Ber. Bunsenges. Phys. Chem.* **1991** 95, 1531-1537

39. Scofield, J. H., J. Electro. *Spectrosc. Rel. Phenom.* **1976** 8, 129-137

40. Schmidt, V. S.; Reich, R., *Berichte der Bunsen-Gesellschaft* **1972** 76, 1202-1208

41. Fraser, R. D. B., *J. Chem. Phys.* **1958** 28, 1113-1115.

42. Fox, M. A.; Grant, J. V. Melamed, D.; Torimoto, R.; Liu, C.-y.; Bard, A. J., *Chem. Mater.* **1998** 10, 1771-1776

IMAGE EVALUATION TEST TARGET (QA-3)

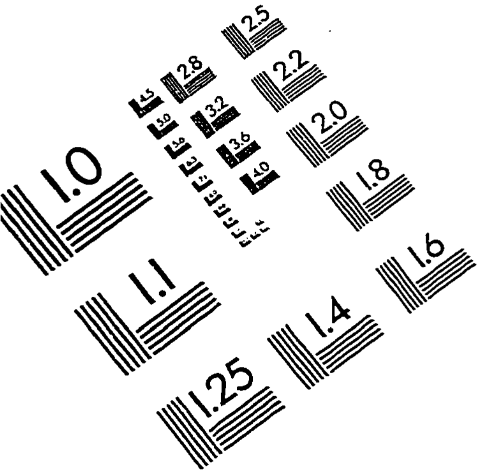

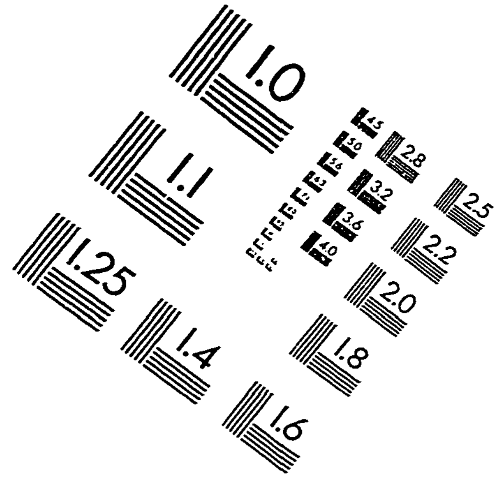

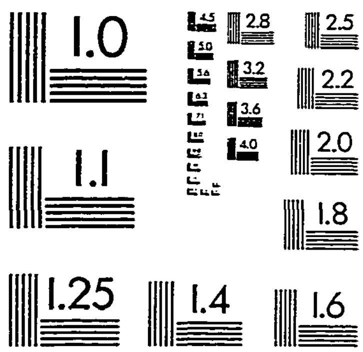

150mm

6"

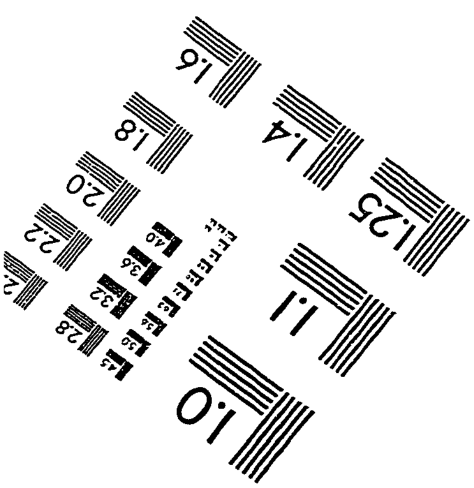

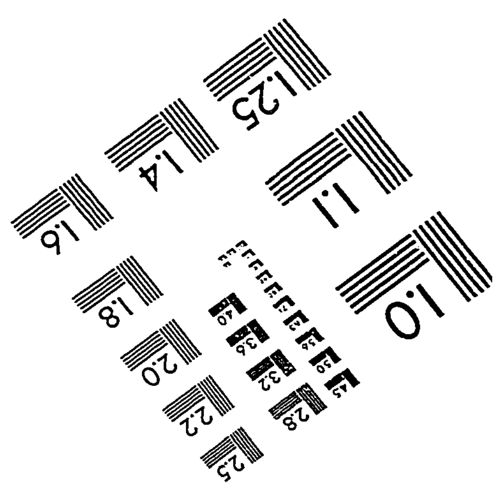

APPLIED IMAGE . Inc
1653 East Main Street
Rochester, NY 14609 USA
Phone: 716/482-0300
Fax: 716/288-5989